

L3HARRIS SECONDARY MIRROR SUPPORT STRUCTURE

Melanie Earle Charles Fleischmann Gabriella Gima Stelios Halioris Christopher Piatek

ABSTRACT

The aerospace industry has embraced additive manufacturing to increase efficiency and lower costs of satellite and rocket components. The goal of this project is to design and develop a satellite component known as a Secondary Mirror Support Structure (SMSS) for aerospace company L3Harris Technologies that can be manufactured using additive manufacturing, specifically 3D metal printing. Additive manufacturing will decrease the cost and time it takes to manufacture a SSMS. There were two approaches taken to solving this design problem. The first incorporated topology optimization to find an ideal geometry defined by the requirements and specifications outlined by the sponsor that can be additively manufactured. The second approach used the success of the previous 2022 senior design team's final SMSS model to influence a new model that focused specifically on the ability for the model to be additively manufactured and the incorporation of lattice acting as an infill for a 3D print. The report will review the design process of the SMSS, the Finite Element Analysis that was used to analyze the SMSS model, and the items that were manufactured to support the SMSS design. The final SMSS model in this report passed all the specifications and requirements given by L3Harris and has a final mass of 14.58 lbm.

PROBLEM DEFINITION

Reflector telescopes use a system called Optical Telescope Assembly (OTA), where components such as Secondary Mirror Support Structures (SMSS) are integral to their function. Satellite components should endure extreme vibrations, thermal loads, and accelerations. Components like the SMSS are time-consuming and costly to manufacture with traditional manufacturing methods.

The aerospace industry has embraced additive manufacturing to construct rockets and satellites components to decrease manufacturing time for more launches. L3Harris aims to use metal additive manufacturing to improve the efficiency of

traditional manufacturing methods, reduce cost and provide reliable support for the secondary mirror. Using properties of the previous SMSS design, a new SMSS will be modeled and further optimized by analyzing the topology, determining thermal stability, and improving the inner lattice to reduce weight and overall cost.

REQUIREMENTS, SPECIFICATIONS, DELIVERABLES

The deliverables requested by L3Harris and agreed upon by the senior design team were guided by requirements and specifications set by the sponsor. There are seven requirements and specifications each, listed below. The requirements for the deliverables are as follows:

1. Project scope is the design, analysis, and prototype of the SMSS only.
2. The project will focus on additive manufacturing solutions to the problem statement.
3. The SMSS will have interfaces for and support the Secondary Mirror and Mounts, Actuator Assembly, Shade Assembly, Misc. Thermal Hardware.
4. Design will be producible with additive manufacturing methods.
5. The following design factors of safety will be used:
 - a. Yield: 2.0
 - b. Micro-yield: 1.0
 - c. Ultimate: 2.5
 - d. Buckling: 4.0
6. Mass Contingency factors will be used
 - a. Concept Design: 20%
 - b. Preliminary Design: 15%
 - c. Final Design: 10%
 - d. Post Final Design
 - e. 5%, Measured Hardware: 0.10%
7. There shall be no trapped cavities in the SMSS.

The specifications for the deliverables given by L3Harris are outlined below in Table 1.

Specifications:

<i>Specification</i>	<i>Verification</i>
The outer diameter of the SMSS must be 48 ± 0.005 ".	A circle with a diameter of 48" can be made around the model to confirm that it fits within the bounds.
The SMSS will interface with the Forward Metering Structure at three locations 120 degrees apart.	A Faro Arm or protractor can be used to measure the angles.
The first mode of the SMSS shall be 120 Hz or greater when grounded at the FMS interface and supporting all hosted hardware.	A hammer test can be performed to find the first mode. NX can also simulate vibrational modes.
The goal mass is a maximum of 18 lbm.	The model can be inspected in NX to find its mass.
The SMSS shall have positive margins of safety against yield and ultimate failure when exposed to a quasi-static load of 12G laterally and 18G axially simultaneously, (lateral swept 15 deg increments) combined with a 5C to 35C temperature range (nominal room temp is 20C) while supporting all hosted hardware.	The ultimate yield and failure can be found through Nastran analysis.
The SMSS and hosted hardware shall not obstruct more than 14% of the Primary Mirror (PM) clear aperture area (assume 1.1m diameter clear aperture).	Using NX, the area of the mirror that is covered can be calculated.
The SMSS should provide a stable mounting platform for the Secondary Mirror in thermal environments. The average motion of the SM interfaces under a 1 degree C isothermal load should be 0.66 micro-inches translation (RSS of X and Y) or less and 0.037 micro-radians rotation (RSS of Rx and Ry) or less.	Thermal simulation can be used to estimate the movement of the structure in low temperature environments.

Table 1: Specifications provided from L3 Harris for the SMSS.

The agreed upon deliverables between the sponsor of L3Harris and the senior design group are as follows below.

1. A Finite Element model of the Secondary Mirror Support Structure in Nastran.
2. CAD file prototypes and 2D drawings of Secondary Mirror Support Structure.
3. A Technical Report
4. Host design review meetings and provide supporting slides for L3Harris Sponsor. Three meetings will be a

Concept Design Review, Preliminary Design Review, and Final Design Review. CAD and FEA analysis will be presented and provided at these meetings.

5. 3D Printed Prototype of Secondary Mirror Support Structure which can be scaled and composed of materials other than Invar-36.
6. Model validations will be included within the final technical report and provided at design review meetings. These model validations will be conducted through simulations and experimental data.

The critical path management and work break down structure that were formed to meet the requirements, specifications, and deliverables are present in Appendix A, Figures 1 and 2.

CONCEPTS

The L3Harris team developed four concepts for the SMSS. Concept A (Appendix B, Fig. 3) is a final design of the SMSS developed by last year’s team. This design’s objective was to be a topologically optimized design of the beams within the SMSS. This design meets all the requirements and specifications of the project as outlined by L3Harris. This design is also under the 18 lbm mass requirement. However, the topological analysis of the design relied on approximations including linear approximations for stiffness equations and curve-fitting onto voxel-based geometry to produce smooth surfaces, which impacted the correlation between the NX model and the physical product. The design also would need to be further optimized to get rid of useless protrusions in the model.

Concept B (Appendix B, Fig. 14) depicts an SMSS that uses I-beams as the appendages of the structure. The inclusion of I-beams into the design is for ease of manufacturing, which is a key goal for this project. The mirror plate in the middle is made of simple cylindrical rings held together by beams in a truss formation, which serves to avoid the keep-out zone discussed in the specifications. The beam appendages can be screwed or bolted to fins which stick out from the rings. Concept B could serve as a foundation for Concept C (Appendix B, Fig.15), which could utilize the simple design provided by the I-beams, combined with an inner lattice to retain strength, reduce weight, and ease manufacturability.

Concept C (Appendix B, Fig. 15) presents an SMSS that is composed of a gyroid lattice which are 10 mm unit cells and have a 40% solidity. This model was composed in Fusion 360. The lattice provides a way to lower the weight of the SMSS and allow for ease of manufacture. To determine if it was possible to 3D print a gyroid lattice, Figure 15 depicts a scaled down model of Concept C as proof of concept. Concept C provides an optimistic path forward if the team chooses to use an inner lattice in the final model. This design does not include the important interface interactions necessary for the final design. Concept C does

incorporate the keep-put zone and is within the 48” circle described above in the specifications.

Concept D (Appendix B, Fig. 16) presents an SMSS that is made from hollow cylindrical members stemming from the support blocks. The shape of the beams allows each support to function similarly to I-beams while allowing for inner lattice structures to be created, potentially increasing the strength of each support. To further optimize the strength to weight ratio of the supports, the cross-section could be made oblate to increase the bending moment in a certain direction while decreasing the moment in another. The structure surrounding the keep-out zone is also constructed of hollow tubes.

The concepts above were compared using a Pugh Matrix. The factors selected to compare the concepts were manufacturability, weight, technology readiness level, and the projected area. The weight and projected area factors were used to analyze the concept’s ability to meet the requirements and specifications outlined by L3Harris, to understand if it would be a drain on resources to ensure that the concept could meet the required values. The manufacturability factor was used to understand if the model could be manufactured using additive manufacturing (3D Printing), which is a critical factor to consider as it is defined as the scope of the project in the problem statement. The technology readiness level factor is to understand the team’s current scope on the methods of manufacturing that would be used to develop the product, meaning if resources such as time would have to be spent on learning the method or technology needed to develop the product. The comparison of the concepts in the Pugh Matrix can be seen below in Table 2.

Concepts:	A	B	C	D
Manufacturability	0	+	+	+
Weight	0	-	+	-
Technology Readiness Level	0	+	0	-
Projected Area	0	-	-	-
Total	0	0	1	-2

Table 2: Pugh Matrix for concept selection and evaluation.

Concepts B and C tie in the Pugh Matrix (Table 2). Using the Pugh Matrix, the team decided to develop a model based on concept B, which used simple beam geometry. After developing a “shell” using beam geometry, the weight of the SMSS will be reduced by using an inner lattice within the beams, which will not only reduce the weight of the final design, but possibly increase ease of manufacturing and decrease time of manufacturing. The final design will encompass design elements from concept B and C, moving away from the difficulty manufacturing concept A presents due to the curvature of rods. This approach allowed the team to take advantage of the technology readiness level that comes from concept B, as the team is more familiar with beam geometry than latticing.

Latticing provides an opportunity to optimize an already strong design, as the team’s current understanding of the benefits of having an inner lattice is reduction of mass to meet the requirement of a product that is less than 18 lbm, and more significantly, allows for ease of manufacturability. The team used the Pugh Matrix results as a basis for the final design, which incorporates having a beam geometry foundation, and latticing to remove weight.

MODEL OPTIMIZATION

The team took two approaches to the design problem. The first, which was the approach that the previous design team had chosen, was topology optimization. The goal of this project is to design an SMSS that can be additively manufactured, but L3Harris turned to additive manufacturing to have a more time efficient and lower-cost satellite component manufacturing process. Additive manufacturing can be costly and less efficient if not approached correctly, such as having redundant material used in a component. Topology optimization removes redundant material from a component by considering the loads, conditions, and boundaries placed on a component. The previous year’s model focus of topology optimization was to maximize the stiffness of their model, and target material that lowered the stiffness of the model to meet the mass requirement and loading conditions.

Topology optimization was conducted using Solution 200 Topology Optimization in NX NASTRAN with the goal of minimizing compliance and reducing the total weight of the model. To make the analysis simple, the face of a non-optimized model was used to make a simple solid model of extruded meshes in the FEM. The mass limits of the Finite Element Model (FEM) were set to be between 5 and 18 lbm ;18 lbm being the maximum mass allowed and 5 lbm is slightly less than the mass of concept A. Manufacturing constraints were included to have result that is manufacturable when considering additive manufacturing. The manufacturing constraints included having a minimum member size of 0.75 inches, a maximum overhang of 30° degrees, and checkerboarding control to prevent misrepresentation of the optimal distribution of material. Steel was used as the material in the model since it has similar material properties to Invar-36. The final optimization solution was set for 500 iterations to observe convergence in design for both a laterally loaded case and a non-laterally loaded case for symmetry. For both cases, a model verification was done to check deflection, stress, and modes against the pre-optimize model (Appendix C, Fig.17 through 22). The verification showed expected differences between the reduced weight model and the original model considering the reduction of material. The results of the topology optimization solution are used to inspire a later design of the model to further reduce weight (Appendix C, Fig. 23).

MECHANICAL ANALYSIS

The second approach that was taken to the design problem was using last year’s design as a foundation for a new design. Concept A can be considered a semesters worth of classes when thinking about the design problem, and two lessons, in particular, were selected to focus on. The first was the benefit of using an interior lattice within the design. 3D printers use infill while printing an object, and these infills are how the printer will build up. These infills can be different designs depending on user preference. For example, using a triangle or a spiral design. An interior lattice, instead of using a traditional infill, would allow for less material to be used while additively manufacturing and retain the stiffness of the structure. The lattice that would work best for the SMSS is a QuadDiametal lattice, as it retains uniform stiffness in the XY, XZ, and YZ planes. The team decided to incorporate an interior lattice within the design due to the benefits of reducing material use and retaining stiffness. The second, and more important contribution from the previous year’s design, is the topology optimization that was conducted last year showed where redundant material would be on the SMSS with the requirements provided by L3Harris. The approach that was taken with these two lessons in mind started with a model which included interface mounting features where the SMSS would interact with other pieces of hardware within the satellite. These three different mounting interfaces were connected to a 4 lbm shade assembly 4 inches above the origin, a 6 lbm actuator assembly 2 inches above the origin, and the 11 lbm secondary mirror 1 inch below the origin. An additional miscellaneous 2 lbm was divided amongst these three mounting locations. The first iteration of this design considered and used concept B and C as inspiration. Then, using the previous year model, redundant material was cut from the design, resulting in the second iteration (Appendix C, Fig.24) From the second iteration, an interior lattice was incorporated into the design, where the interior of the second iteration was shelled out to reduce weight and replaced with an interior QuadDiametal lattice with an edge length of 0.5 inches and a rod diameter of 0.1 inches to retain stiffness (Appendix C, Fig. 25). These dimensions are changed in later models to try and optimize the weight of the structure. Holes were placed on the sides of the model to provide venting for the structure as it is launched into space where the internal pressure will continuously increase if not released. After running the finite element model (Appendix C, Fig.26), and simulations on this model, the largest displacement was 0.205 inches (Appendix C, Fig. 25), and the highest Von-Mises Stresses were located at sharp corners having a value of 27.54 ksi (Appendix C, Fig. 28). To reduce these high stresses, the model was updated to include edge blends and the sketch was fixed so that any sharp corners were filleted (Appendix C, Fig. 29). To assist with the analysis of the model, the venting holes were removed in the current model, but will likely need to be added in for future iterations.

The first step the team took in this project was comparing last year’s physical prototype to a Siemens NX simulation of concept A. This allowed for a stronger comprehension of the design problem and a understanding of where last year’s design was successful. The two tests conducted include a deflection and a free-free strike modal test to compare the physical prototype and the simulation. The deflection test, shown in Appendix A, Figures 4 and 6, used two different subcases to understand the physical models’ deflection. The two subcases used a 4.9 N lbf weight, but differed in where the weight was placed on the model. The physical model was simply supported on three gauge pins, respective to the three arms of the prototype. A dial indicator was used to measure the deflection of the model. The first subcase resulted in a 0.016 inch deflection and the second subcase responded to a 0.018 inch deflection. In the corresponding simulations that were conducted to reflect the deflection physical test, (Appendix A, Fig. 5 and 7), the simulated first subcase had a deflection of 0.016 inches and the second subcase, 0.016 inches. The percent error for the first subcase was 1.85% and the second subcase was 8.57%, showing a positive relationship between the physical and simulated results for the deflection tests of last year’s prototype, meaning there is not a significant error present in the prototype or simulation. The results of the deflection test are presented below in Table 3.

Subcase	Deflection Test (inches)	Simulated Deflection (inches)	Percent Error
1	0.016	0.016	1.85%
2	0.018	0.016	8.57%

Table 3: Comparison of physical deflection test on Concept A and NX simulated deflection.

The vibrational test was conducted using a free-free strike modal test. The set-up for the test is shown in Appendix A, Figure 10. The physical prototype was suspended from the ceiling using bungee cords to reflect a free-free modal analysis, as requested by the L3Harris customer. Accelerometers were placed on the arms of the prototype to reflect the coordinate system of the test to the coordinate system that would be used in the following NX simulation (Appendix A, Fig. 11). The free-free strike modal test resulted in a natural frequency of 62.83 Hz (Appendix A, Fig. 12). The simulated free-free modal analysis on NX resulted in a natural frequency of 63.48 Hz (Appendix A, Fig. 13), delivering a percent error of 1.02%, again showing signs of a critical error being absent from the physical and simulated model. By conducting these analyses on the previous year’s final prototype, the team was able to have a solid understanding of the prototype, and validate there were no significant errors that would not allow

the work from last year to be built upon. The results from the strike modal test are shown below in Table 4.

Free-free Modal analysis (Hz)	Simulated Natural Frequency (Hz)	Percent Error
62.83	63.48	1.02%

Table 4: Results of physical and simulated strike modal test.

When the structure is being post-processed in the FEM, the lattices appear as 1D mesh beam collectors. The rest of the model was made to be a 3D TETRA10 Solid Mesh. The shade assembly, actuator assembly, and secondary mirror were all modeled as 0D concentrated masses that were connected using RBE3s to avoid adding additional stiffness to the SMSS. The lattices were originally connected to the inside faces of the structure using 1D Mesh-to-Face CBEAM connections. The process for this was tedious, however, it was necessary to ensure every lattice mesh and all inside faces were selected individually. On top of this, the simulation ran for over thirty minutes. This demonstrates one roadblock the team faced of having long wait time before trying to fix an issue in the FEM, and running a new simulation. Another issue was the internal lattice was oriented in the same direction when they should have been oriented differently depending on where it is located in the structure. In simulations run on previous models, an 18g gravity load was applied in the negative Z-direction and there was a subcase for a 12g gravity load at every 15-degree angle laterally. Different subcases for the temperature difference of 5°C to 35°C were also included within the simulation. Each face of SMSS legs' ends of the model had a fixed constraint. To be concise, in the models mentioned here, the fixed constraints and 18g gravity load remain constant, but there is no longer any temperature subcases. The worst case of 12g lateral gravity load was applied in the negative Y-direction, along the axis of one of the legs. The next step was to take advantage of the symmetry in the model by dividing the SMSS to get a piece that was 1/6 of the full structure. This piece would be mirrored and rotated symmetrically in order to complete the full structure. Having this feature solves the lattice orientation issue. The shell of the SMSS was removed from the part, and was added in the FEM as a 2D thin shell mesh rather than the 3D solid mesh. The problem that had arose with this model is the beams used to mount the actuator assembly are not symmetric to any other part, and would therefore need to be added on once the symmetry was completed (Appendix D, Fig. 30). These beams needed to be modeled as 1D beam elements, but it was difficult to combine 1D and 2D meshes. Without attaching these beams to the structure, the simulation ran relatively fast and showed results. The problem at this stage was the lattices that were oriented in different directions did not connect to each other properly when they came to the point of contact (Appendix D, Fig. 34). This induced high stress in the

structure at these very locations (Appendix D, Fig. 31 & 32). A free-free modal analysis simulation was conducted and showed a frequency of 259.49 Hz (Appendix D, Fig. 33). With this in mind, the sponsor of this project wanted to verify that the lattice had structural integrity, and that the shell was not taking on the majority of the loads and stresses (Appendix D, Fig. 35). As shown in Appendix D, Figure 36, the stress of the model is drastically increased without an internal lattice. From here, two approaches were taken in the advancement of this model. The first approach was to use the original method of connecting each lattice mesh to every inside face individually, even if it meant sacrificing more time. Some issues arose when redoing this model, and to verify that the method was still valid, a piece of one of the legs was created as a separate part. Using the method listed above, this model was able to run without any complications (Appendix D, Fig. 37 & 38). With the time it took to set up the FEM, it felt like the first method was unfortunately reaching a dead end.

The second approach is ultimately the approach that was used moving forward. In this approach, the model was split into different bodies to input a lattice with different orientations in the varying sections of the structure (Appendix D, Fig. 39, 42, & 44). For this method, the lattice meshes were still connecting to the 2D mesh faces using 1D Mesh-to-Face connections, but rather used RBE3 connections over CBEAMs. Looking back on the project from last year, RBE2 connections were used, which is a poor assumption because RBE2 connections will make the structure infinitely stiff (Appendix D, Fig. 47). The material used for this project was Invar-36 due to its low coefficient of thermal expansion. Slowly but surely, more lattices were added to the structure using the split bodies method, and many simulations were run to verify that the simulation would work (Appendix D, Figs 40 & 41). The 2D thin shell, mesh was first put on the entire model with a thickness of 0.1 inch. From there, different shell thicknesses were tried, and it was found that the model would displace more with a thicker shell, which is a counter-intuitive result. It was found that since RBE3 connections do not add any stiffness at all, it would be necessary to use either CBEAM or RBE2 connections. Since RBE2s add infinite stiffness, it would be possible to use them if the mesh they are connected to is extremely fine. A section in the middle of the model was split from the rest of the structure, as this is where higher stresses will occur. The end goal for that section was to make it completely solid using a 3D Tet mesh, and connecting the 2D and 3D meshes in the model together. In the current model shown in Appendix D, Figure 48, the entire model has a 2D mesh, but the center section has a 0.5 inch thickness while the rest of the structure only has a 0.1 inch thickness (Appendix D, Figs. 56 through 59). Moving forward, the next steps are to include the solid mesh and to continue to add lattices until the model is completely filled out. Since the stresses of the current model are very low

compared to the yield stress of the material, the lattice rod diameter and shell thicknesses were able to be reduced to meet the specification of the SMSS being under 18 lbm, leading to a final mass of 14.58 lbm. The subcases were re-run to find the stress and displacement at the given temperatures, and every gravity load angle. Many iterations of simulations were run, and the results are shown in Appendix D, Figures 43, 45, 46, & 49 through 54.

A fastener calculation was used to determine the torque required for the secondary mirror and the SMSS fastened connection. The bolt used for the calculation is a grade 8 ¼-20 with a non-plated black finish bolt condition. The tensile stress area for a ¼-20 bolt is .0318 ksi and the nominal diameter, d , is 0.25 inches [1]. The proof strength for an SAE grade 8 bolt is 120 ksi [2]. Using equation 1,

$$F_p = A_t \cdot S_p \quad (1)$$

F_p is the force on the bolt under proof strength, which is equivalent to 3816 lbf. Assuming this connection is permanent, equation 2 is used to calculate the preload for a permanent connection.

$$F_i = 0.90 \cdot F_p \quad (2)$$

The bolt condition is 0.3 ksi and is used in equation 3 [3].

$$T = K \cdot d \cdot F_i \quad (3)$$

where K is the friction factor, d is the bolt diameter, and F_i is the bolt condition. This equation calculates the torque necessary for one of the permanent fasteners that connects the SMSS to the mirror. The torque specification is 214.65 lbf-in.

A tolerance issue the team faced was the specification of the outer diameter of the SMSS being 48 inches. The SMSS would have to fall within a diameter of $48 \pm .005$ inches from the center point of the SMSS to meet this specification. This 48 inch diameter specification is important for the interaction of the SMSS to other critical components of the satellite. This specification was addressed during the initial conceptual design of the SMSS design, by sketching a 48 inch circle in Siemens NX and keeping the design within the circle (Appendix F, Fig. 70). The specification was validated by measuring the difference between the circle and plane where the SMSS would interact, which resulted in a length of $0 \pm .005$ inches, providing the necessary tolerance for the goal of the sponsor.

The optimal material for the SMSS would be Invar-36. Invar-36 was recommended by the L3Harris sponsor, due to its low coefficient of thermal expansion. Even though the SMSS would be in a controlled climate within the satellite while it is in

space, the sponsor is concerned with thermal expansion during launch. The climate considered for the launch thermal expansion is a typical Florida day, which would be 5°C to 35° temperature range. A low coefficient of thermal expansion can ease concerns over significant thermal expansion of the SMSS during launch. The average thermal coefficient of expansion for Invar-36 is $1.93 \mu\text{m}/\text{m}^\circ\text{C}$. This is the material that was used in the simulations conducted for this project. For manufacturing, ABS was used, as Invar-36 is a costly material and the use of it in manufacturing would place the team over the allotted budget. The team was not able to 3D-print using a metal material as originally expected due to unforeseen circumstances, so prints for this project were composed using ABS. This will be further explained in the manufacturing section below.

Due to the static nature of the SMSS, much of the fatigue analysis on the system is concerned with thermal fluctuations of the Invar-36, and the rest of the concern was given to bending of the structure due to the loads on both the shell and the internal lattice structure. By performing thermal analysis on the structure, the maximum stress due to thermal loading is found to be 1699.96 psi. This is low enough that the structure should not fail due to thermal fatigue after a high number of cycles. To be able to assess the mechanical fatigue, assumptions have to be made about the structure. One assumption is that Invar-36 has very similar properties to steel, so that all properties besides thermal could be accurately estimated with steel. The surface factor of a 3D printed part can be variable and unknown until the part is finished, so an assumption can be made that it will be machined or cold-drawn quality, with the surface condition modification factor coming to a value of 0.86. Since the ends of the arms of the SMSS have a rectangular cross-section, we can also calculate an estimate of the size factor, with it being 0.858. With an ultimate strength of 72.5 ksi, the rotary-beam test specimen endurance limit was found to be 36.25 ksi. Since the SMSS requires high reliability, it can be assumed that a reliability percent of 99% is sufficient, leaving the reliability factor as 0.814. Multiplying these factors together achieves an endurance limit of 21.82 ksi. These results are displayed in Appendix F, Figure 77.

MANUFACTURING

The main goal of this project is to additively manufacture a Secondary Mirror Support Structure. Every decision made during this project involved a consideration of how the decision could affect the additive manufacturing process of the SMSS. For example, the decision to have the top of the SMSS lie on a single plane was so a 3D printer could build off the print bed easily. A true additively manufactured SMSS would be 3D printed using metal, specifically Invar-36, as the chosen material. Invar-36 has a very low coefficient of thermal expansion (CTE)

of $1.93\mu\text{m}/\text{m}^\circ\text{C}$, which is favorable as it will avoid significant expansion and contraction of the SMSS in launch weather (Florida) and in space. The cost of 3D printing using Invar-36 is vastly outside the budget, making it impossible to print a full-scale SMSS at this time. The material that was chosen for the additive manufacturing of this project's final SMSS is 17-4PH Stainless-Steel, due to its' low cost and lower CTE value of $10.8\mu\text{m}/\text{m}^\circ\text{C}$. A full-scale model would not be able to be printed, however, due to the limitations of the metal 3D printers the team has access to and the still significant cost of printing a whole SMSS using 17-4PH Stainless-Steel. The cost of a full-scale SMSS using 17-4PH Stainless-Steel would be thousands of dollars over budget. The group had initially decided to print a 50% scaled model of a single arm on the SMSS, which would allow the team to show that the SMSS could be additively manufactured using metal as a material. However, this plan unfortunately fell through, and the team was not able to 3D print a metal structure. The group approached this roadblock with two different ideas. The first was going to a third party as the design team from the year 2022 had and 3D print a 60% scaled model solid infill of the SMSS. The cost of printing the SMSS with the interior lattice as designed through the third party would fall outside of the team's budget, which made an interior lattice within the SMSS through the third party an impossibility. Another benefit of 3D printing a 60% scaled solid infill model of the SMSS was time. With the remaining time, working with a third party for the 60% scaled solid infill model of the SMSS would provide time to compare the printed model to a simulated model using the experimental results of a strike modal test.

To manufacture the 60% SMSS model, several third parties were considered by the team. Ultimately, Xometry was chosen, due to its ability to give the team instant quotes for models, the capability to 3D print with metal materials, and the relatively low fabrication and delivery times compared to other companies. For a 60% solid infill model (Appendix E, Fig. 63), the price to print and ship the model was quoted to be \$523.36 dollars with standard shipping and tax exemption. With standard shipping, however, the model would arrive the day before the Final Design Review due date and would not give us enough time to conduct thorough tests on it. We instead opted for expedited shipping, and we were unable to get tax exemption on time, so the final price for the model came to be \$601.58 dollars. With faster shipping, the new model arrived on Monday April 17th and we were able to conduct tests on the model the next day. The team also considered creating a dog bone model out of 3D printed steel to be able to study the differences between traditionally manufactured metal and 3D printed metal structures. Due to the quoted price of a steel dog bone being \$433.68 dollars though, it did not fit within the team's budget and would not be worth the price.

The second idea would allow the team to showcase the lattice infill of the SMSS model, which is a significant design feature that would be missing from the third-party 60% scaled solid infill model. As part of the earlier stages of the project, to verify that the lattice would be able to 3D printed, an open shelled lattice cube was created using NX and printed in-house (Appendix E, Fig. 60 & 61). This idea revolved around using the printers located on the University of Rochester campus and breaking the SMSS model apart into pieces that could fit on the print beds of the 3D printers on campus. The pieces would then be glued together after they were printed, to display what the interior lattice design would physically look like. The "puzzle piece" model will allow the group to display the ability of the whole SMSS to be additively manufactured. Two significant considerations for the puzzle piece model were the timing it would take to 3D print each piece and the cost of the filament used to construct each piece. Due to the time it would take to print the full model and the amount of filament that would be used to print the full model, the team decided to print a single arm scaled to the original model size. The arm would not be printed with the full lattice, instead having a 3 inch portion with the lattice (Appendix E, Fig. 63). This decision was made to reduce the complexity and time of the printing as the lattice increases the time to print significantly using the current printers on the University of Rochester campus. The time it took to print the arm was 30 hours and 5 minutes. The total filament used for the puzzle piece model was 31.5 in^3 , and the cost of a cubic inch of filament is \$2.50 dollars, generating the full cost of the puzzle piece model to be \$78.85 dollars.

The final piece that was manufactured for this project was a test coupon (Appendix E, Fig. 64) which would allow the group to analyze the stiffness of lattices used within the SMSS using an MTS (MTS Criterion Model 43). The original concept for the test coupon had a selected material of 17-4PH Stainless-Steel as it is a low-cost material to use. Due to the complications, the test coupons were instead printed at the University of Rochester using ABS plastic as the material. The test coupons had a print time of 5 hours and 20 minutes and cost \$10.27 dollars to manufacture.

The total cost of the pieces manufactured for this project are displayed below in Table 6, which is \$690.70 dollars. The team's hours spent manufacturing the 60% scaled solid infill model, test coupon, and puzzle piece arm were 25 hours in total, resulting in a total cost of \$2,500 dollars, which is represented in Table 5. The final cost of this project considering the cost to print the models and teams' hours spent is \$3,190.70 dollars. It is difficult to estimate the cost of a full-scale SMSS model using Invar-36 as the selected material. Sigma Aldrich [4] has a supplier who sells 500 grams of powder Invar-36 at the cost of \$1,450.00 dollars. The amount of Invar-36 needed to manufacture the

SMSS using 3D printing depends on the printer and its capabilities. It is unknown currently the amount of Invar-36 that would be necessary to print a full-size SMSS and the operating costs of using a 3D printer. If it was requested that 1,000 SMSS be manufactured, considerations that would be made is the amount of material used to manufacture a SMSS. The SMSS would need to be fully optimized to use the least amount of material as possible. More material in a SMSS means a higher cost to print and a longer manufacturing time. It may be a worthwhile investment if printing 1,000 SMSS to have an army of 3D printers to simultaneously print the SMSS. It would be impossible to print a 1,000 SMSS with only a few printers in a reasonable amount of time.

Team Member	Hours	Cost
Melanie Earle	5	\$500
Charles Fleischmann	5	\$500
Gabriella Gima	5	\$500
Stelios Halioris	5	\$500
Christopher Piatek	5	\$500
Total	25	\$2,500

Table 5: Cost of team’s hours spent on manufacturing.

	Cost
60% Scaled Solid Infill Model	\$601.58
Puzzle Piece Arm	\$78.85
Test Coupons	\$10.27
Team Manufacturing Time	\$2,500.00
Total Cost	\$3,190.70

Table 6: Final cost of project.

TEST PLAN AND RESULTS

	Specification	Verification	Passed or Failed Verification?
1	The outer diameter of the SMSS must be 48 ± 0.005 ".	A circle with a diameter of 48" can be made around the model to confirm that it fits within the bounds.	Pass
2	The SMSS will interface with the Forward Metering Structure at three locations 120 degrees apart.	A Faro Arm or protractor can be used to measure the angles.	Pass

3	The first mode of the SMSS shall be 120 Hz or greater when grounded at the FMS interface and supporting all hosted hardware.	A hammer test can be performed to find the first mode. The results will be compared with simulated vibrational modes computed with NX Solution	Pass
4	The goal mass is a maximum of 18 lbm.	The model can be inspected in NX to find its mass.	Pass
5	The SMSS shall have positive margins of safety against yield and ultimate failure when exposed to a quasi-static load of 12G laterally and 18G axially simultaneously, (lateral swept 15 deg increments) combined with a 5C to 35C temperature range (nominal room temp is 20C) while supporting all hosted hardware.	The ultimate yield and failure can be found through Nastran analysis.	Pass
6	The SMSS and hosted hardware shall not obstruct more than 14% of the Primary Mirror (PM) clear aperture area (assume 1.1m diameter clear aperture).	Using NX, the area of the mirror that is covered can be calculated.	Pass
7	The SMSS should provide a stable mounting platform for the Secondary Mirror in thermal environments. The average motion of the SM interfaces under a 1 degree C isothermal load should be 0.66 micro-inches translation (RSS of X and Y) or less and 0.037 micro-radians	Thermal simulation can be used to estimate the movement of the structure in low temperature environments.	Fail

rotation (RSS of Rx and Ry) or less.		
--------------------------------------	--	--

Table 7: Specifications of project and evaluation/validation of specifications.

Specification 2 was verified with use of the Faro Arm. Three points of the 60% Solid Infill SMSS model’s arm were selected as the area of interest, as depicted. The angles between the points of interest were measured using the Faro Arm, resulting in an angle of 119.53 ° (Appendix F, Fig. 71&72). The resulting percent difference between 119.53° and 120° degrees is 0.39%. Even though the 60% Solid Infill SMSS model is not full scale, the angle between the 3 arms would not change as a reduction in size would still retain the geometry of the SMSS. This allows the 60% Solid Infill SMSS model to be used for validation. The Faro Arm angle measurements verify that the SMSS passes specification 2.

A deflection test was performed on the 60% Solid Infill SMSS model to compare it to a simulation using the same subcases in NX to compare the physical model and the simulated model (Appendix F, Fig.65 &66). The results of the deflection test are presented in Table 8, where the percent error is 0.9%.

Deflection Test (inches)	Simulated Deflection (inches)	Percent Error
1.1E-03	1.11E-03	0.90%

Table 8: Physical and NX Simulated Deflection of 60% Solid Infill SMSS model.

A free-free modal strike test was carried out on the 60% Solid Infill SMSS model, resulting in a natural frequency of 168.75 Hz (Appendix F, Fig.68). This test was performed in the same manner as described in Mechanical Analysis as it was done on the SMSS from last year’s group (Appendix F, Fig. 67). The simulated free-free modal in NX resulted in a natural frequency of 176.29 Hz, which resulted in a percent error of 4.27% (Appendix F, Fig. 69). The results of the deflection test and validates the physical 60% Solid Infill SMSS model and simulation, allowing us to conclude that there is not a significant error present in the prototype or simulation. Since there is no significant error present, we assume that the simulation of full-scale SMSS with the lattice will have values that are approximately close to the true values, allowing us to validate the required specifications through NX simulations.

Specifications 1,3, 4,5,6, and 7 were verified using Siemens NX. Specifications 1 and 6 were verified using dimensional analysis in NX Siemens. Specification 1 was analyzed by encompassing the SMSS with a 48" diameter circle and the length was measured between the circle’s edge and the face of the SMSS interacting with the circle (Appendix F, Fig. 70). The resulting length was 0.0 inches, verifying that specification was met.

Specification 3 was validated through an NX simulation of the vibrational modes. The natural frequency of the SMSS (Appendix F, Fig.74), is 157.23 Hz, which passes specification 3. Specification 4 was verified using NX’s solid properties check. The SMSS model’s selected material in NX was Invar-36. With the SMSS’s lattice, the SMSS had a mass of 14.58 lbm, which passes specification 4 (Appendix F, Fig. 78). Specification 5 is verified by taking the highest Von-Mises Stress from the structure and comparing it against the yield stress and ultimate stress of Invar-36 as shown in Table 9 below. The equation for margin of safety is shown in equation 4 below,

$$MS = \frac{\sigma_{max}}{\sigma_{VM}} - 1 \quad (4)$$

Where MS is the margin of safety, σ_{max} is the ultimate or yield stress, and σ_{VM} is the von-mises stress. The margin of safety for yield stress and ultimate stress are positive values of 1.24 and 2.90, respectively. The equation for factor of safety is shown in equation 5 below.

$$FS = \frac{\sigma_{max}}{\sigma_{VM}} \quad (5)$$

Here, FS is the factor of safety and the values for yield and ultimate Stresses are 2.24 ksi and 3.9 ksi, respectively. These results pass specification 5.

Stress	Stress Value (ksi)	Von-Mises Stress (ksi)	Margin of Safety (ksi)	Factor of Safety
Yield Stress	33.3	14.86	1.24	2.24
Ultimate Stress	58	14.8	2.90	3.9

Table 9: Stresses present in NX simulation of SMSS using conditions specified in requirements.

Specification 6 was verified by using NX to measure the projected area of the bottom surface of the SMSS and dividing it over the project area of the satellite’s secondary mirror (Appendix F, Fig. 73). The obstruction resulting from the SMSS is 10.93%, which verifies specification 6 being met.

Specification 7 was tested by comparing subcases with different temperature loads in Siemens NX simulations. Each subcase was compared with another that had identical gravity loads but had a 1 °C difference in temperature loads. A subcase with no gravity loads was also created with a temperature load of 21 °C. The maximum displacement in this subcase was determined to be 13.81 micro-inches, higher than the maximum allowed translation in the specification (Appendix F, Fig. 77). When comparing the two subcases, the greatest change in displacement was found with an axial gravitational force at 90° from the x-axis and the difference between maximum displacements was found to be 8 micro-inches.

To understand how the lattice affects the stiffness of the SMSS, a test coupon was created that mimicked the arm of the SMSS (Appendix F, Fig. 64). Two test coupons were printed, one with the lattice present in the SMSS, which is the interior QuadDiametal lattice with an edge length of 0.5 inches and a rod diameter of 0.1 inches, and one that is hollow without the lattice present. Both test coupons were analyzed using a MTS (Material Test System) machine. The MTS increases the load that is placed on to the test coupon using a weight, and the force and extension of the length of the test coupon is measured. The stiffness of the test coupon is calculated using the equation 6,

$$k = \frac{F}{\delta} \quad (6)$$

Where k is stiffness, δ is displacement, and F is force. The resulting stiffness of the test coupon with a lattice and the hollow test coupon are respectively $1.05E+04 \frac{lb}{in}$ and $8.02E+3 \frac{lb}{in}$. The percentage difference between the lattice and hollow test coupon is 26.67%, meaning the lattice provided 26.67% more stiffness than the hollow test coupon. A simulation was conducted to mimic the results of the MTS machine to find if there were any major errors. The percentage error for the hollow test coupon is 11% and for the lattice test coupon it is 6.8%. Cracking was heard from the hollow test coupon, so a deformation from the force applied to the hollow test coupon can explain the percent error. When the mass of each test coupon was divided over the stiffness of the coupon, it was found there is a 1.87% difference between the test coupons (Appendix F, Figs. 75,76, &80). There is more stiffness while using the lattice within the test coupon, but while comparing it to the mass used with the addition of the lattice, there is still a benefit to using the lattice within the arm. The test coupon stiffness analysis allows us to assume that the lattice will provide maximum stiffness, meaning it is worthwhile and valuable to have there be a form of infill within the SMSS.

INTELLECTUAL PROPERTY

The team's Secondary Mirror Support Structure is patentable due to originality. This is the conclusion last year's group made due to the topology optimization process NX uses. NX's topology process creates a unique computation dependent on customizable factors. The team from last year concluded that due to the process of NX to reduce material to make a unique geometry with the addition of lattices makes the SMSS novel. Designs for other Secondary Mirror Support Structures from the companies Lockheed Martin Company and Boeing Company are covered under patents of satellite components owned by the respective companies. These patents (Appendix G, Fig. 81 & 82) use rods as a critical element in the design of their Secondary Mirror Support Structure, which differs from the approach taken by the

team from this year and the past year, where a cantilever beam was the critical component in the design. Instead of using rods to connect the SMSS to other hardware or to the satellite itself, the legs of the SMSS act as a cantilever beam. This difference makes the design of the SMSS, combined with the unique geometry resulting from the NX topology optimization software, patentable due to originality.

SOCIETAL AND ENVIRONMENTAL IMPLICATIONS

In March, Relativity Space launched one of the first rockets to be mostly manufactured through the use of 3D printing [5]. While the rocket, named Terran 1, failed to reach orbit, there was 85% 3D printed mass. After the orbit failure, Relativity Space switched gears on the 3D printed rocket concept, as they plan to create a rocket that can be reused named the Terran R. The Terran R will still incorporate 3D printed mass. Relativity Space is not the only company within the aerospace market incorporating additive manufacturing into its products. A review of metal additive manufacturing written in 2021 estimated that due to the increase of additive manufacturing within the aerospace industry, the market will increase to \$3.187 billion by 2025 [6]. The societal implications of the increase of additive manufacturing becoming commonplace within the market can be seen through the record-breaking year of 2022 for space launches. There were 180 successful rocket launches in 2022, beating out 2021 by 44 more launches [7]. More and more launches are taking place each year, and additive manufacturing can increase the number of launches by providing less time and cost for parts to be manufactured. One concern that arises from more launches, rockets, and satellites is the number of satellites in space. In 2022, it was recorded that there are 5,465 active satellites in space, which does not include the estimated 36,500 pieces of debris orbiting Earth [8] [9]. The question that has arisen for those in the space industry is what a safe number of satellites is to have in orbit, which is a question that does not currently have an answer. This question has implications for telecommunications, the internet, imaging, and other services offered through the use of satellites. While additive manufacturing can offer a shorter timeline for satellite manufacturing, a question that should be considered is how many satellites should be launched.

The impact of additive manufacturing on the environment should also be considered. A report written in 2020 [10] sponsored by the Additive Manufacturer Green Trade Association (AMGTA) found that additive manufacturing had a larger carbon footprint ten times larger than traditional manufacturing and processing energy was also higher than traditional machining. To confront the issue of additive manufacturing having a larger carbon footprint, a more critical view should be taken on how much material is necessary for a

component to be 3D printed. Topology optimization reduces unnecessary material, making it a valuable solution when considering the carbon footprint of additive manufacturing. To minimize the processing energy, the material itself should be considered. Materials with lower melting points, thermal conductivity, and reflectance allow for less energy to be used in the additive manufacturing process. For example, titanium requires higher processing energy, so while titanium could be useful, environmentally, it can be harmful. When using additive manufacturing methods such as 3D printing, the amount of material used should be considered as more material in a product means a higher carbon footprint and more processing energy, which are both harmful for the environment. Materials with lower melting points, thermal conductivity, and reflectance will lower processing energy, so these materials should be looked at first when considering additive manufacturing. A topology optimization analysis should also be run on a product being 3D printed to reduce insignificant material.

RECOMMENDATIONS FOR FUTURE WORK

Further simulations should be run to understand how the SMSS is thermally expanding under the current simulation conditions, and what could be done to improve the SMSS considering specification 7 (Table 7), as specification 7 is not passed. A goal to understand specification 7 further would be to run a physical experiment to see how a metal SMSS would react when undergoing thermal expansion and contraction in an oven test where a range of temperatures are selected to cycle through. An oven test could provide the opportunity to understand what stress occurs due to thermal expansion and contraction. For the oven test to be conducted, a 3D metal printed scaled model of the SMSS would have to be manufactured. A strong recommendation for further work on this project would be to manufacture a scaled model of the SMSS with a metal as the selected material. It may not be possible to use Invar-36 as the chosen material for a scaled model of the SMSS, but it would be beneficial to find an accurate cost of a full-scaled SMSS model manufactured using 3D printing with Invar-36 as the selected material.

One area for future work is a continued effort to research and develop the lattice, with the intention of creating a test coupon manufactured with metal as the material. The metal test coupon would allow for further understanding of how the lattice can improve the stiffness of the SMSS, and a comprehension of if the added mass from the lattice to the SMSS is a worthwhile investment. In terms of the SMSS itself, the creation of venting holes would need to be added to the SMSS, so there are no trapped cavities on the model, which would allow us to fulfill all the requirements provided by L3Harris. A convergent study should be considered to find the optimal element mesh size for the FEA, which will help with 1D mesh-to-face RBE2 connections. Finally, future work should take advantage of the

symmetry of the model, so that when there is a finer element mesh size, the simulations will have a faster run-time.

Based on the hundreds of cycles run for topology and the optimum design being found towards the end of the runs, more cycles may be run to find a further optimized design from topology. It would be recommended that the topology should be run for at least 1000 cycles to allow an analysis of a properly converged model. The constraints used within topology use estimated best values in terms of the minimum size of members and overhang angles which could be toggled and optimized individually to obtain more optimal sizing.

ACKNOWLEDGMENTS

The L3Harris team would like to show our gratitude and give thanks to the sponsor of this project, Patrick Ellsworth, Chris Pratt, Mike Pomerantz, Jim Alkins, Bill Mildenberger, Paul Osborne, Alex Prideaux, Lyrica Yanaway, along with a special thanks to Professor Muir for his continued help throughout the duration of the project.

REFERENCES

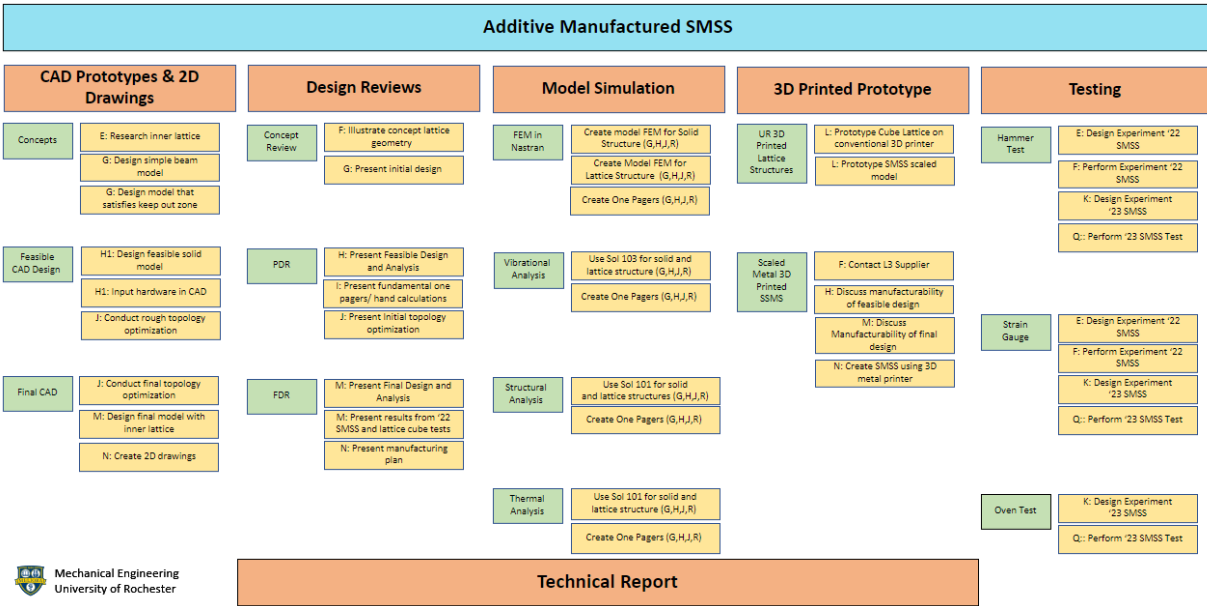
- [1] Budynas, R., Nisbett, J. and Shigley., 2011. Shigley's mechanical engineering design. 9th ed. New York: McGraw-Hill, p.413.
- [2] Budynas, R., Nisbett, J. and Shigley., 2011. Shigley's mechanical engineering design. 9th ed. New York: McGraw-Hill, p.433.
- [3] Budynas, R., Nisbett, J. and Shigley., 2011. Shigley's mechanical engineering design. 9th ed. New York: McGraw-Hill, p.439.
- [4] "Invar 36 Alloy Powder | Sigma-Aldrich." *Invar 36 Alloy Powder* | Sigma-Aldrich, www.sigmaaldrich.com/US/en/search/invar-36-alloy-powder?focus=products&page=1&perpage=30&sort=relevance&term=invar%2036%20alloy%20powder&type=product_name.
- [5] @SPACEDotcom. "Relativity Space Launches World's First 3D-printed Rocket on Historic Test Flight, but Fails to Reach Orbit." *Space.com*, 23 Mar. 2023, www.space.com/relativity-space-terran-1-test-launch-failure.
- [6] Blakey-Milner, Byron, et al. "Metal Additive Manufacturing in Aerospace: A Review." *Materials & Design*, vol. 209, Elsevier BV, Nov. 2021, p. 110008. *Crossref*, <https://doi.org/10.1016/j.matdes.2021.110008>.
- [7] "2022 Was a Record Year for Space Launches." *2022 Was a Record Year for Space Launches*, 11 Jan. 2023, www.nature.com/articles/d41586-023-00048-7.
- [8] @SPACEDotcom. "How Many Satellites Can We Safely Fit in Earth Orbit?" *Space.com*, 27 Feb. 2023, www.space.com/how-many-satellites-fit-safely-earth-orbit.

[9] “How Many Satellites Are in Space? - NanoAvionics.” *NanoAvionics*, 20 Dec. 2022, nanoavionics.com/blog/how-many-satellites-are-in-space.

[10] Van Sice, Corrie, and Jeremy Faludi. “COMPARING ENVIRONMENTAL IMPACTS OF METAL ADDITIVE MANUFACTURING TO CONVENTIONAL MANUFACTURING.” *Proceedings of the Design Society*,

vol.1, Cambridge UP (CUP), July 2021, pp. 671–80. *Crossref*, <https://doi.org/10.1017/pds.2021.67>.

Appendix A: WBS and CPM



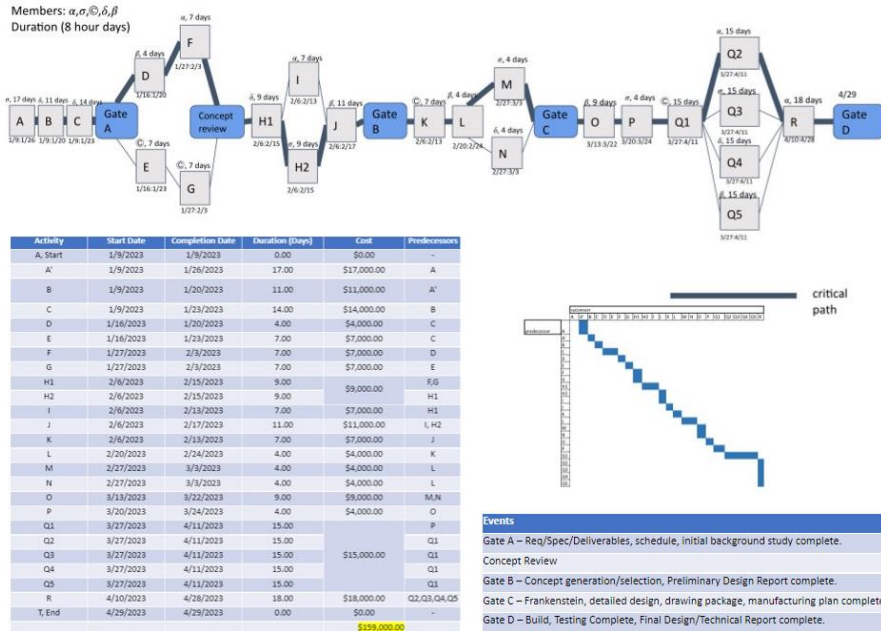
Mechanical Engineering
University of Rochester

Figure 1: Work Breakdown Structure (WBS).

Melanie Earle, Charles Fleischmann, Gabriella Gima, Stelios Halioris, Christopher Piatek L3Harris Project Gate A- CPM 2-1-23

Members: $\alpha, \sigma, \rho, \delta, \beta$
Duration (8 hour days)

Activity	Start Date	Completion Date	Duration (days)	Cost	Predecessors
A, Start	1/9/2023	1/9/2023	0.00	\$0.00	-
A'	1/9/2023	1/26/2023	17.00	\$17,000.00	A
B	1/9/2023	1/20/2023	11.00	\$11,000.00	A'
C	1/9/2023	1/23/2023	14.00	\$14,000.00	B
D	1/16/2023	1/20/2023	4.00	\$4,000.00	C
E	1/16/2023	1/23/2023	7.00	\$7,000.00	C
F	1/27/2023	2/3/2023	7.00	\$7,000.00	D
G	1/27/2023	2/3/2023	7.00	\$7,000.00	E
H1	2/6/2023	2/15/2023	9.00	\$9,000.00	F,G
H2	2/6/2023	2/15/2023	9.00	\$9,000.00	F,G
I	2/6/2023	2/13/2023	7.00	\$7,000.00	H1, H2
J	2/6/2023	2/17/2023	11.00	\$11,000.00	L, H2
K	2/6/2023	2/13/2023	7.00	\$7,000.00	J
L	2/20/2023	2/24/2023	4.00	\$4,000.00	K
M	2/27/2023	3/3/2023	4.00	\$4,000.00	L
N	2/27/2023	3/3/2023	4.00	\$4,000.00	L
O	3/13/2023	3/22/2023	9.00	\$9,000.00	M,N
P	3/20/2023	3/24/2023	4.00	\$4,000.00	O
Q1	3/27/2023	4/11/2023	15.00	\$15,000.00	P
Q2	3/27/2023	4/11/2023	15.00	\$15,000.00	P
Q3	3/27/2023	4/11/2023	15.00	\$15,000.00	Q1
Q4	3/27/2023	4/11/2023	15.00	\$15,000.00	Q1
Q5	3/27/2023	4/11/2023	15.00	\$15,000.00	Q1
R	4/10/2023	4/28/2023	18.00	\$18,000.00	Q2,Q3,Q4,Q5
T, End	4/29/2023	4/29/2023	0.00	\$0.00	-
\$159,000.00					



Events

- Gate A – Req/Spec/Deliverables, schedule, initial background study complete.
- Concept Review
- Gate B – Concept generation/selection, Preliminary Design Report complete.
- Gate C – Frankenstein, detailed design, drawing package, manufacturing plan complete.
- Gate D – Build, Testing Complete, Final Design/Technical Report complete.

Mechanical Engineering
University of Rochester

Figure 2: Figure 2: Critical Path Method (CPM).

Appendix B: Concepts

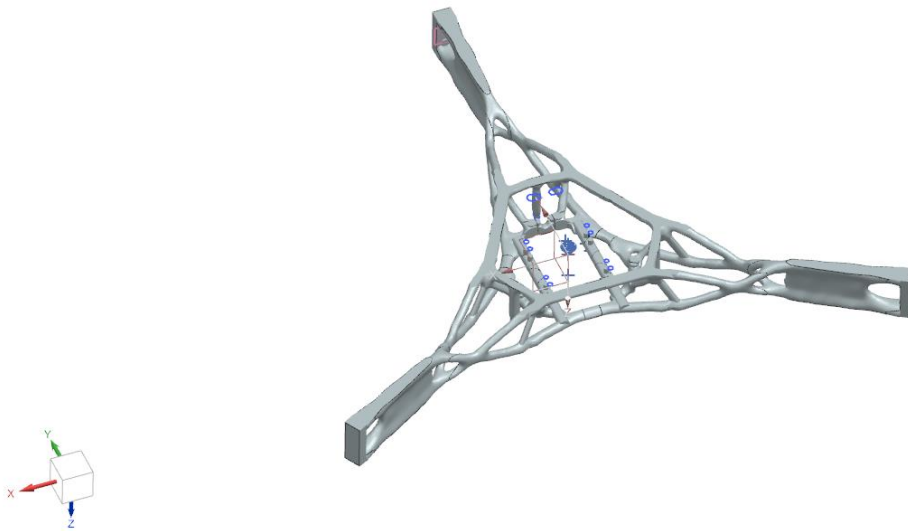


Figure 3: Concept A

60 % Scaled SMSS Subcase 1 Deflection Test L3Harris SSMS: Charles Fleischmann

Results

Subcase 1: 0.0162" deflection



4.9N lbf load

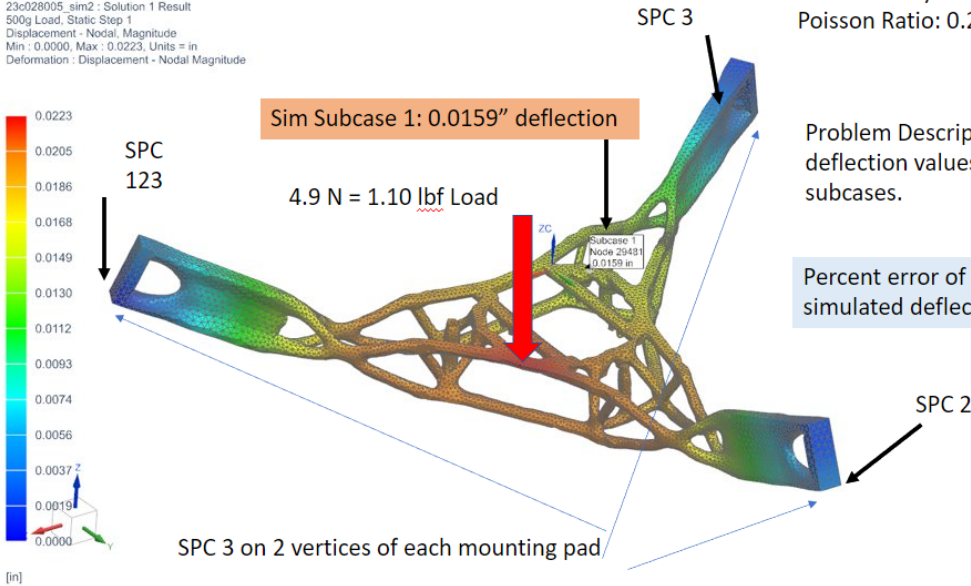
All 3 sides simply supported on gauge pins



Figure 4: Concept A physical deflection test for subcase 1.

60 % Scaled SMSS Subcase 1 One Pager
 L3Harris SSMS: Charles Fleischmann

23c028005_sim2 : Solution 1 Result
 500g Load, Static Step 1
 Displacement - Nodal Magnitude
 Min: 0.0000, Max: 0.0223, Units = in
 Deformation : Displacement - Nodal Magnitude



Materials: ABS
 E: 2 MPA = .29 KSI
 Mass Density: $1.05 \times 10^{-6} \text{ kg/mm}^3 = .0379 \text{ lbf/in}^3$
 Poisson Ratio: 0.26

Problem Description: Match real world deflection values in NX with two different subcases.

Percent error of real-world deflection and simulated deflection: **1.85% Error**

Real World Subcase 1: 0.0162" deflection

Mechanical Engineering
 University of Rochester

Figure 5: Concept A NX simulated deflection test for subcase 1 and comparison to Fig 2.

60 % Scaled SMSS Subcase 2 Deflection Test
 L3Harris SSMS: Charles Fleischmann

Results

Subcase 2: 0.0175" deflection

All 3 sides simply supported on gauge pins



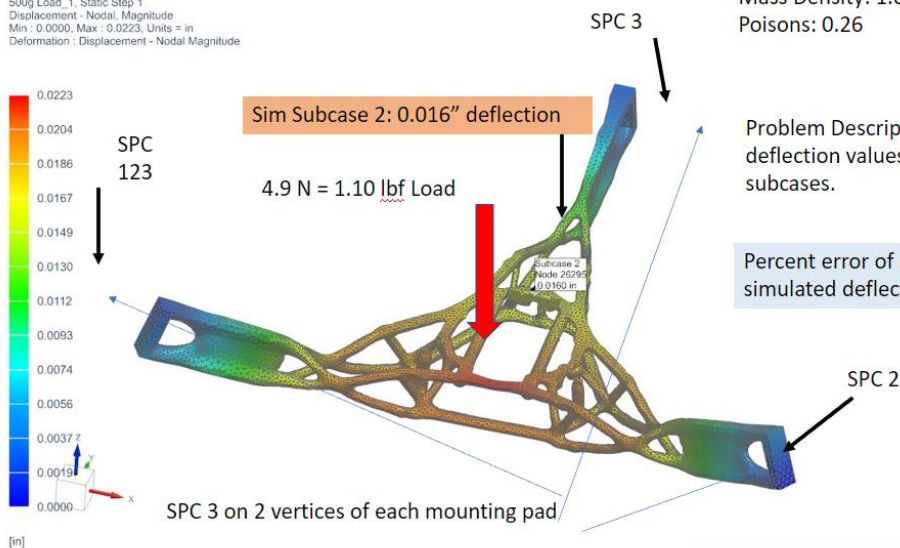
4.9N lbf load

Mechanical Engineering
 University of Rochester

Figure 6: Concept A physical deflection test for subcase 2.

60 % Scaled SMSS Subcase 2 One Pager
L3Harris SSMS: Charles Fleischmann

23c028005_sim2 : Solution 1 Result
 500g Load_1, Static Step 1
 Displacement - Nodal, Magnitude
 Min : 0.0000, Max : 0.0223, Units = in
 Deformation : Displacement - Nodal Magnitude



Materials: ABS
 E: 2 MPA = .29 KSI
 Mass Density: $1.05e-6 \text{ kg/mm}^3 = .0379 \text{ lbm/in}^3$
 Poisons: 0.26

Problem Description: Match real world deflection values in NX with two different subcases.

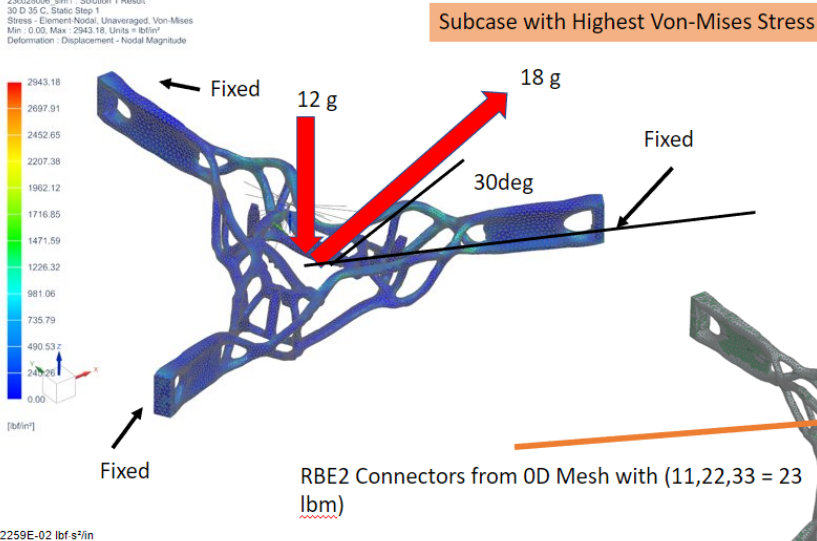
Percent error of real-world deflection and simulated deflection: **8.57% Error**

Real World Subcase 2: 0.0175" deflection

Figure 7: Concept A NX simulated deflection test for subcase 2 and comparison to Fig 4.

'22 SMSS Sim Baseline Concept A (60 % Scaled, Invar)
L3Harris SSMS: Charles Fleischmann

23c028006_sim1 : Solution 1 Result
 30 D 35 C, Static Step 1
 Stress - Element Nodal, Unaveraged, Von-Mises
 Min : 0.00, Max : 2943.18, Units = lbf/in^2
 Deformation : Displacement - Nodal Magnitude



Invar-36	
Mass Density	0.291 lbm/in ³
Young's Modulus	$1.9 \cdot 10^7 \text{ lbf/in}^2$
Poisson's Ratio	0.26
Ultimate Stress	64251.7 lbf/in^2
CTE	$5.5558E-7 \text{ in/in/}^\circ\text{F}$

Problem Description: Perform a simplified Simulation of a 15-degree lateral swept subcase and axial gravity loading

Figure 9: Stress Results from NX simulation of Concept A with 15-degree lateral swept and axial gravity loading.



Figure 10: Strike modal test experimental set up. Concept A is hung off the ground with bungee cords for free-free constraints.



Figure 11: Accelerometers placed on Concept A for strike test to record data.

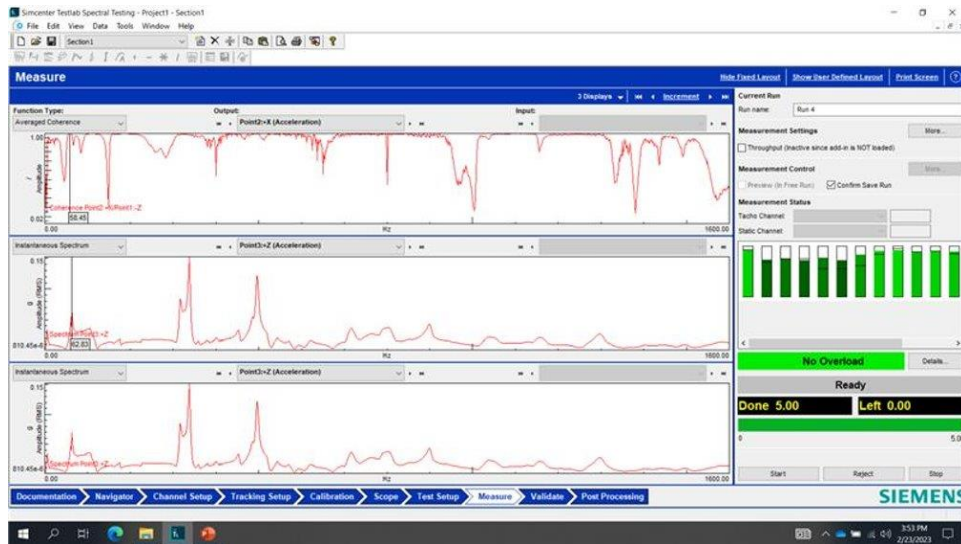


Figure 12: Recorded data from Concept A strike test.

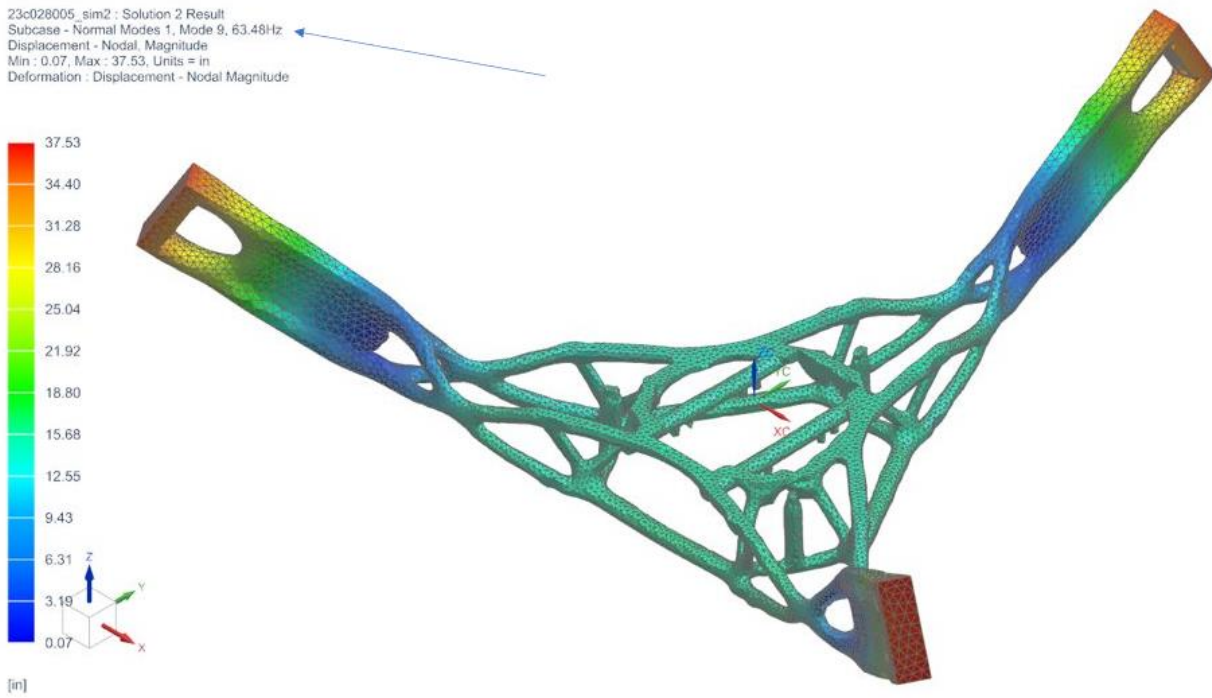
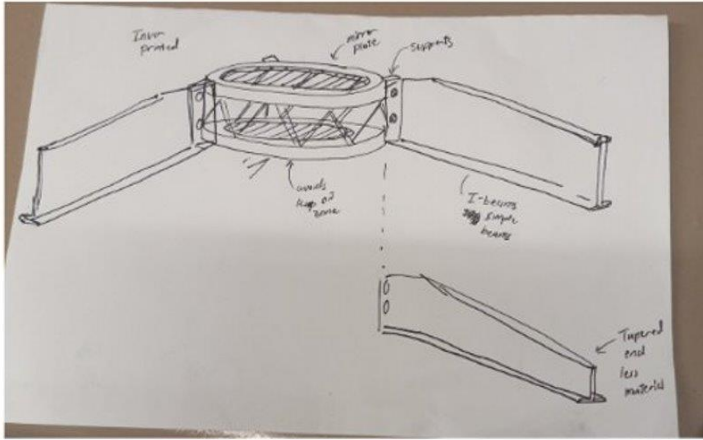
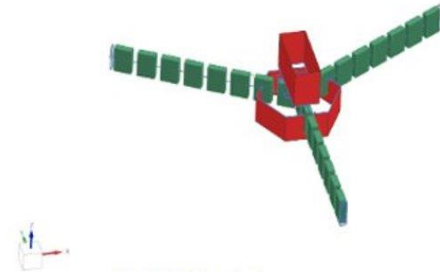


Figure 13: NX Simulation using Solution 103 of free-free modal strike test. The resulting natural frequency is 63.48 Hz.

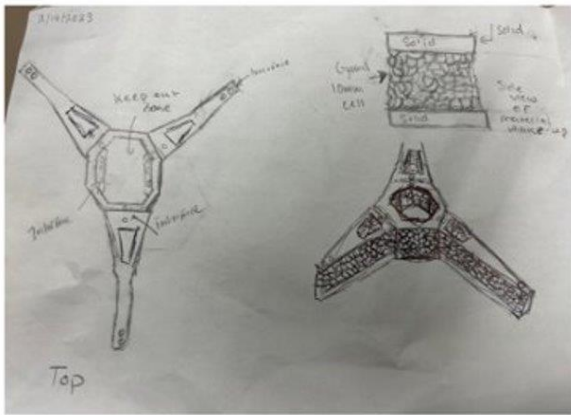


Concept Drawing



FEM Model

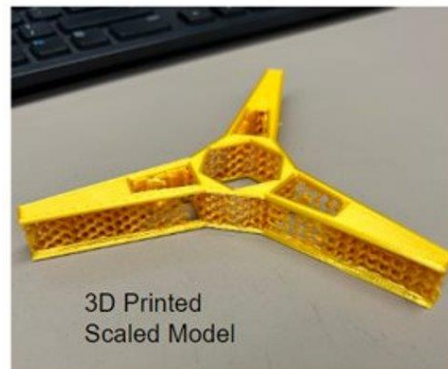
Figure 14: Concept B drawing and FEM model. I-Beams are integral to this design.



Concept Sketch



FEM Model



3D Printed Scaled Model

Figure 15: Concept C drawing, FEM model, and 3D printed concept of proof. Lattices are integral to this design.

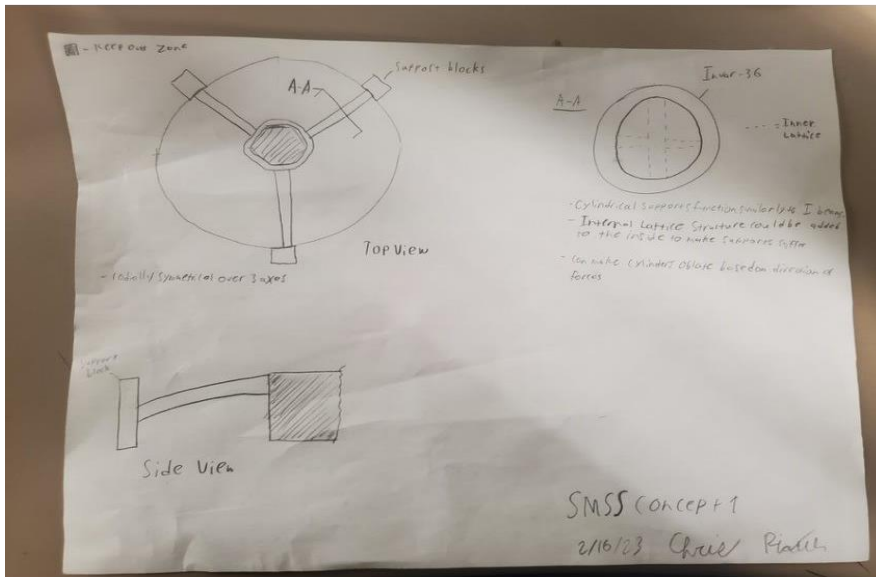


Figure 16: Concept D drawing. Hollow Cylinders are integral to this design.

APPENDIX C: MODEL OPTIMIZATION

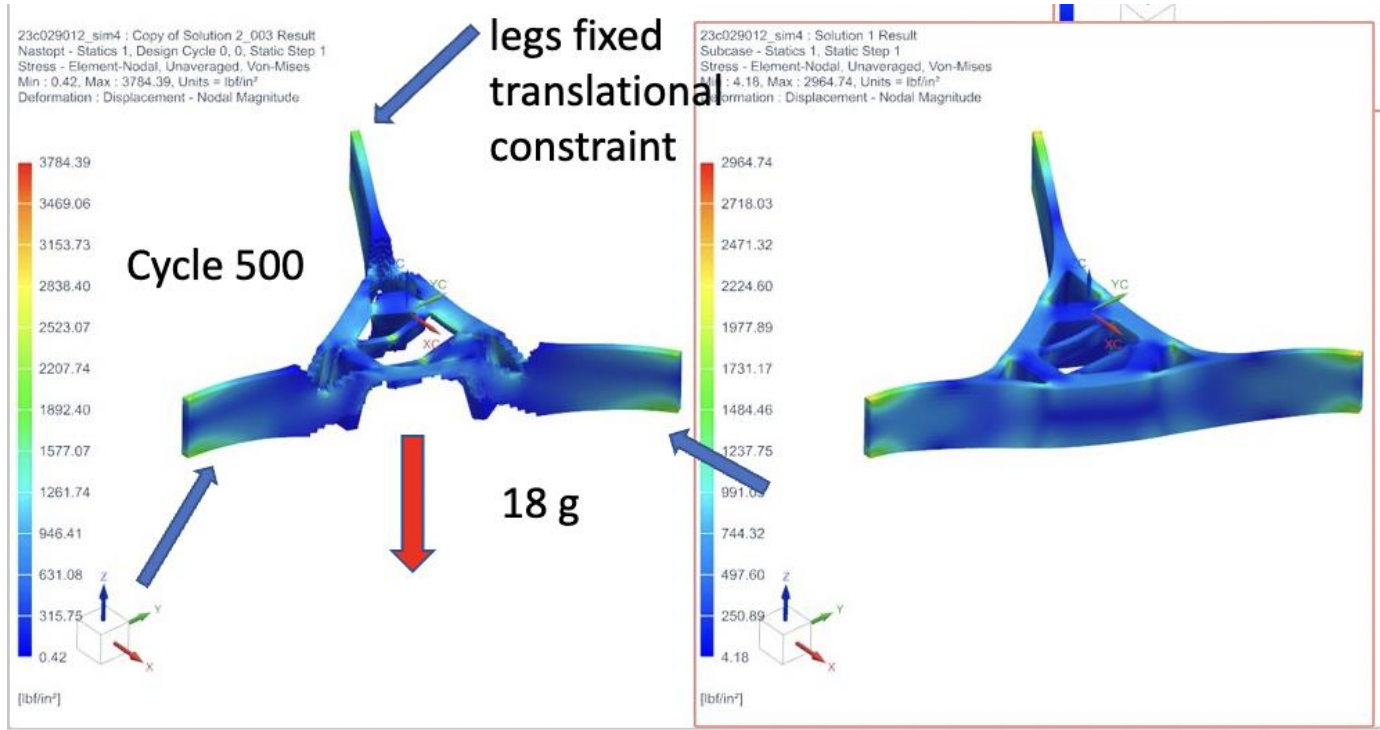


Figure 17: NX Solution 200 Topology Optimization von-mises stress verification for 18 g gravitational load.

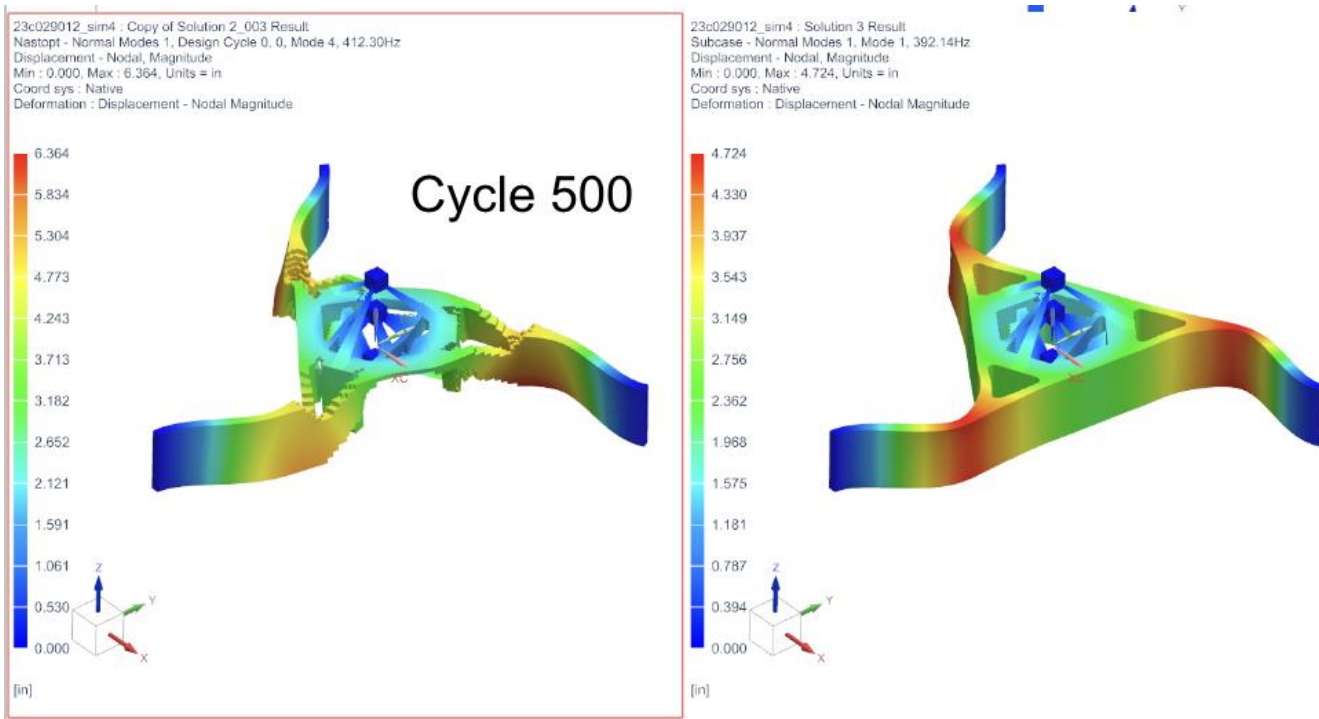


Figure 18: NX Solution 200 Topology Optimization modal analysis verification for 18 g gravitational load.

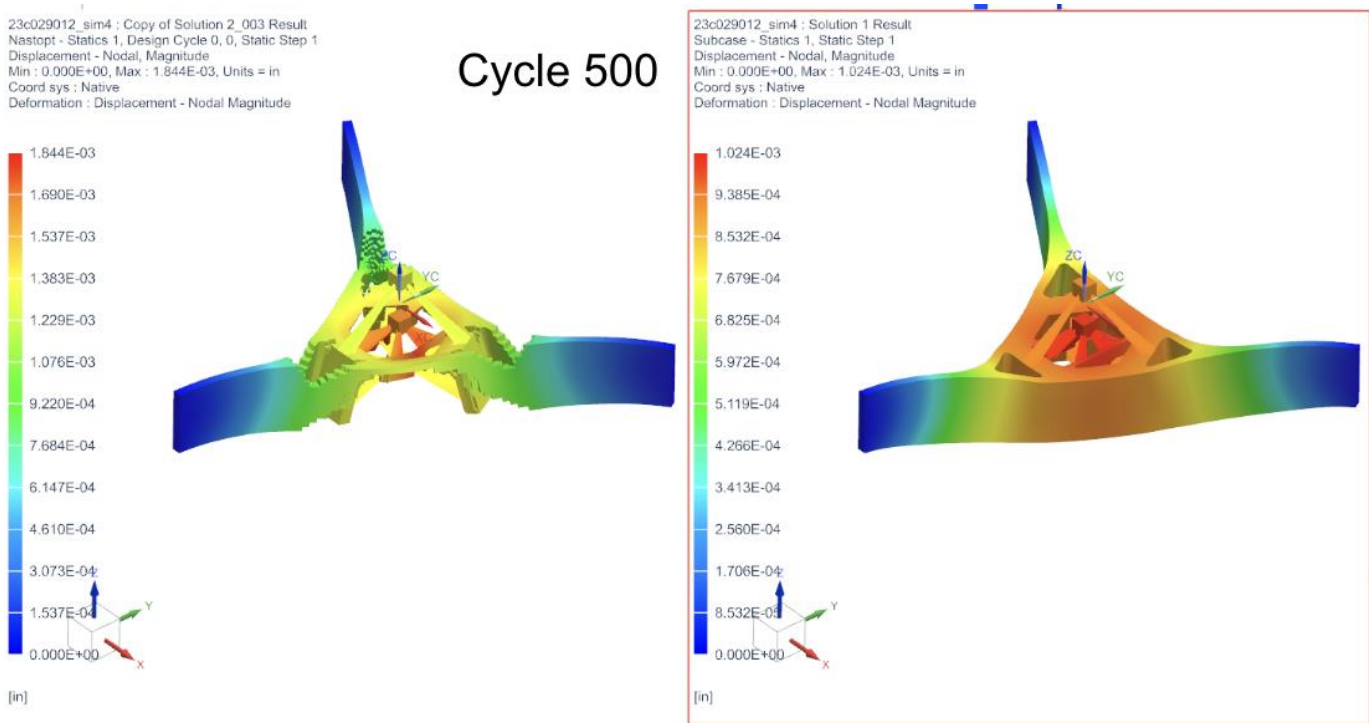


Figure 19: NX Solution 200 Topology Optimization displacement verification for 18 g gravitational load.

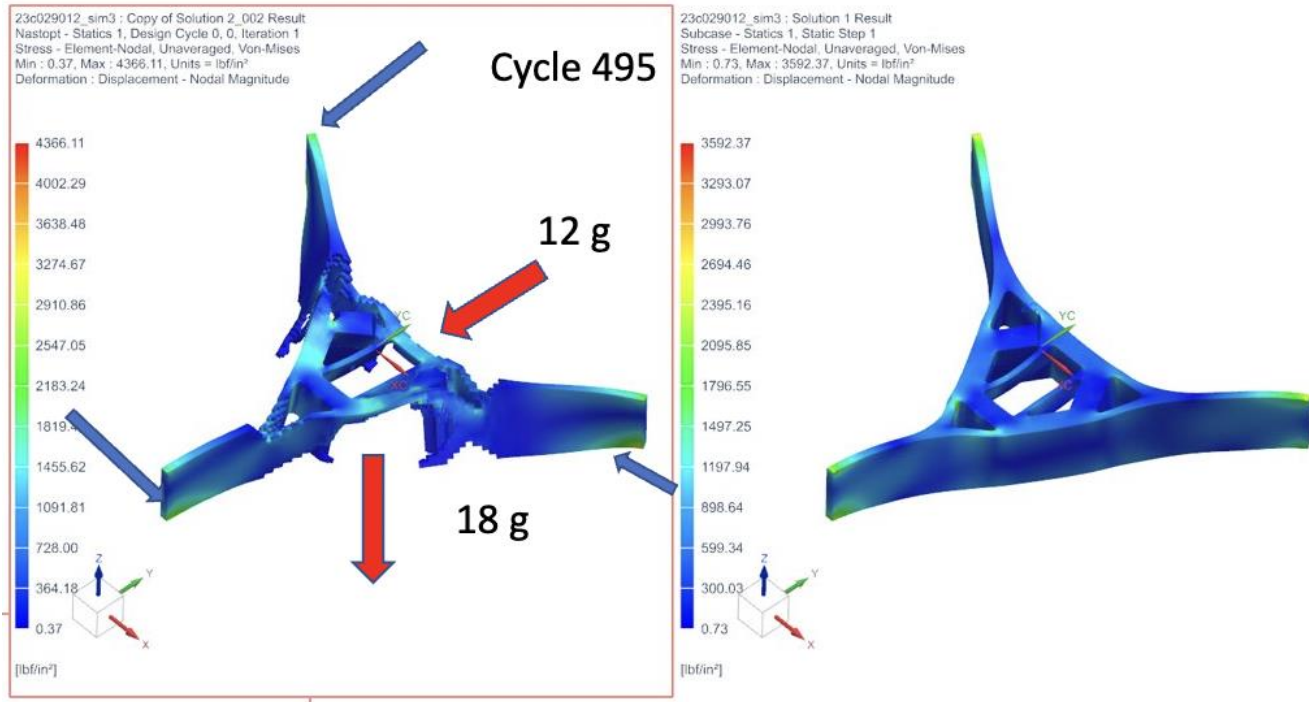


Figure 20: NX Solution 200 Topology Optimization Von-mises stress verification for 18 g gravitational load with 12 g lateral load.

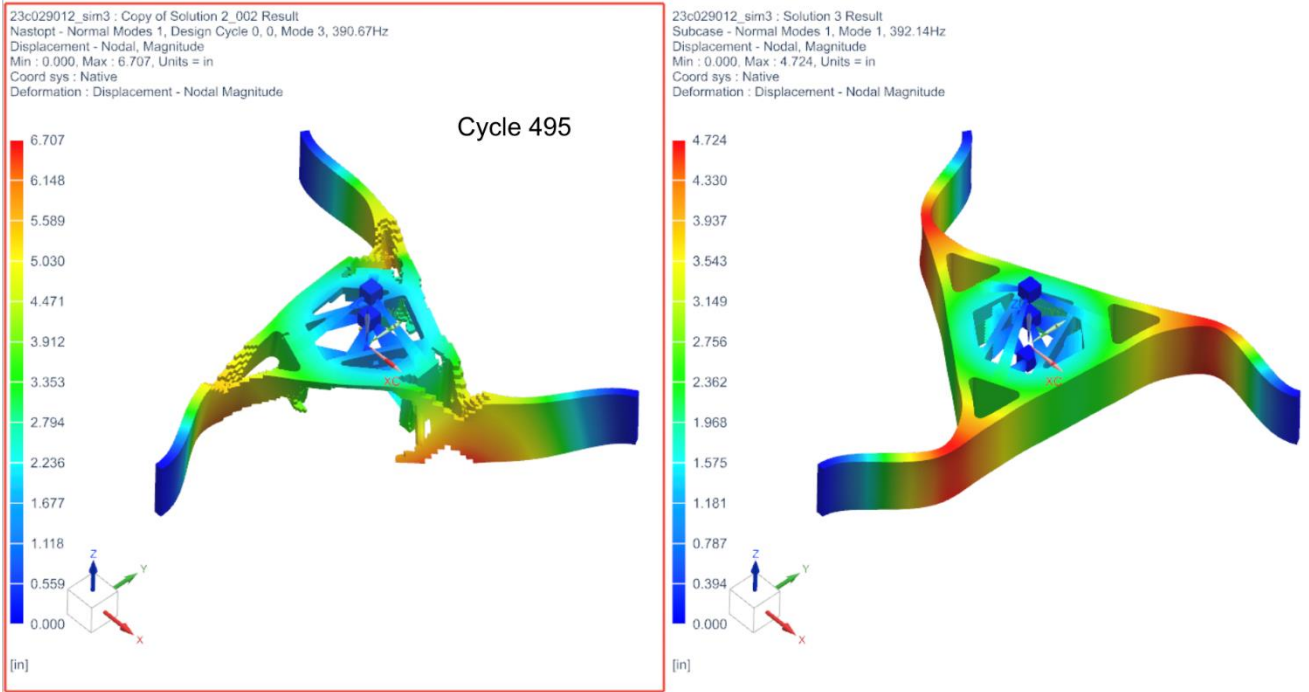


Figure 21: NX Solution 200 Topology Optimization modal analysis verification for 18 g gravitational load with 12 g lateral load.

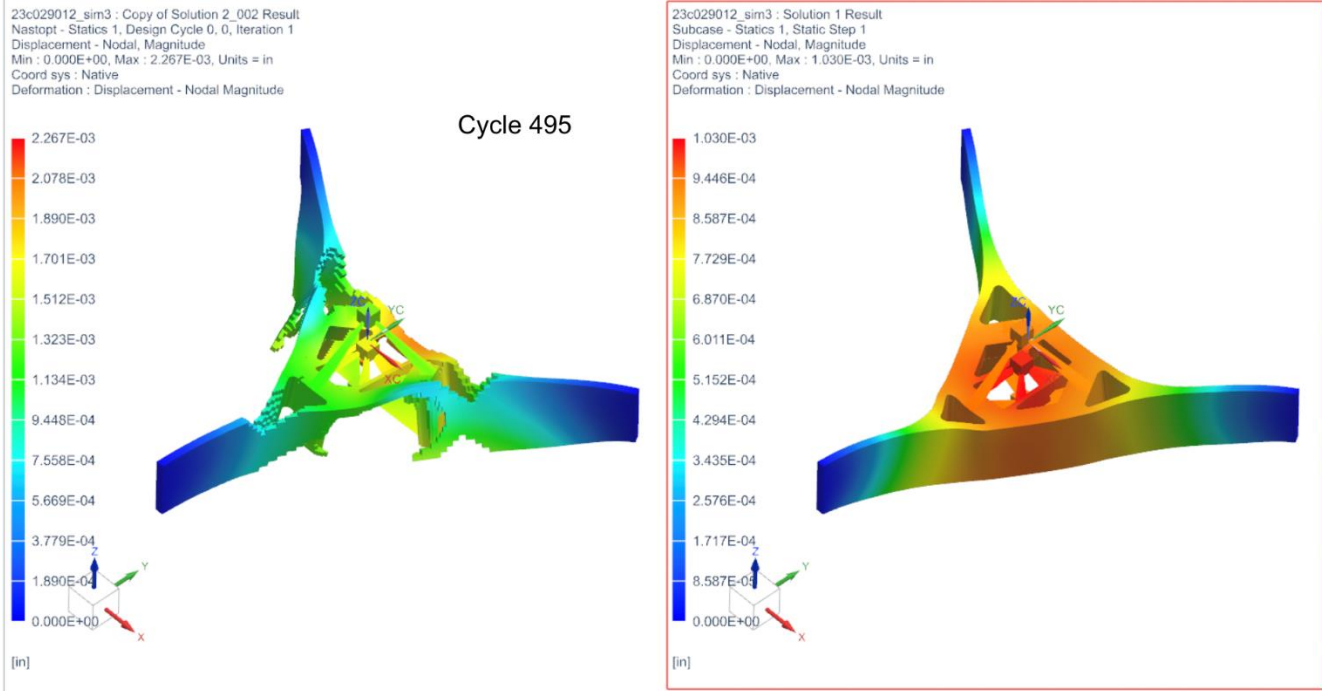


Figure 22: NX Solution 200 Topology Optimization displacement verification for 18 g gravitational load with 12 g lateral load.

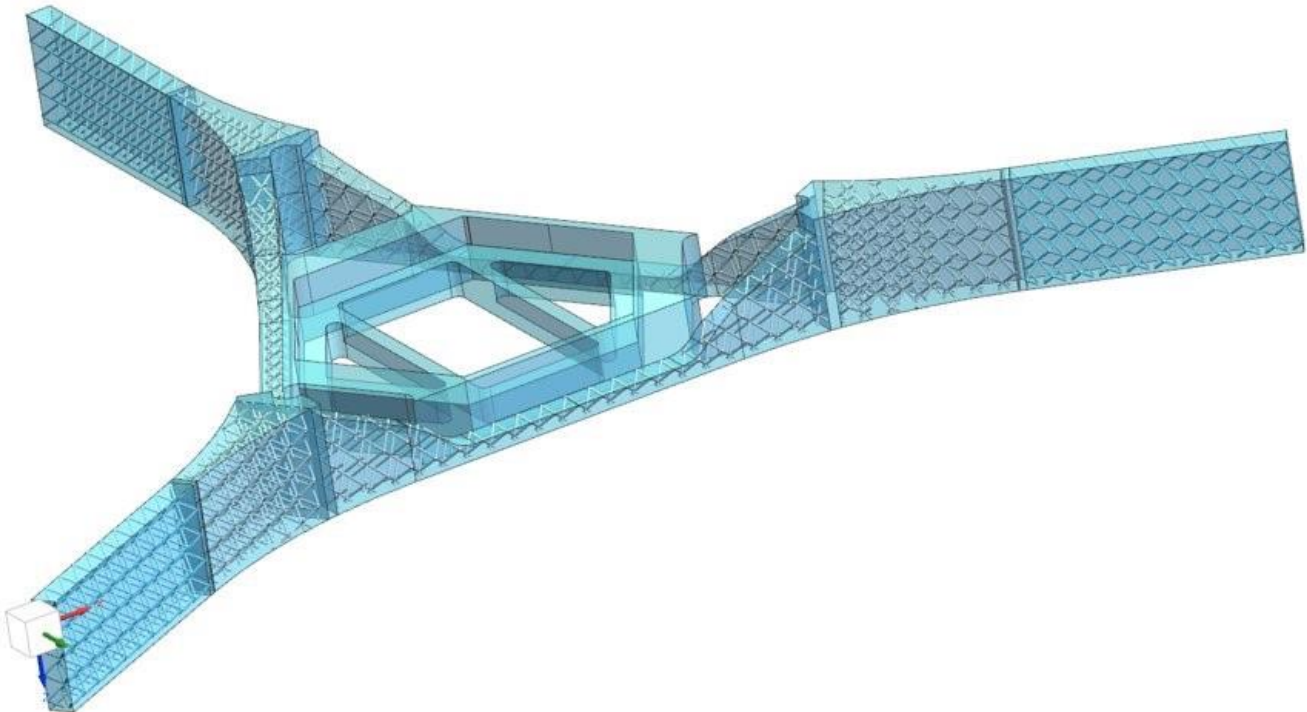


Figure 23: Topologically optimized model with lattice.

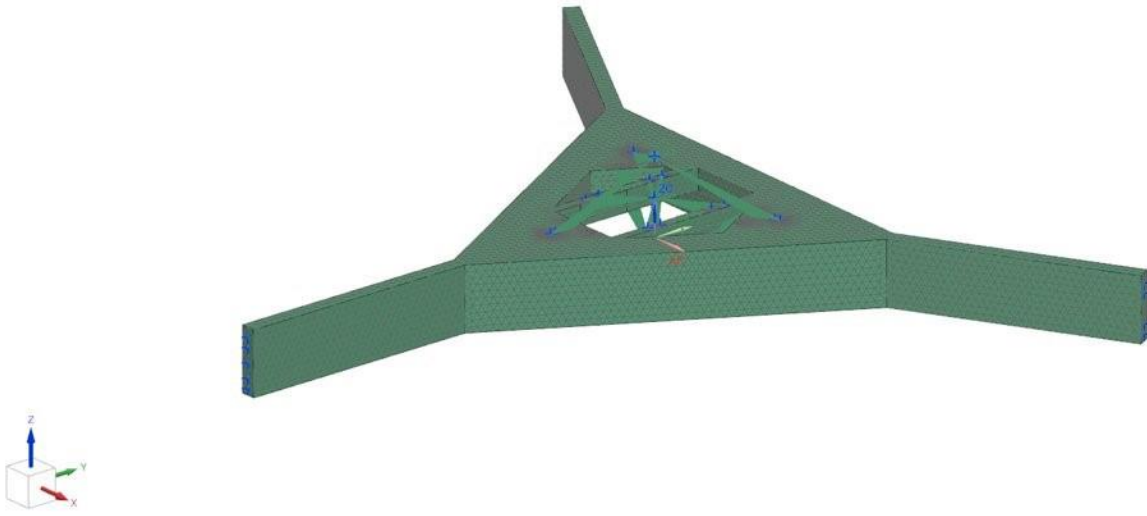


Figure 24: Finite element model (FEM) with RBE3 connections.

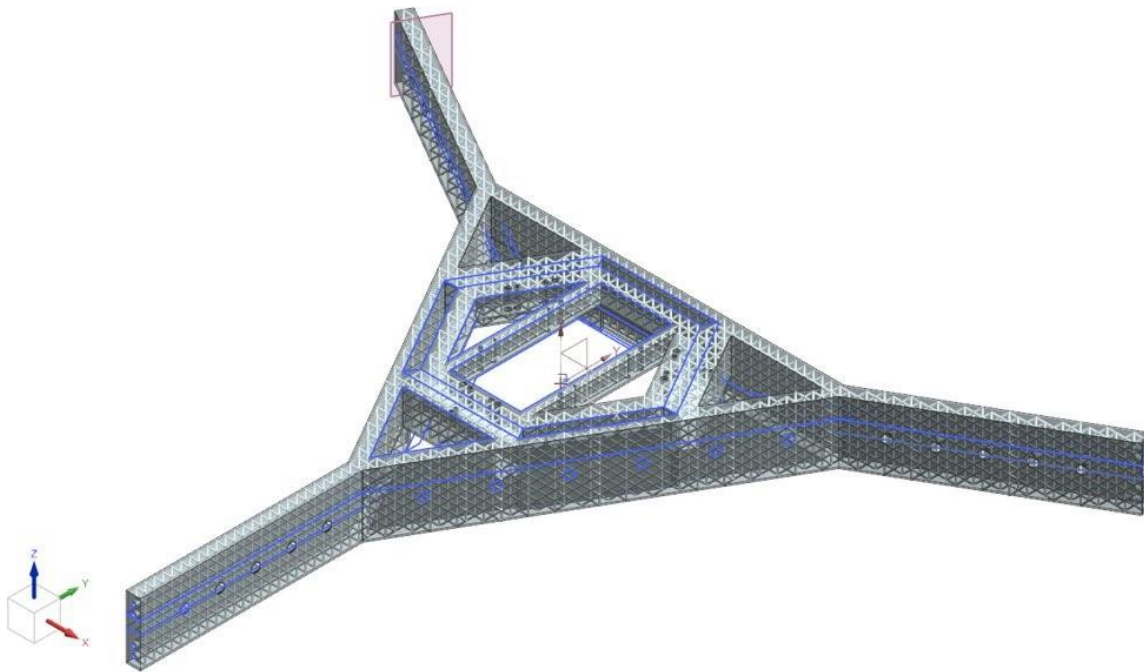
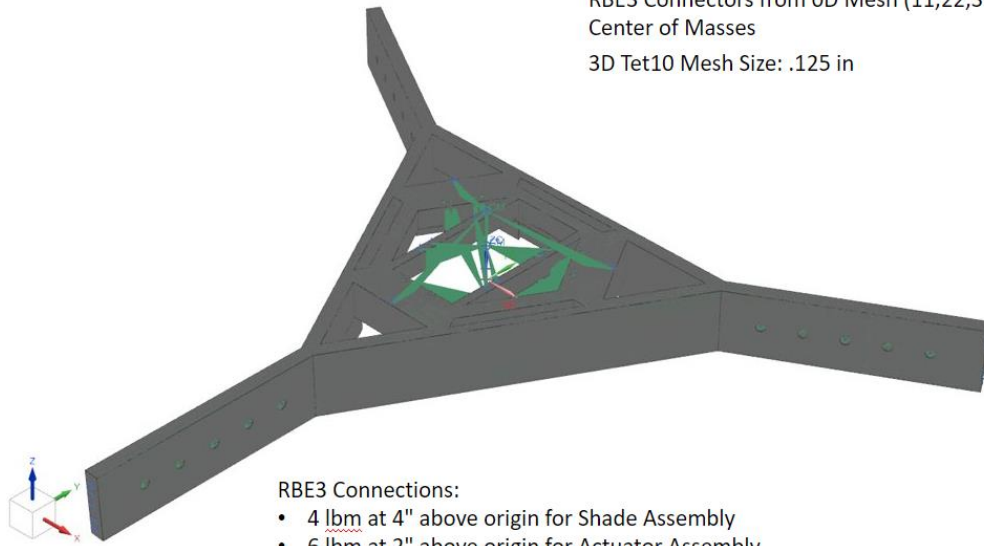


Figure 25: First rendition of SMSS through approach 1. Mass in this design is 33.28 lbm.

RBE3 Connectors from OD Mesh (11,22,33) at three
Center of Masses
3D Tet10 Mesh Size: .125 in



RBE3 Connections:

- 4 lbm at 4" above origin for Shade Assembly
- 6 lbm at 2" above origin for Actuator Assembly
- 11 lbm at 1" below origin for Secondary Mirror and Mounts
- 2 lbm added and distributed evenly at all three points for Miscellaneous Mass

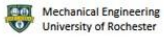


Figure 26: Finite element model with lattice.

FDR Lattice SIM (Displacement)

23c031008_sim2 : Solution 1 Result
Subcase - Statics, Iteration 1
Displacement - Nodal, Magnitude
Min : 0.0000, Max : 0.0205, Units = in
Deformation : Displacement - Nodal Magnitude

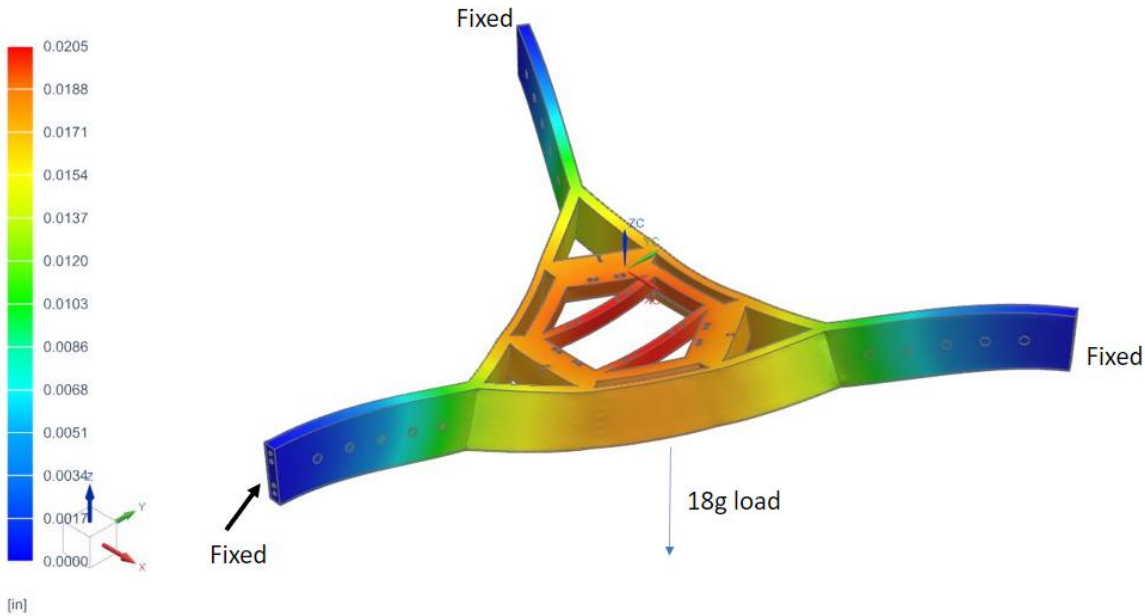


Figure 27: Displacement analysis for latticed model.

23c031008_sim2 : Solution 1 Result
 Subcase - Statics, Iteration 1
 Stress - Element-Nodal, Unaveraged, Von-Mises
 Beam Section : Recovery Point C
 Min : 2.309E-03, Max : 2.754E+04, Units = lb/in²
 Beam Coord sys : Local
 Deformation : Displacement - Nodal Magnitude

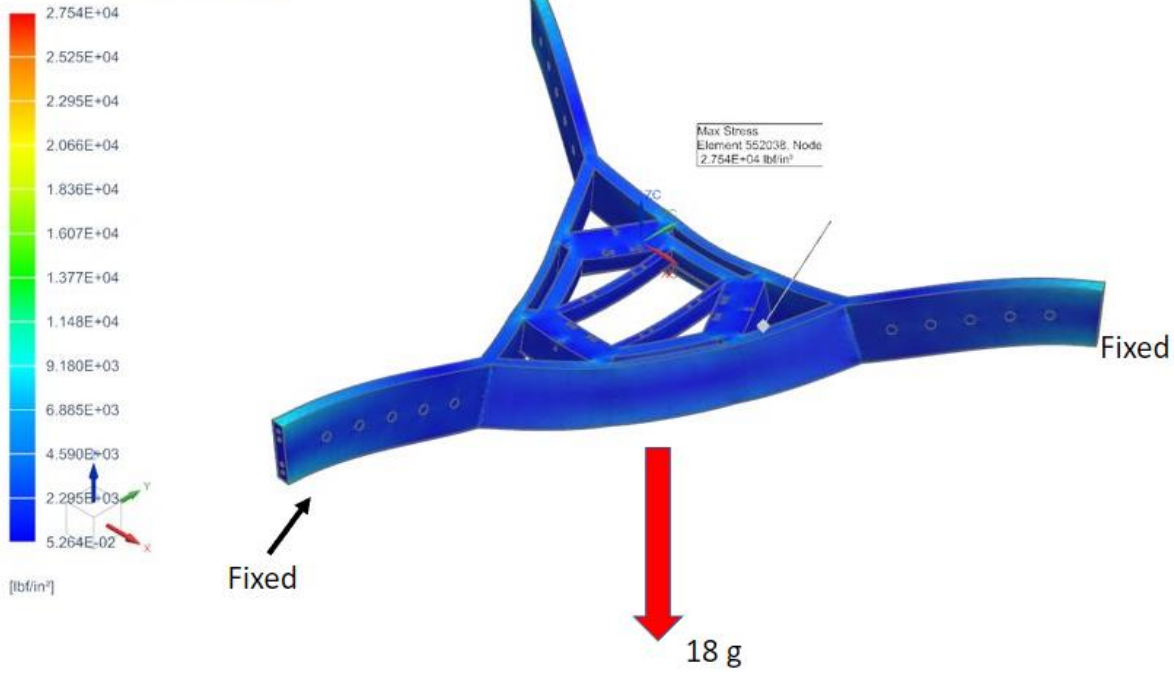


Figure 28: Von-mises stress analysis for latticed model.

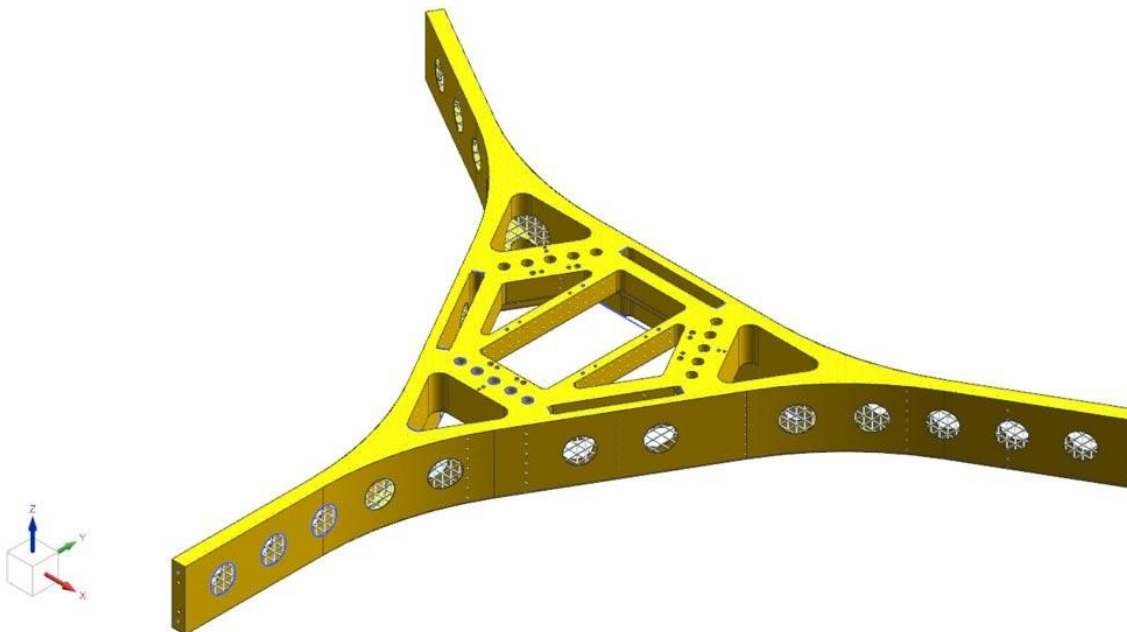


Figure 29: Second rendition of SMSS through approach 1. Mass in this design is 17.23 lbm.

APPENDIX D: MECHANICAL ANALYSIS –SIMULATION OF SMSS

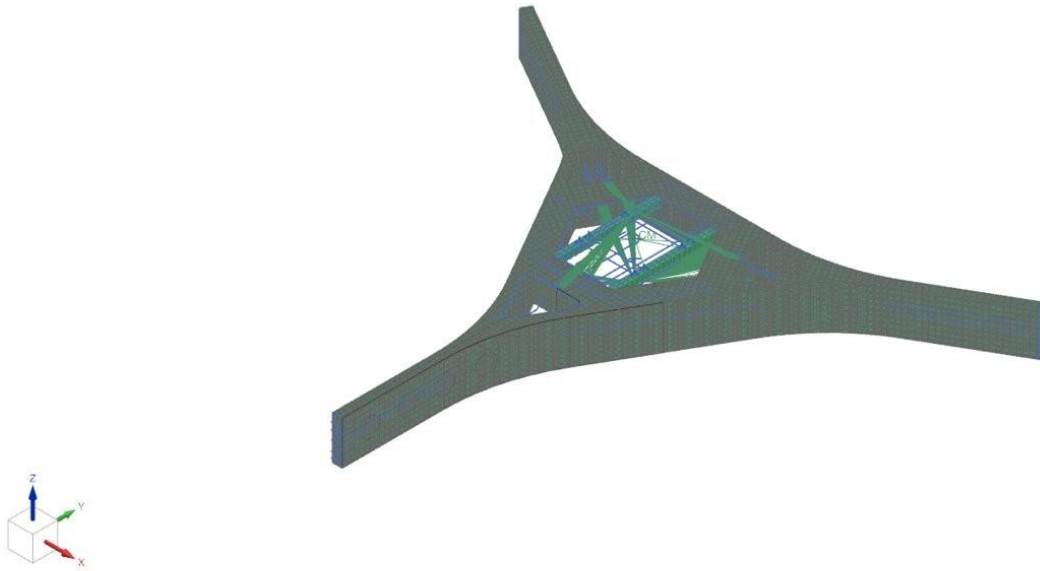


Figure 30: Finite element model of second rendition of SMSS.

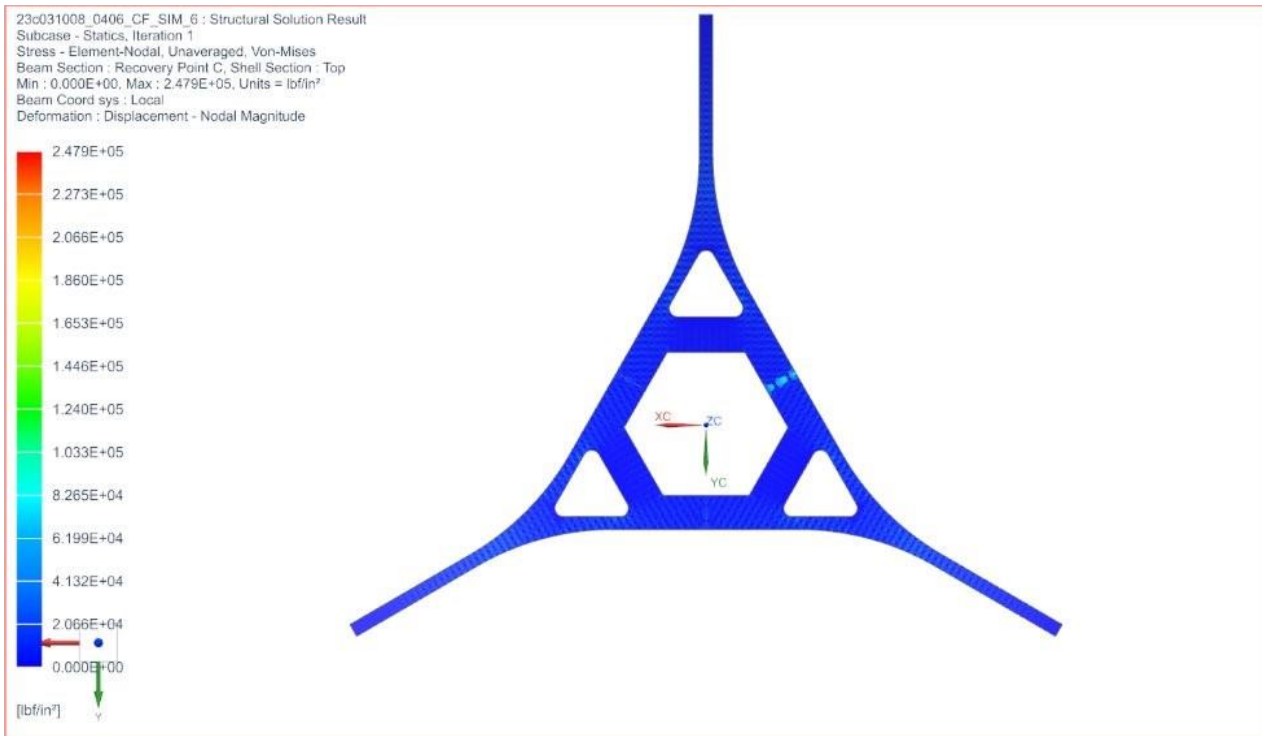


Figure 31: Von-mises stress analysis for second rendition model.

23c031008_0406_CF_SIM_3 : Structural Solution Result
Subcase - Statics, Iteration 1
Stress - Element-Nodal, Unaveraged, Von-Mises
Beam Section : Recovery Point C, Shell Section : Top
Min : 0.00, Max : 68.54, Units = lbf/in²
Beam Coord sys : Local
Deformation : Displacement - Nodal Magnitude

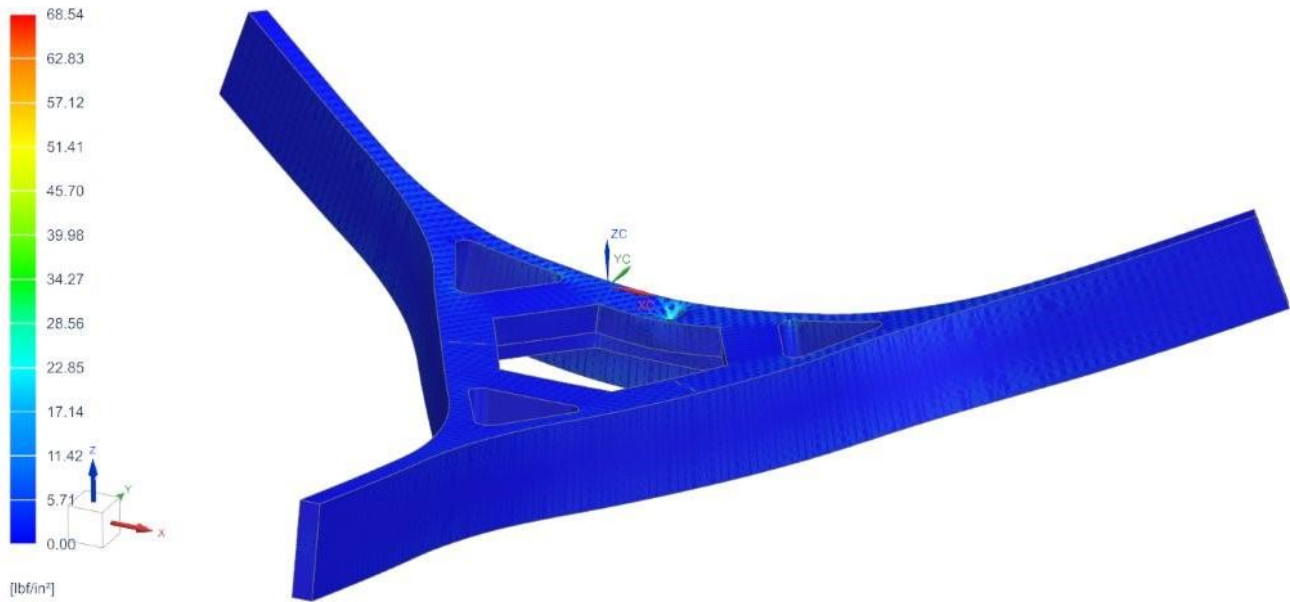
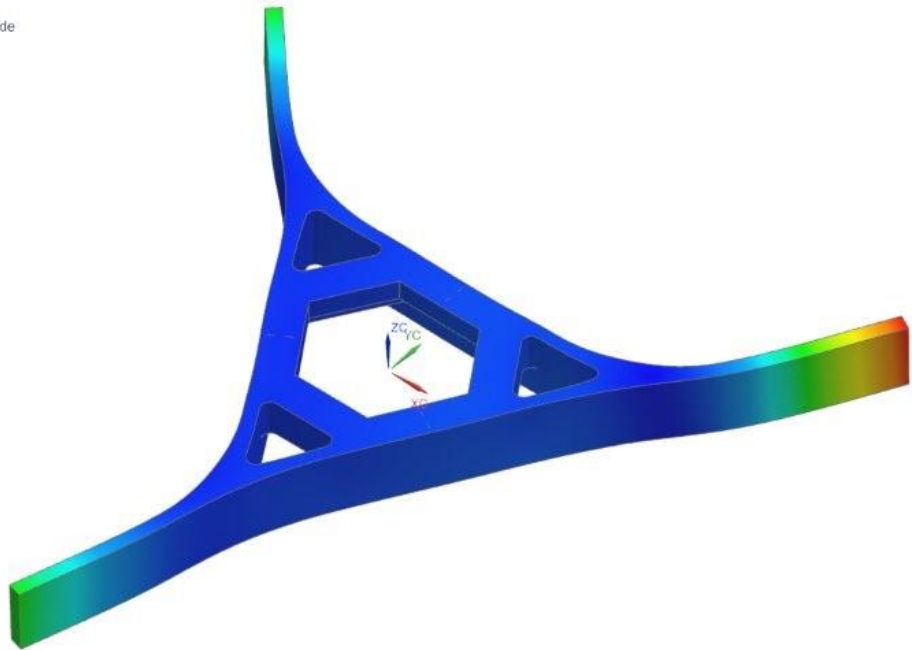


Figure 32: Von-mises stress analysis for second rendition model.

23c031008_0406_CF_SIM_3 - Solution 1 Result
Subcase - Normal Modes 1, Mode 7, 259.49Hz
Displacement - Nodal Magnitude
Min : 0.00, Max : 13.24, Units = in
Deformation : Displacement - Nodal Magnitude



[in]

Figure 33: Modal analysis for second rendition model.

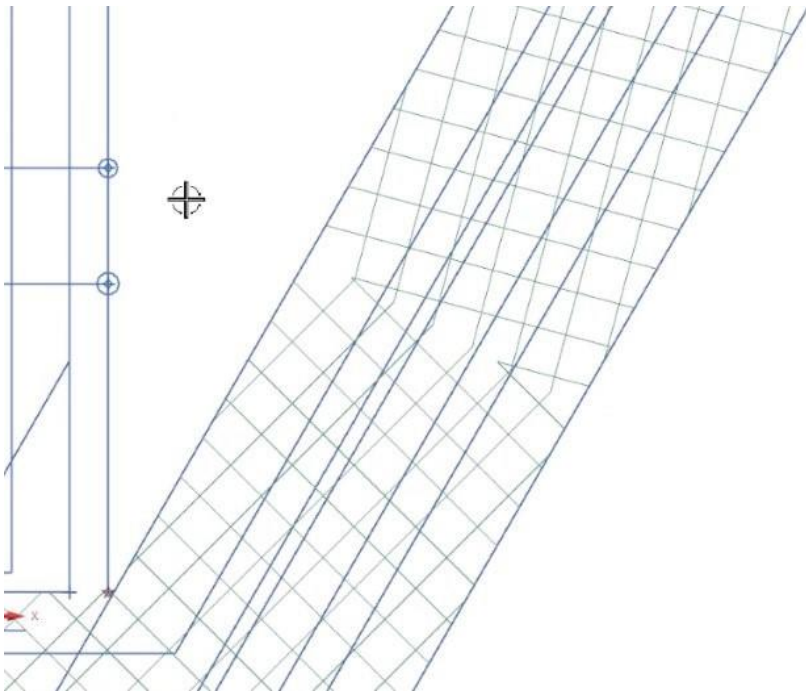


Figure 34: View of lattice orientation in center support of SMSS.

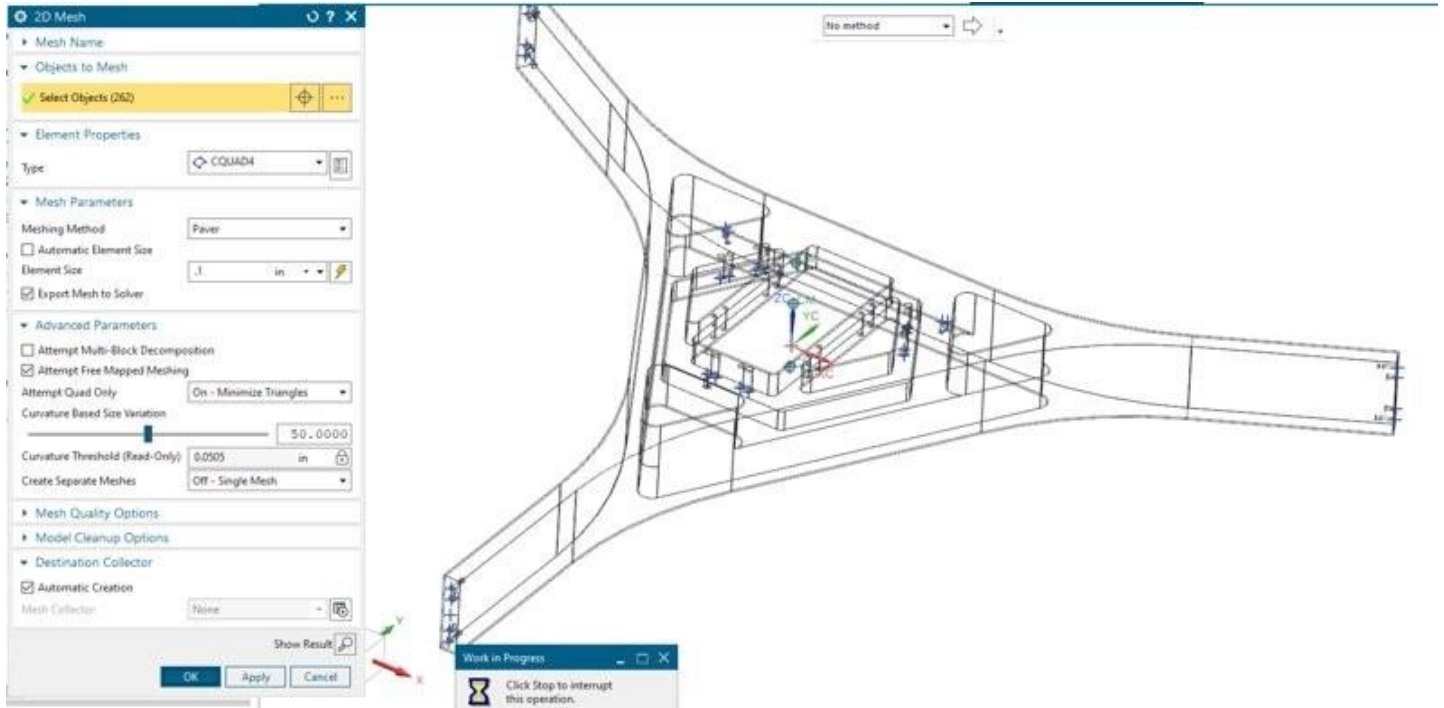
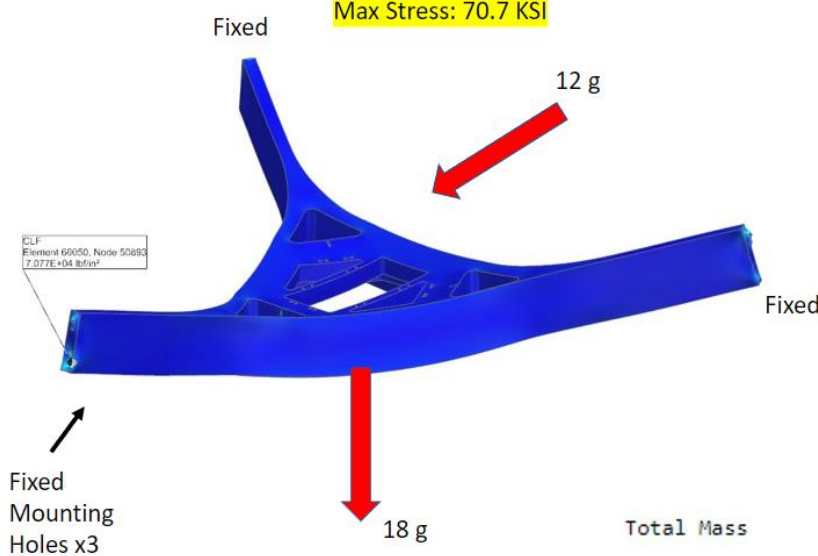
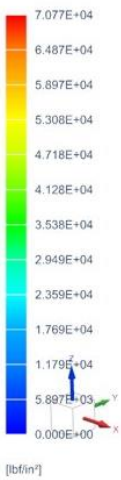


Figure 35: 2D mesh creation for third rendition of SMSS.

Shell Simulation (Von Mises)

23c031008_CF_0411_sim1 : Solution 1 Result
 Subcase - Statics, Iteration 1
 Stress - Element-Nodal, Unaveraged, Von-Mises
 Shell Section : Top
 Min : 0.000E+00, Max : 7.077E+04, Units = lbf/in²
 Deformation : Displacement - Nodal Magnitude



Problem Description: Run a simulation using a 2D mesh to compare with a model with a lattice.

Mat Properties:

Density = .291 lbfm/in³
 Yield Stress = 33.33 KSI
 Ult Strength = 58 KSI
 CTE = 1.0722e-6 in/in°F
 Poisson Ratios = .26

0.1" Shell 2D MESH

Total Mass : 7.586155E-02 lbf·s²/in

Weight: 29.31 lbf

Figure 36: Von-mises stress analysis on shell model.

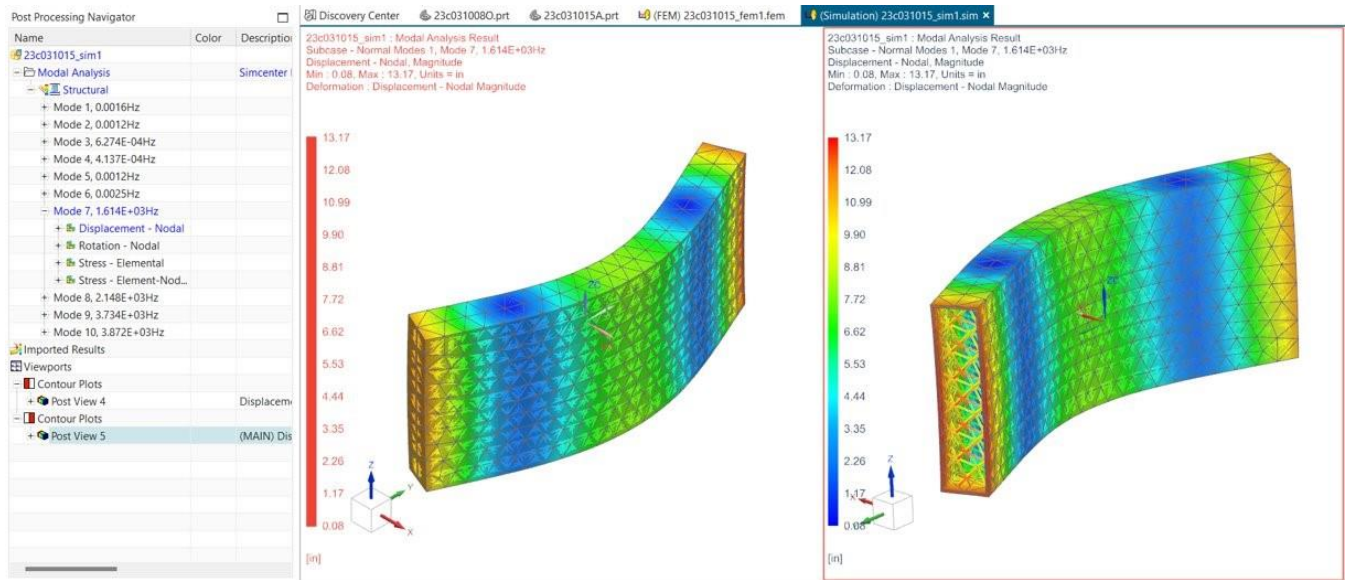


Figure 37: Modal analysis on leg of final rendition of SMSS.

4-13-23

Leg simulation with loads and constraints

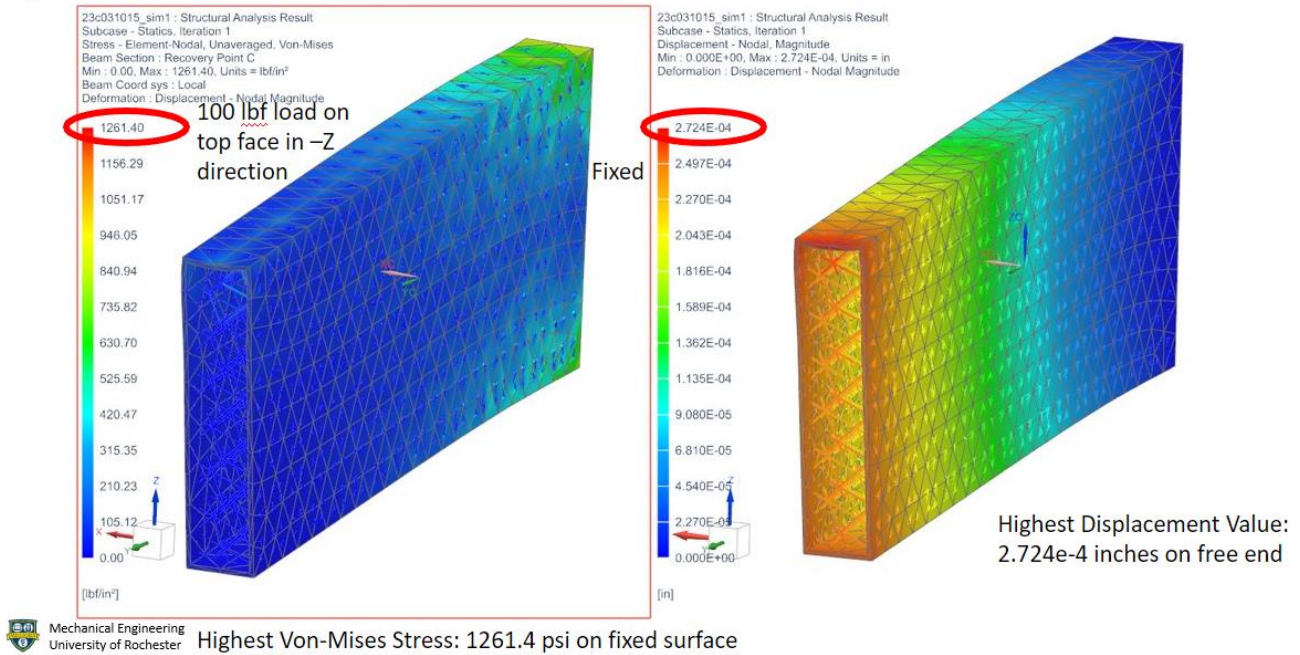
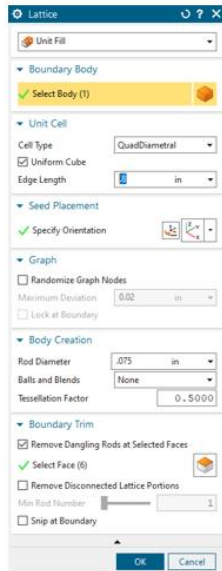


Figure 38: Von-mises stress analysis on leg of final rendition of SMSS.

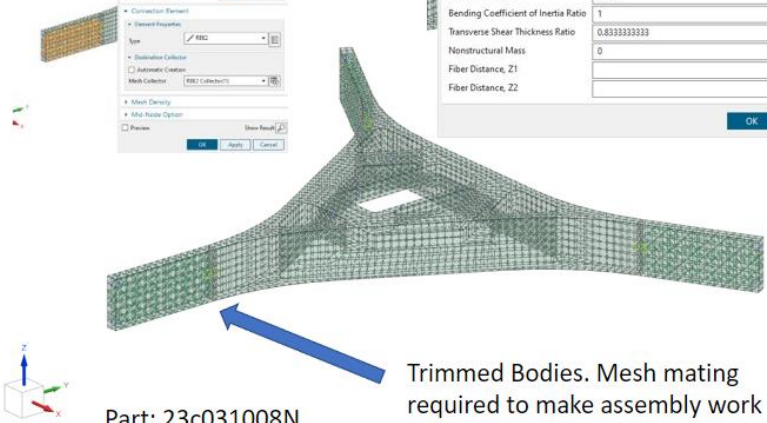
FEM with lattices in Legs Only

File: 23c031008_CF_0413_fem1

Leg Lattice: RBE2 Connection Mesh to face.



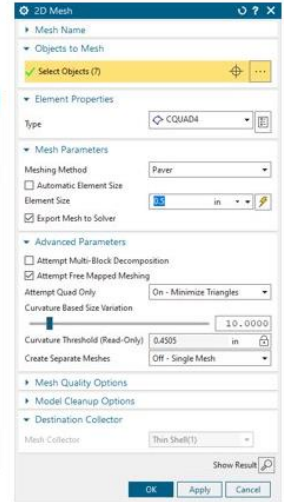
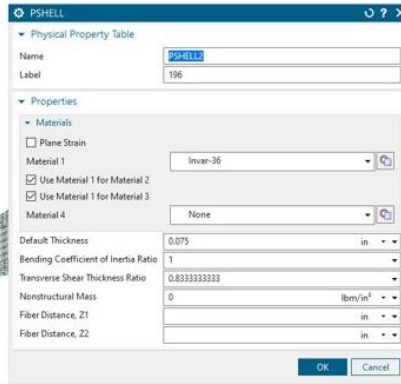
Mechanical Engineering
University of Rochester



Part: 23c031008N

Trimmed Bodies. Mesh mating required to make assembly work

2D Mesh



Mat Properties:

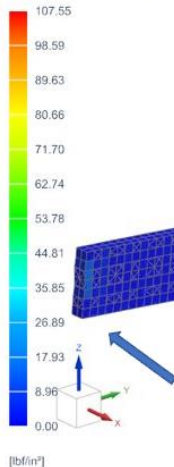
Density = .291 lbm/in³
Yield Stress = 33.33 KSI
Ult Strength = 58 KSI
CTE = 1.0722e-6 in/in°F
Poisson Ratios = .26

Figure 39: Finite element model with lattice only in legs.

SIM with lattices in Legs Only

File: 23c031008_CF_0413_sim1

23c031008_CF_0413_sim1 : Solution 1 Result
Subcase - Statics, Iteration 1
Stress - Element-Nodal, Unaveraged, Von-Mises
Beam Section : Recovery Point C, Shell Section : Top
Min : 0.00, Max : 107.55, Units = lb/in²
Beam Coord sys : Local
Deformation : Displacement - Nodal Magnitude



[lb/in²]

Mechanical Engineering
University of Rochester

$F = 1 \text{ lbf}$

Single Node on each Leg Constrained

2D Mesh

Figure 40: Von-mises stress simulation with lattice only in legs.

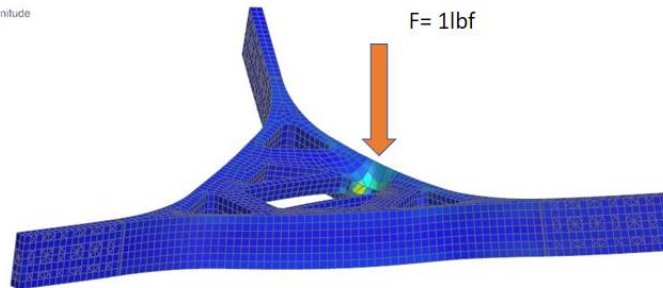
RBE3 Connection Recipe

File: 23c031008_CF_0413_sim3

Same as FEM/SIM 1

Using RBE3 Connection recipes for lattice

23c031008_CF_0413_sim3 : Solution 1 Result
Subcase - Statics, Iteration 1
Stress - Element-Nodal, Unaveraged, Von-Mises
Beam Section : Recovery Point C, Shell Section - Top
Min : 0.00, Max : 107.97, Units = lbf/in²
Beam Coord sys : Local
Deformation : Displacement - Nodal Magnitude



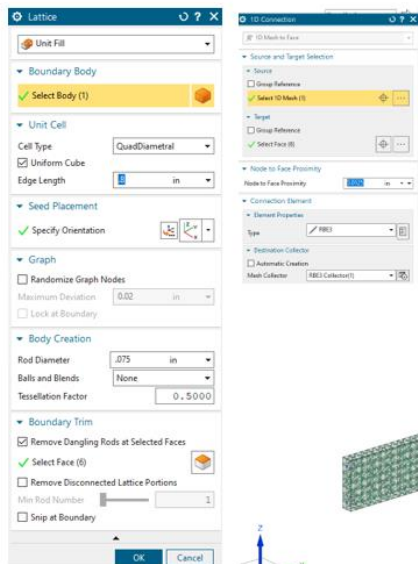
Mechanical Engineering
University of Rochester

Figure 41: Example of von-mises stress analysis to determine split bodies.

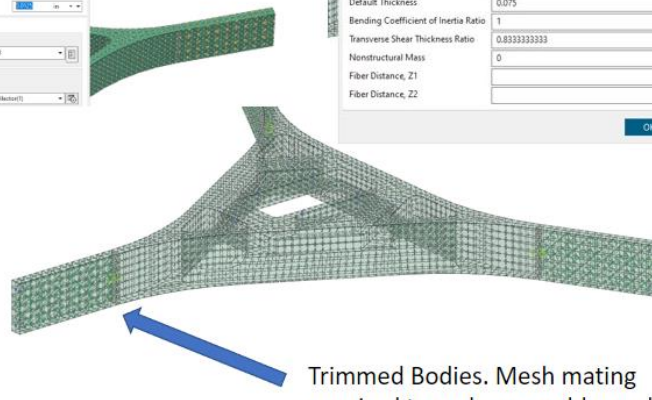
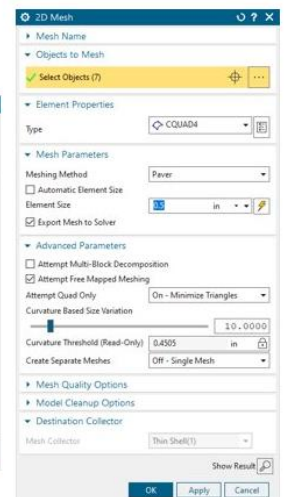
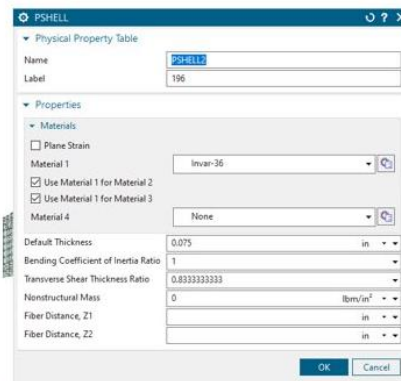
FEM with lattices in Legs Only

File: 23c031008_CF_0413_fem4

Leg Lattice: RBE3 Connection Mesh to face.



2D Mesh



Part: 23c031008N

Mechanical Engineering
University of Rochester

Mat Properties:

Density = .291 lbm/in³
Yield Stress = 33.33 KSI
Ult Strength = 58 KSI
CTE = 1.0722e-6 in/in°F
Poisson Ratios = .26

Figure 42: Finite element model with lattice only in legs.

23c031008_CF_0413_sim4 : Solution 1 Result
 Subcase - Statics, Iteration 1
 Stress - Element-Nodal, Unaveraged, Von-Mises
 Beam Section : Recovery Point C, Shell Section : Top
 Min : 1.229E-01, Max : 2.648E+04, Units = lbf/in²
 Beam Coord sys : Local
 Deformation : Displacement - Nodal Magnitude
 Animation Frame 8 of 8

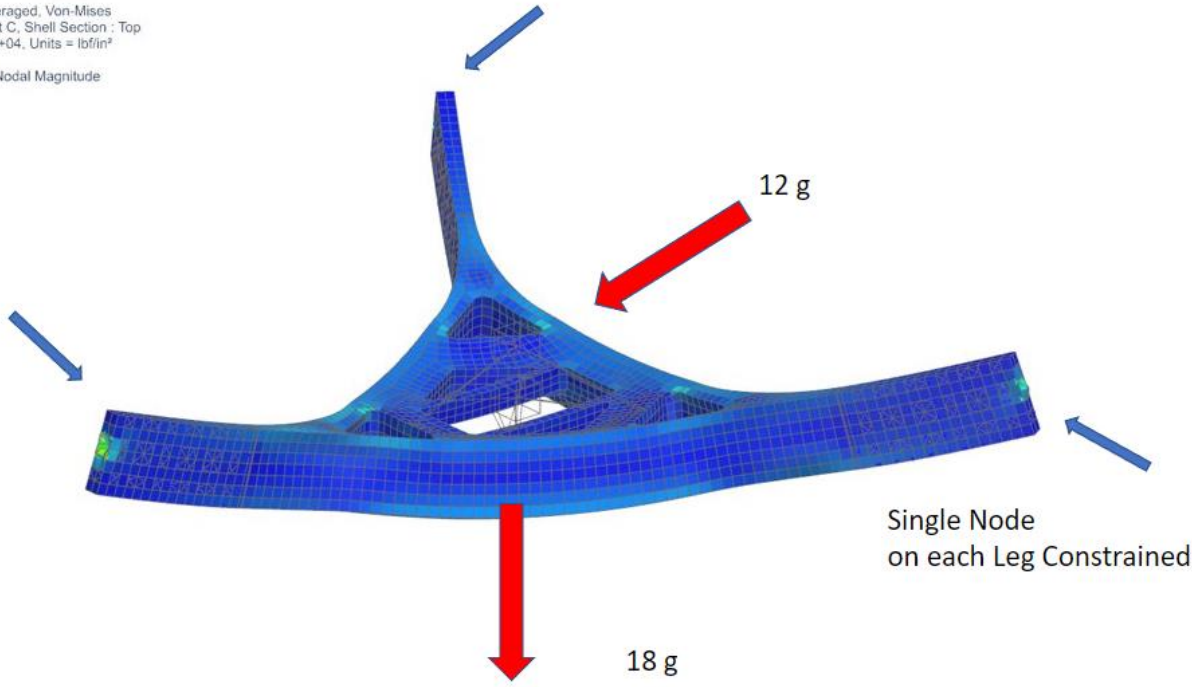


Figure 43: Von-mises stress analysis on model with lattice only in legs.

FEM With No Lattice

File: 23c031008_CF_0413_fem5

Part: 23c031008N

Trimmed Bodies. Mesh mating required to make assembly work

2D Mesh

PSHELL

Name: PSHELL1
Label: 196

Properties

Materials

Material 1: Invar-36
Material 2: Use Material 1 for Material 2
Material 3: Use Material 1 for Material 3
Material 4: None

Default Thickness: 0.075 in
Bending Coefficient of Inertia Ratio: 1
Transverse Shear Thickness Ratio: 0.8333333333
Nonstructural Mass: 0 lbfm/in³
Fiber Distance, Z1: in
Fiber Distance, Z2: in

2D Mesh

Mesh Name

Objects to Mesh

Element Properties

Type: CQUAD4

Mesh Parameters

Meshing Method: Paver
Curvature Threshold (Read-Only): 0.4505 in

Mat Properties:

Density = .291 lbfm/in³
 Yield Stress = 33.33 KSI
 Ult Strength = 58 KSI
 CTE = 1.0722e-6 in/in°F
 Poisson Ratios = .26

Figure 44: Finite element model with trimmed bodies and no lattice.

Same as SIM 4,
deleted Lattice from
FEM

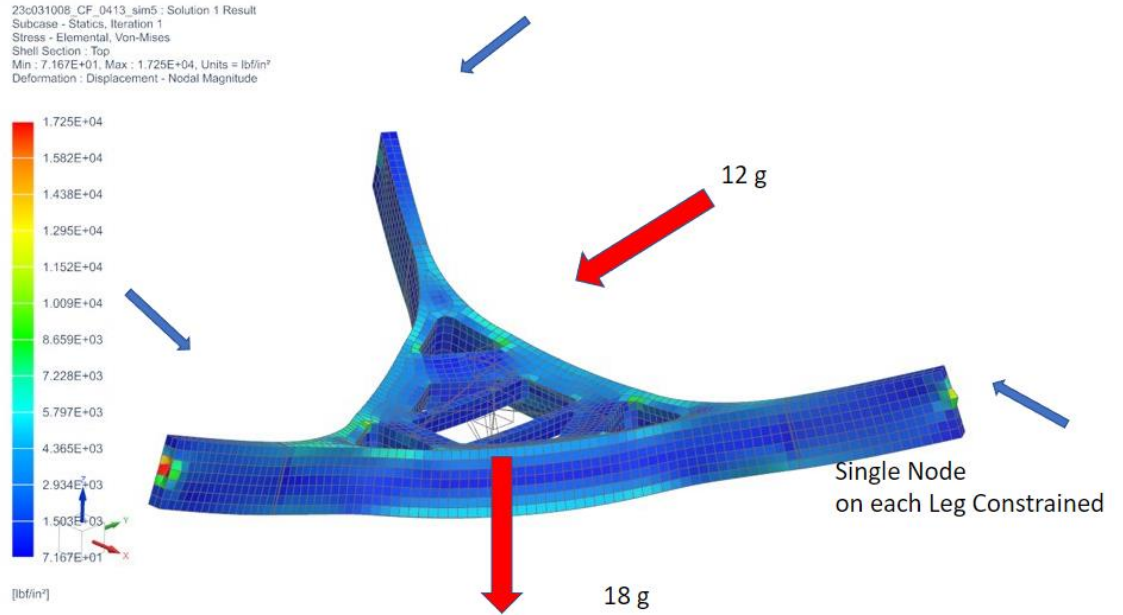
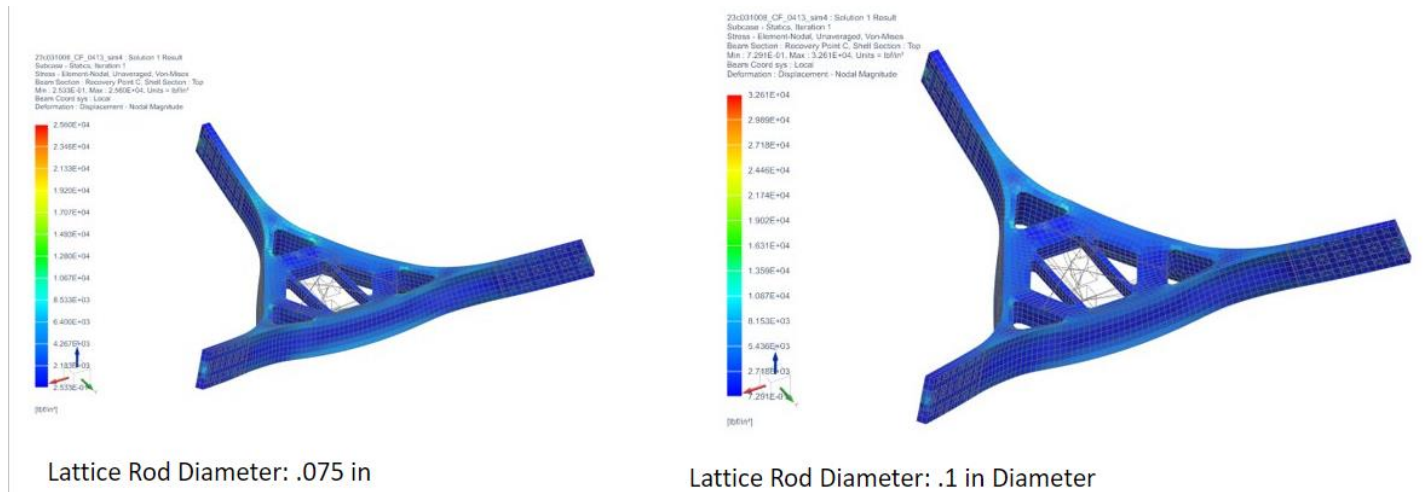


Figure 45: Von-mises stress analysis with trimmed bodies and no lattice.



Lattice Rod Diameter: .075 in

Lattice Rod Diameter: .1 in Diameter

Figure 46: Simulations to show the effects of changing the lattice rod diameters in the trimmed bodies.

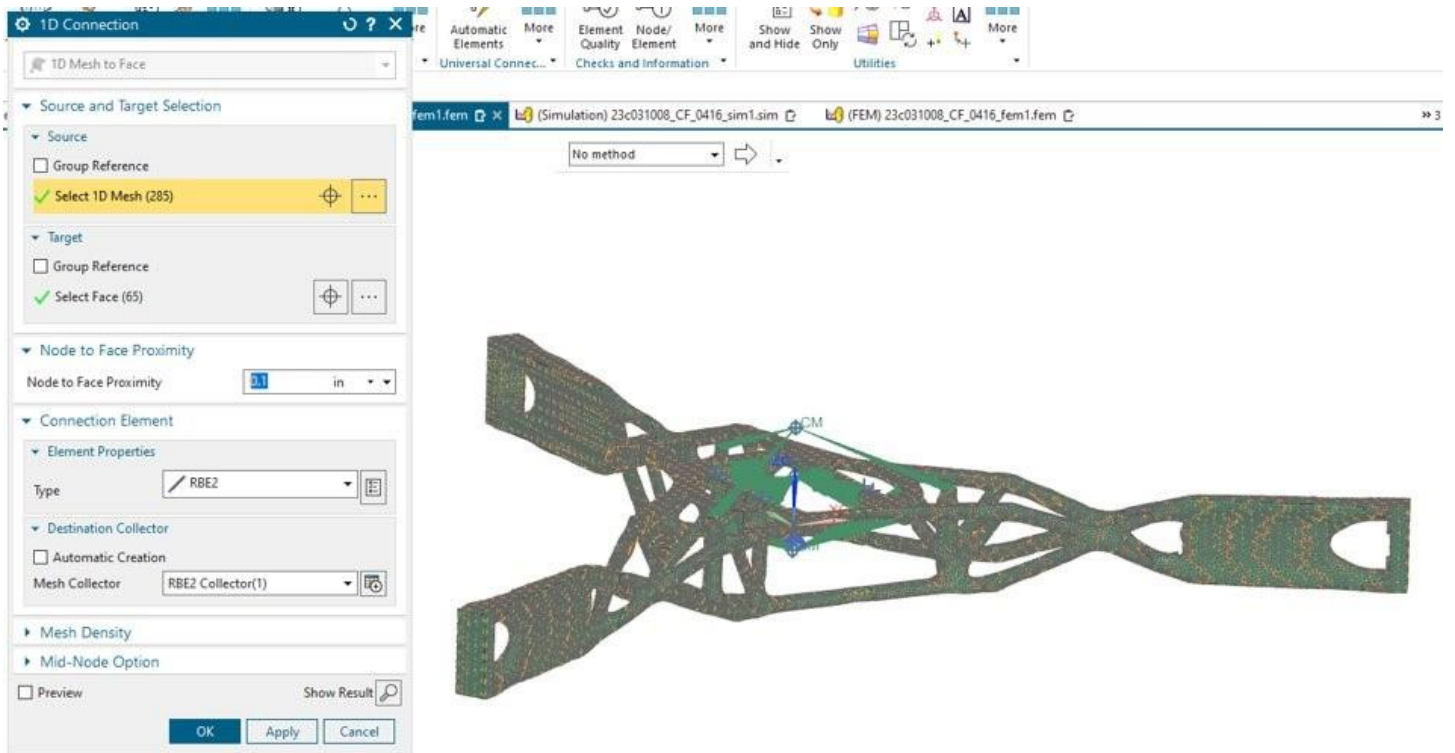


Figure 47: RBE2 connections are shown as used in last year's project.

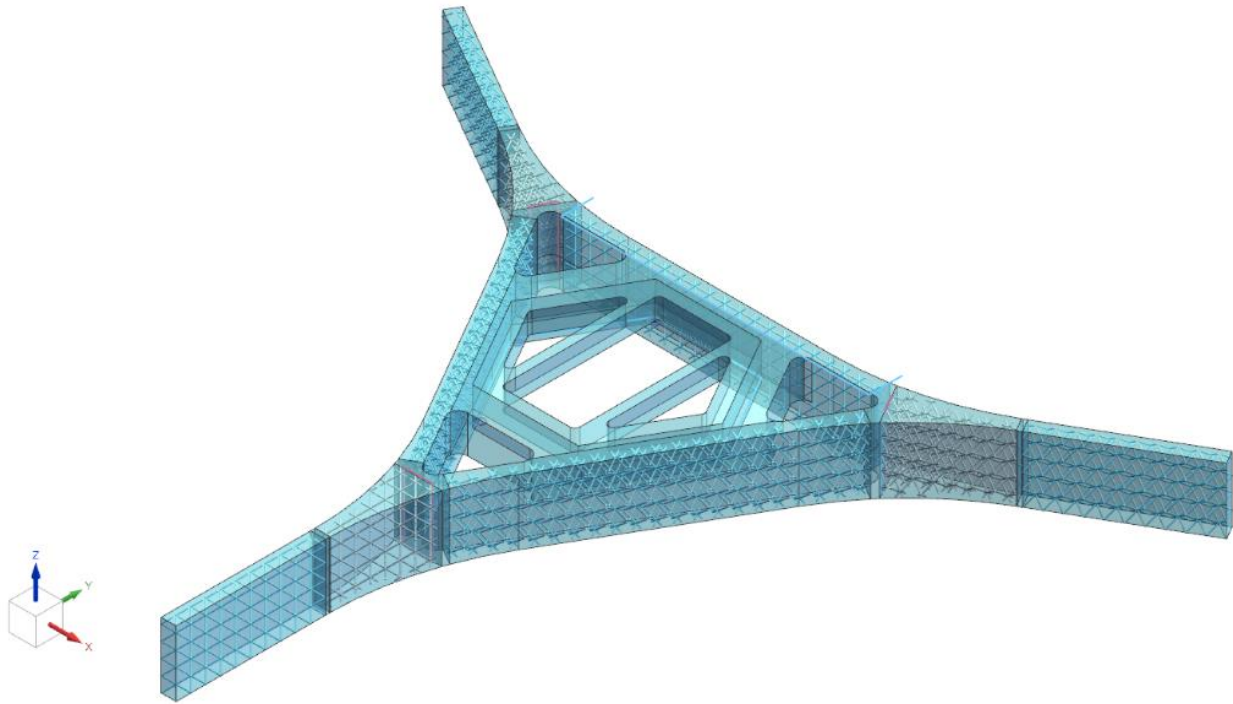


Figure 48: Final rendition of SMSS through approach 1. Mass in this design is 14.58 lbm.

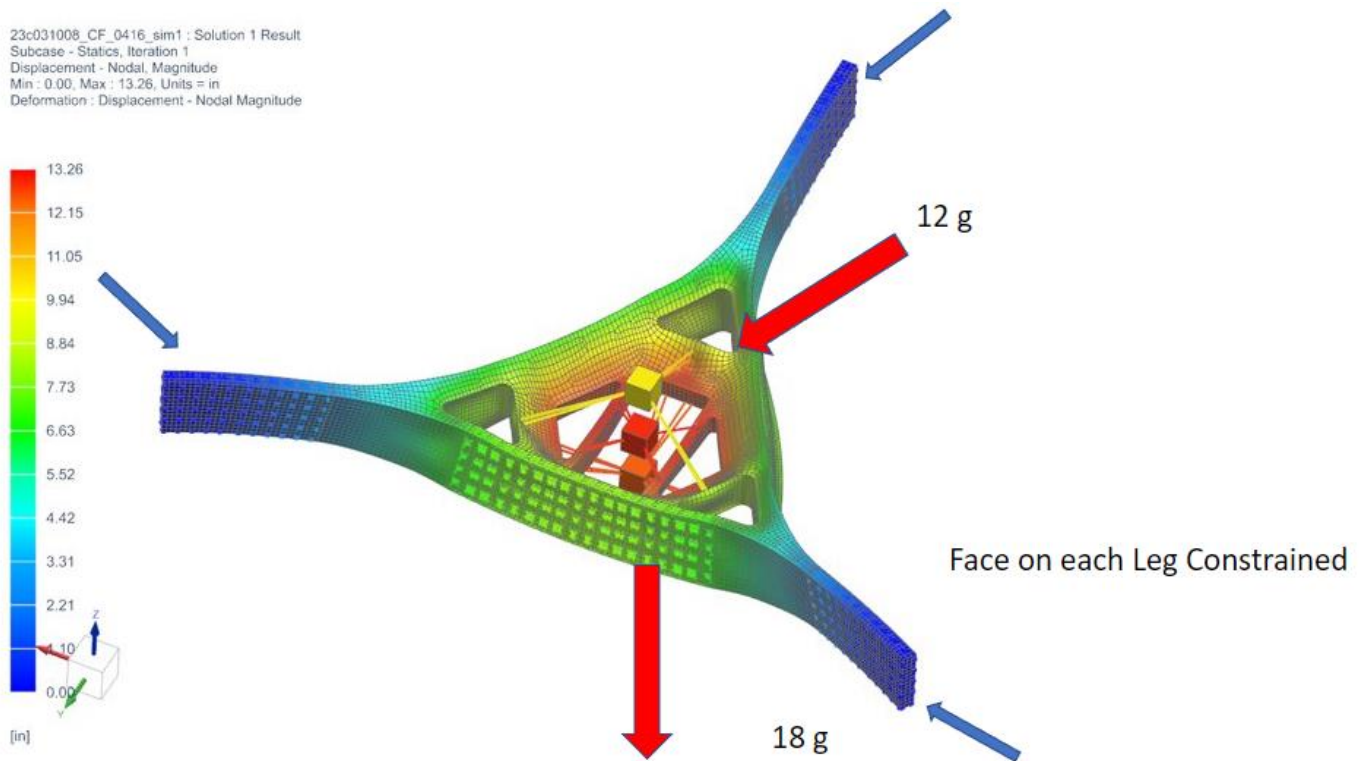


Figure 49: Displacement analysis of SMSS iteration with trimmed bodies and internal lattices.

3 Leg Lattice, and Base 1 and 2 Lattice

File: (Simulation) 23c031008_CF_0416_sim4.sim

23c031008_CF_0416_sim4 : Solution 1 Result
 Subcase - Statics, Iteration 1
 Stress - Element-Nodal, Unaveraged, Von-Mises
 Beam Section : Recovery Point C, Shell Section : Top
 Min : 0.000E+00, Max : 1.307E+04, Units = lb/in²
 Beam Coord sys : Local
 Deformation : Displacement - Nodal Magnitude

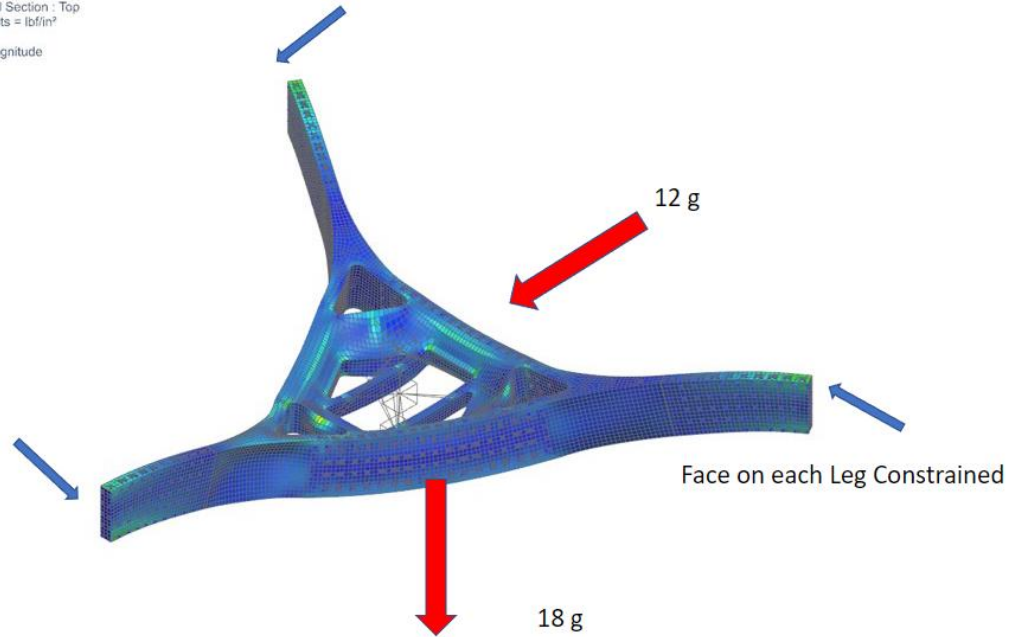


Figure 50: Stress simulation of model with trimmed bodies and internal lattices.

3 Leg Lattice, and Base 1,2, And 3 Lattice

File: (Simulation) 23c031008_CF_0416_sim5.sim

23c031008_CF_0416_sim5 : Solution 1 Result
 Subcase - Statics, Iteration 1
 Stress - Element-Nodal, Unaveraged, Von-Mises
 Beam Section : Recovery Point C, Shell Section : Top
 Min : 0.000E+00, Max : 1.303E+04, Units = lb/in²
 Beam Coord sys : Local
 Deformation : Displacement - Nodal Magnitude

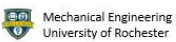
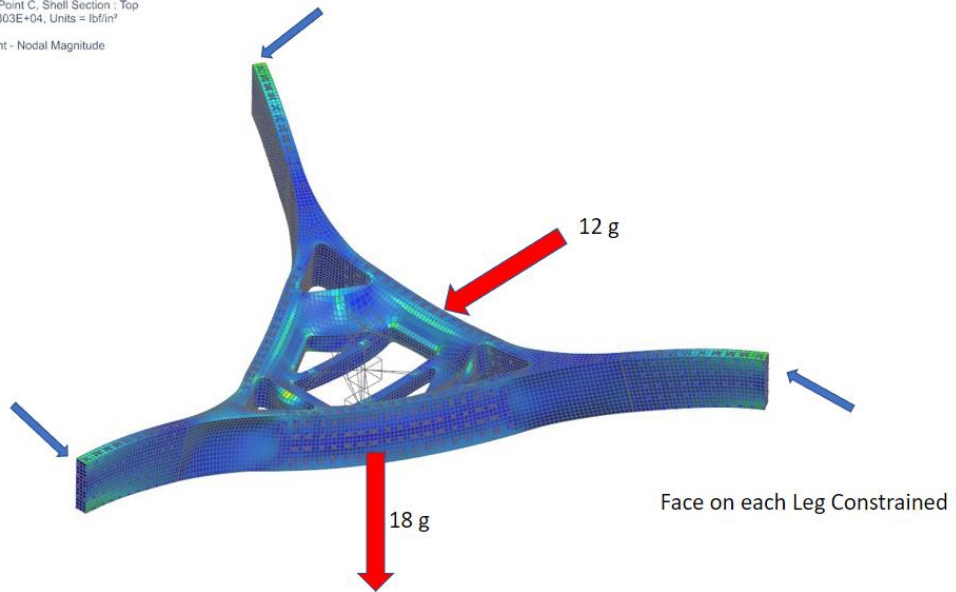


Figure 51: Stress simulation of model with trimmed bodies and internal lattices. This simulation has reduced stress from Figure 50.

Displacement, Middle Hex Shell .1 " Outside Shell .1"

File: (Simulation) 23c031008_CF_0416_sim11.sim

23c031008_CF_0416_sim11 : Solution 1 Result
 Subcase - Statics, Iteration 1
 Displacement - Nodal, Magnitude
 Min : 0.000, Max : 5.905, Units = in
 Deformation : Displacement - Nodal Magnitude

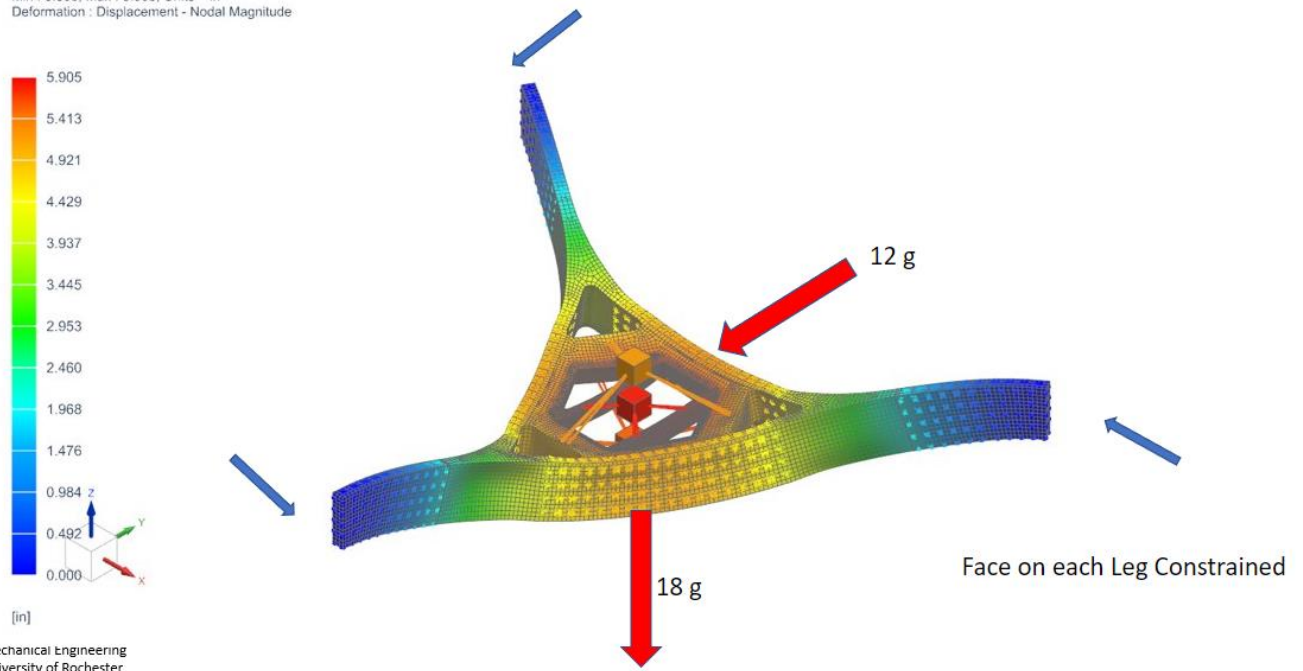


Figure 52: Displacement analysis of model with trimmed bodies, internal lattices, and varying shell sizes in the model.

Von Mises, Middle Hex Shell .1 " Outside Shell .1"

File: (Simulation) 23c031008_CF_0416_sim11.sim

23c031008_CF_0416_sim11 : Solution 1 Result
 Subcase - Statics, Iteration 1
 Stress - Element-Nodal, Unaveraged, Von-Mises
 Beam Section : Recovery Point C, Shell Section : Top
 Min : 0.000E+00, Max : 1.633E+04, Units = lbf/in²
 Beam Coord sys : Local
 Deformation : Displacement - Nodal Magnitude

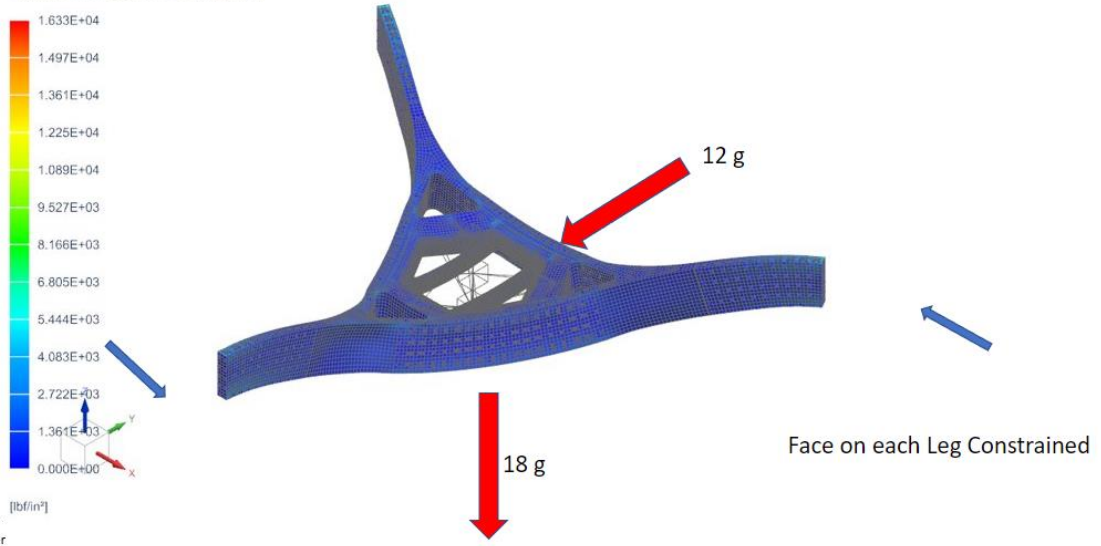
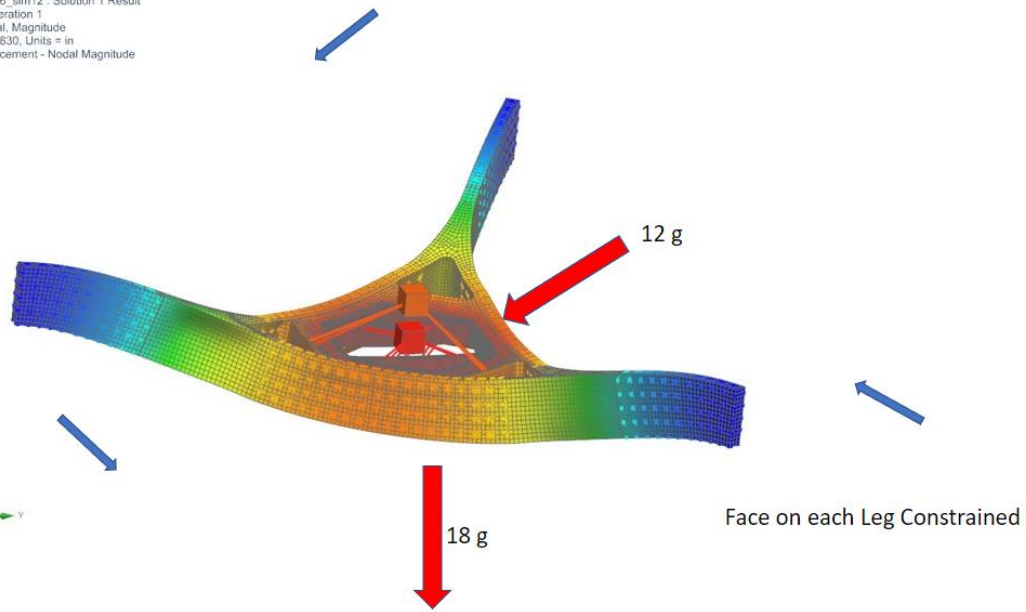
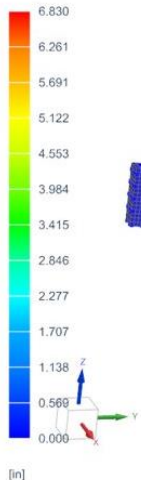


Figure 53: Von-mises stress analysis of model with trimmed bodies, internal lattices, and varying shell sizes in the model.

Whys is Middle Hex Shell at .5" create more displacement than .1" Shell?

File: Sim 12

23c031008_CF_0416_sim12 : Solution 1 Result
Subcase - Statics, Iteration 1
Displacement - Nodal, Magnitude
Min : 0.000, Max : 6.630, Units = in
Deformation : Displacement - Nodal Magnitude



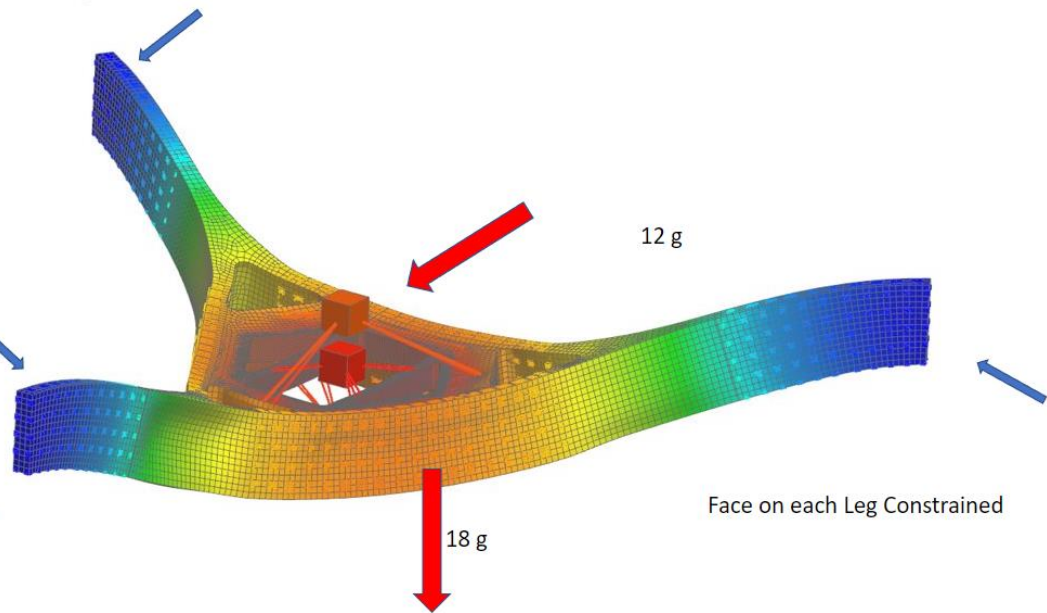
Mechanic
University of Rochester

Figure 54: Continued displacement verification of model with trimmed bodies, internal lattices, and varying shell sizes in the model.

Outside 0.1", Middle 0.5" and RBE2 connections

File: Sim 14

23c031008_CF_0416_sim14 : Solution 1 Result
Subcase - Statics, Iteration 1
Displacement - Nodal, Magnitude
Min : 0.000E+00, Max : 8.181E-03, Units = in
Deformation : Displacement - Nodal Magnitude



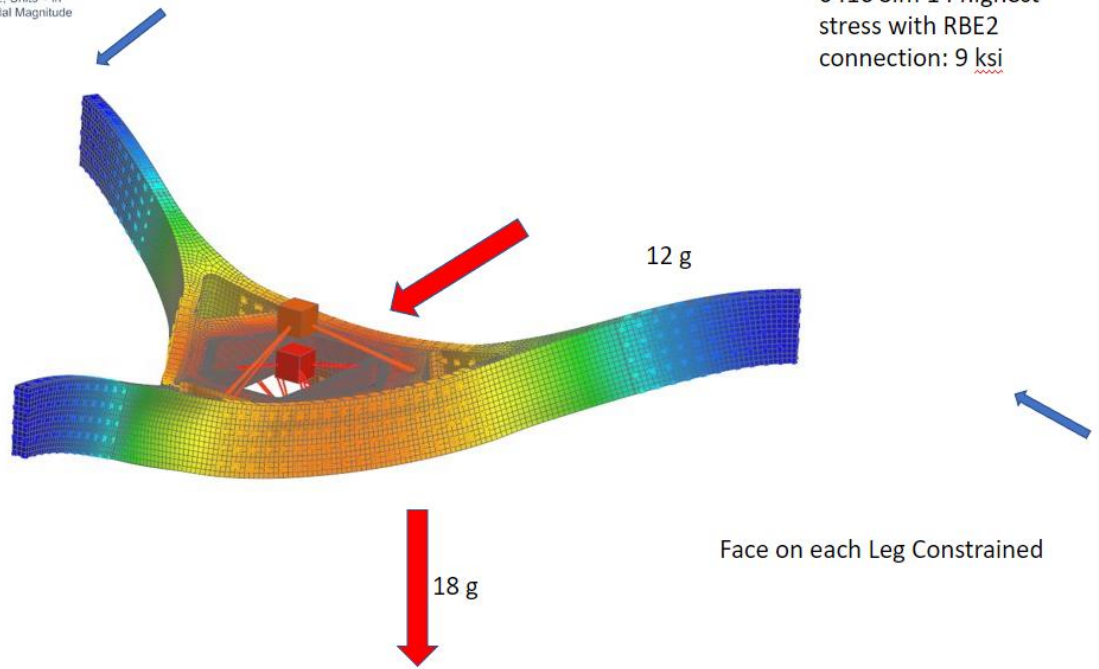
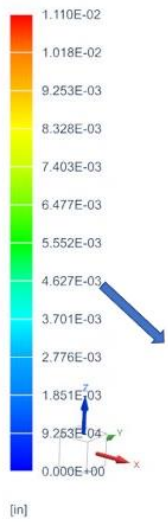
Mechanical Engineering
University of Rochester

Figure 55: Displacement verification of model with trimmed bodies, internal lattices, RBE2 connections, and varying shell sizes in the model.

Outside 0.1", Middle 0.5" and RBE3 connections

File: 0417 Sim 1

23c031008_CF_0417_sim1 : Solution 1 Result
 Subcase - Statics, Iteration 1
 Displacement - Nodal, Magnitude
 Min : 0.000E+00, Max : 1.110E-02, Units = in
 Deformation : Displacement - Nodal Magnitude



0416 Sim 14 highest stress with RBE2 connection: 9 ksi

Mechanical Engineering
 University of Rochester

Figure 56: Displacement verification of model with trimmed bodies, internal lattices, RBE3 connections, and varying shell sizes in the model.

Outside 0.1", Middle 0.5" and RBE3 connections

File: 0417 Sim 1

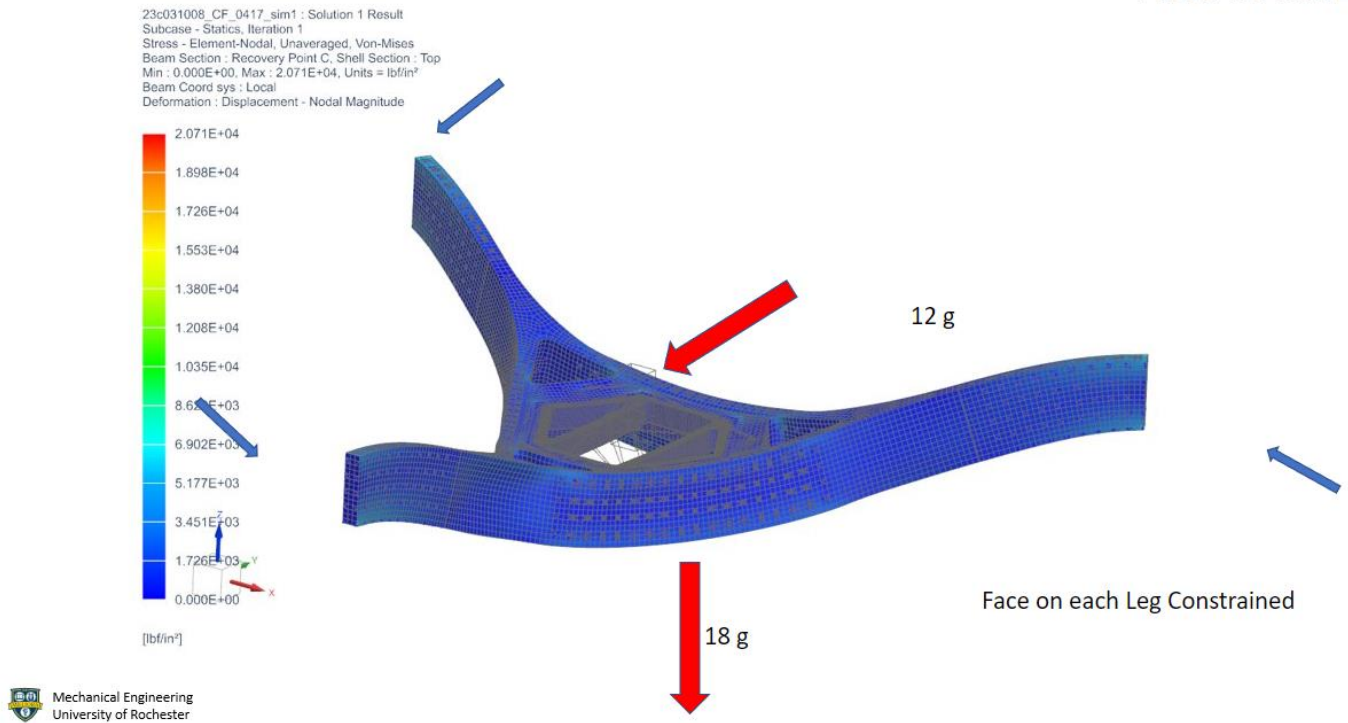


Figure 57: Stress verification of model with trimmed bodies, internal lattices, RBE3 connections, and varying shell sizes in the model.

3 Leg Lattice, and Base 1,2, And 3 Lattice, Shell Split

File: (Simulation) 23c031008_CF_0417_sim5.sim

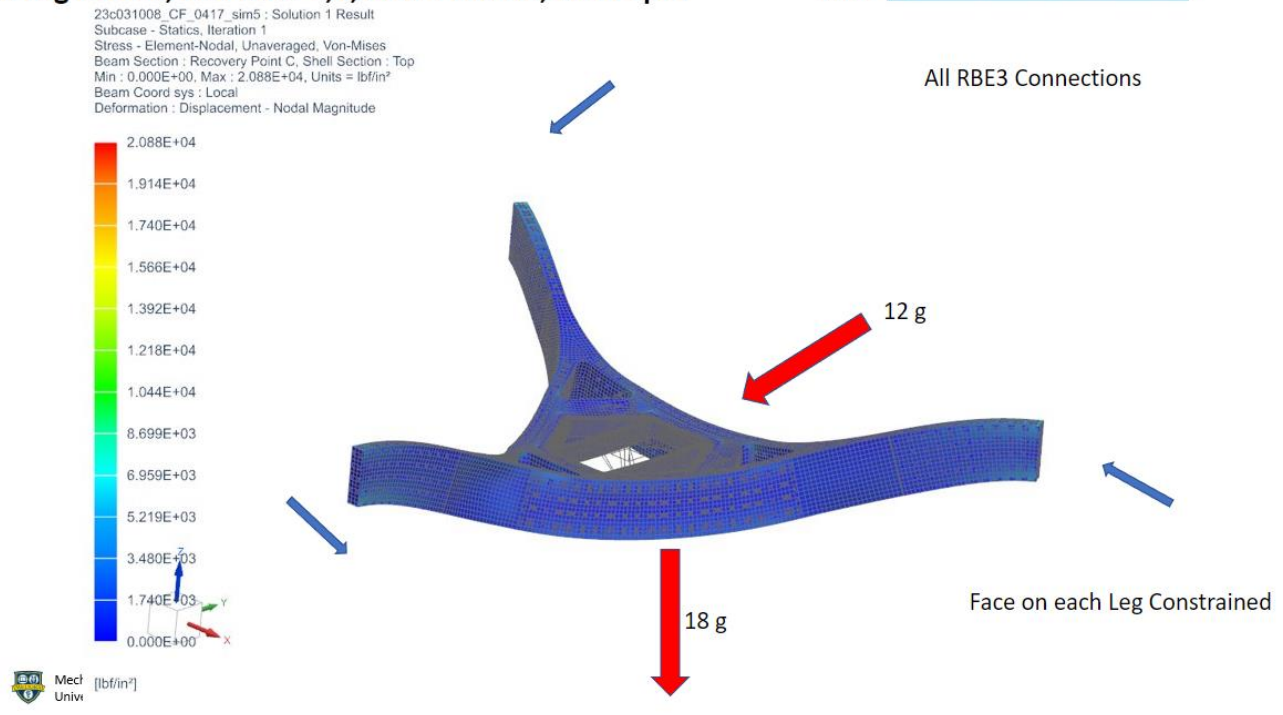


Figure 58: Stress verification of model with internal lattices and shelled split bodies.

**3 Leg Lattice, and Base 1,2,3 Lattice, Split Lattice 1,2,3
2D Shell All Around**

File: 0417 FEM/SIM 7

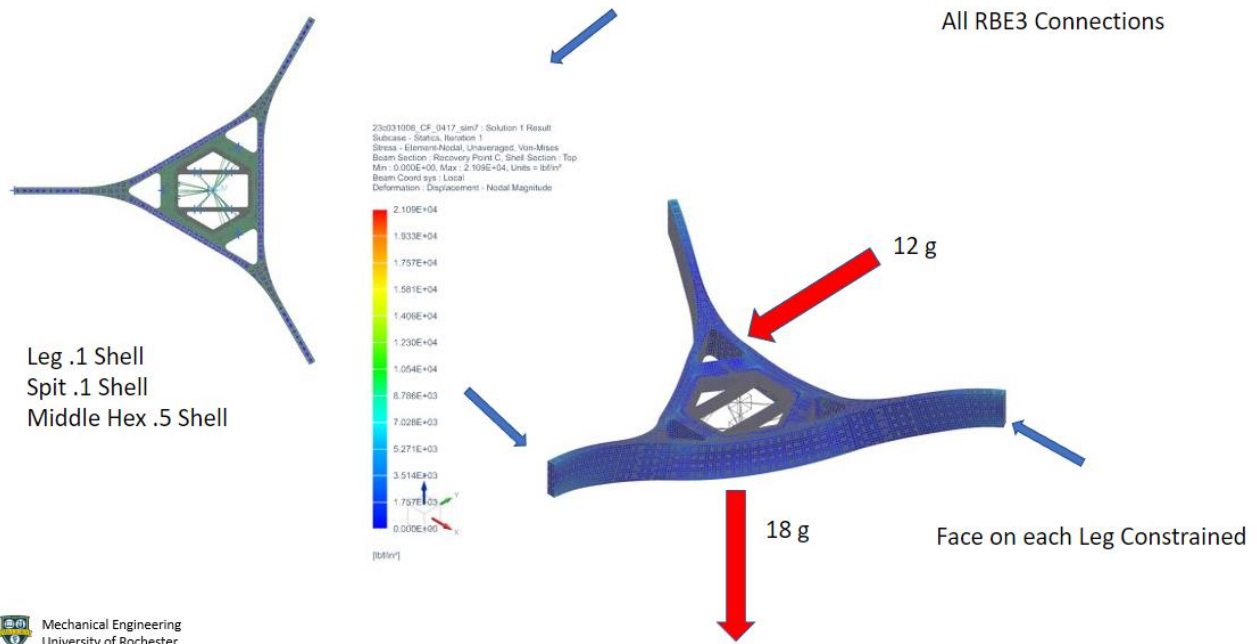


Figure 59: Stress verification of shelled model with trimmed internal lattices and split bodies with additional lattices. This is the basis for the final rendition.

APPENDIX E: MANUFACTURING

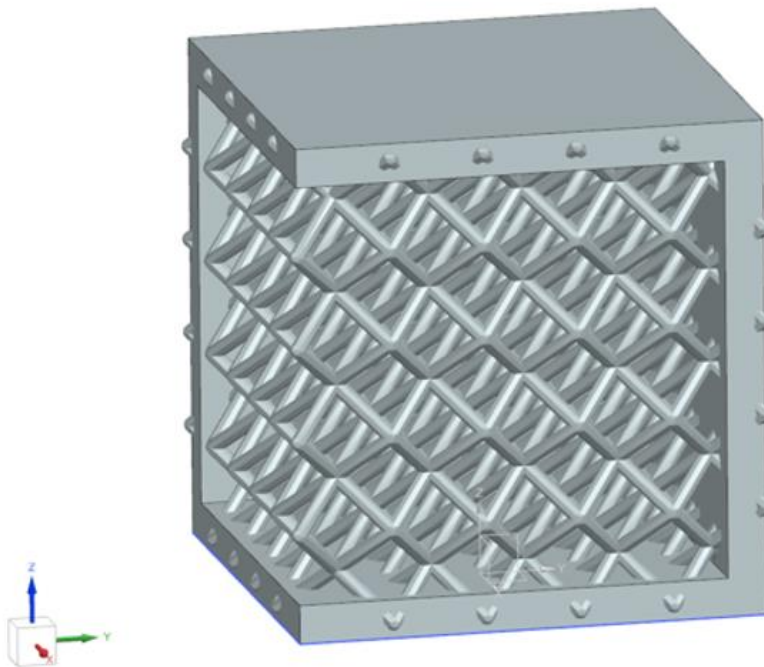


Figure 60: Model of shell cube with internal lattice.

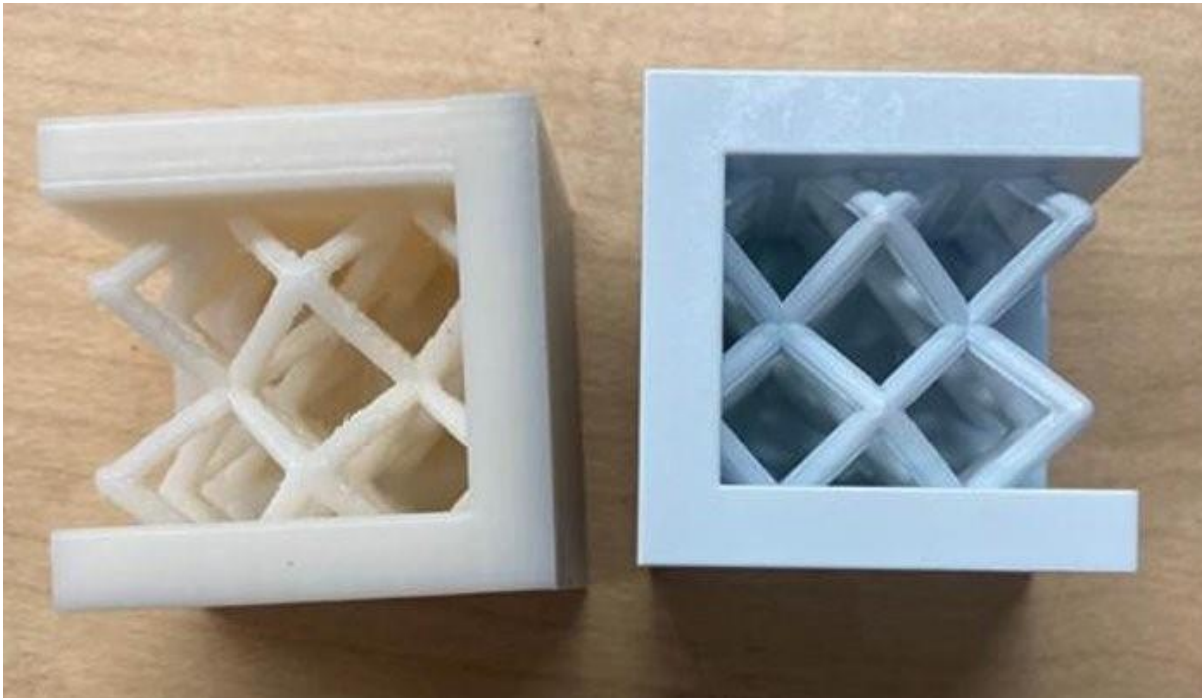


Figure 61: 3D printed shell cubes with internal lattice.

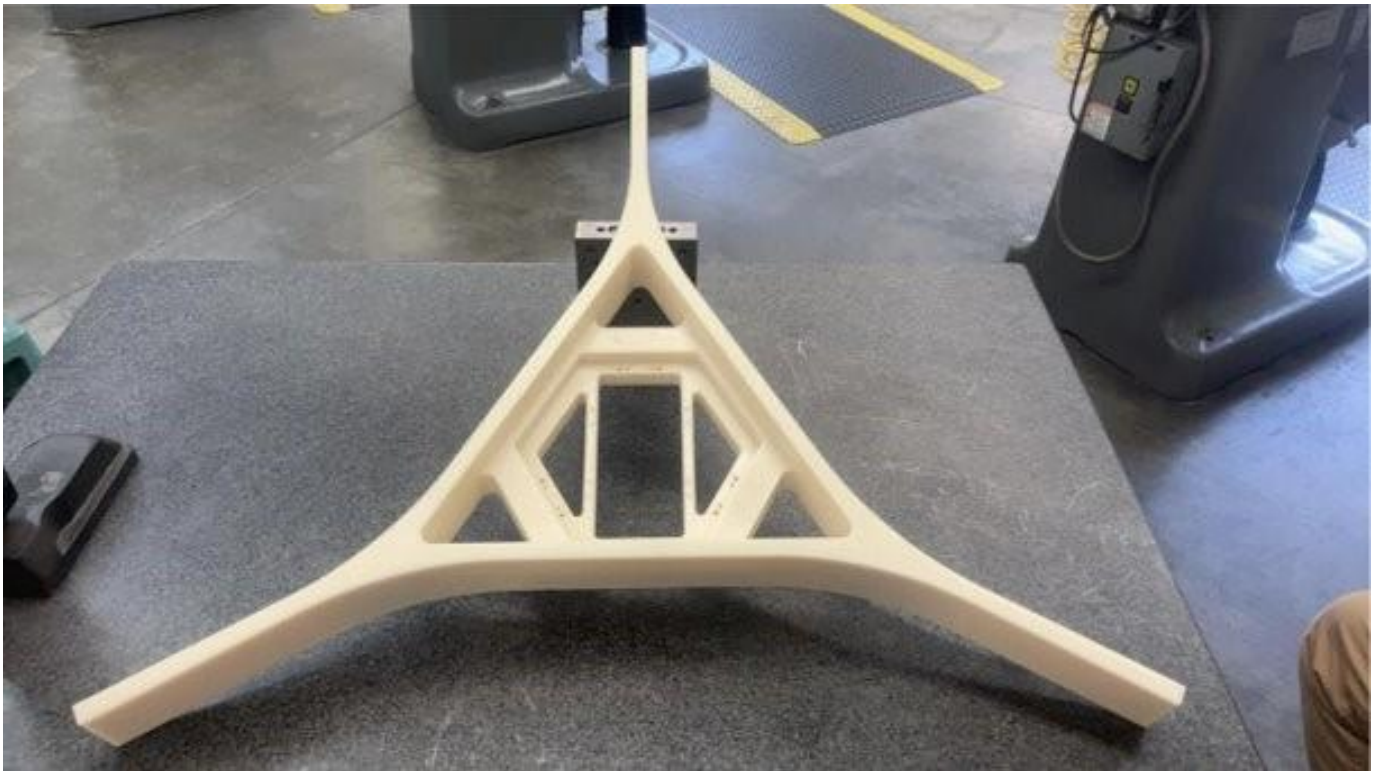


Figure 62: 60% scaled 3D printed SMSS with solid infill.

Puzzle Piece Arm

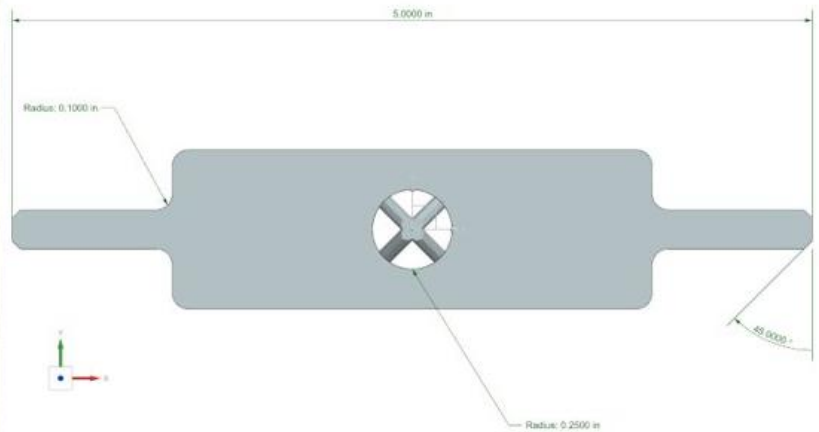
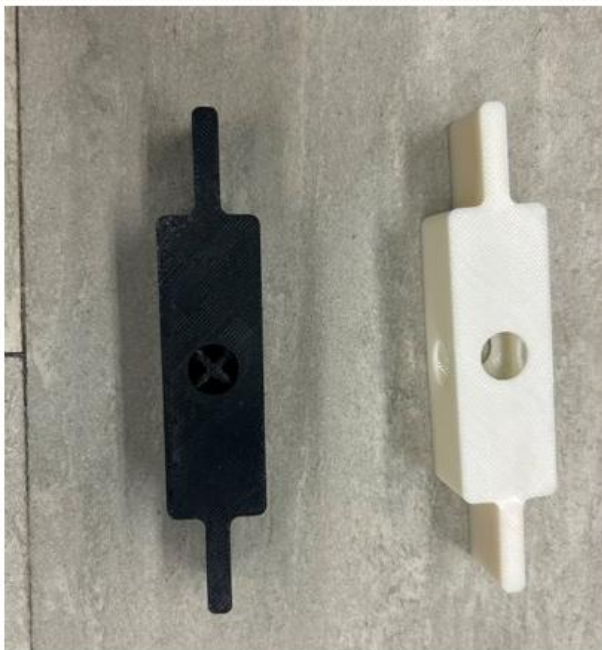


3-inch Lattice Infill

QuadDiametral Lattice
Edge Length = 0.5 inches
Rod Diameter = 0.1 inches



Figure 63: 3D printed arm with 3-inch of lattice infill. The arm was printed in sections that fit together.



QuadDiametral Lattice
Edge Length = 0.5 inches
Rod Diameter = 0.1 inches

Figure 64: 3D printed lattice and hollow test coupons on the left. CAD of lattice coupon on the right.

APPENDIX F: TESTING AND RESULTS

4/25/23

Set up and measurement for deflection test



Figure 65: Set up and measurement for deflection test with 8.9 lbf load.

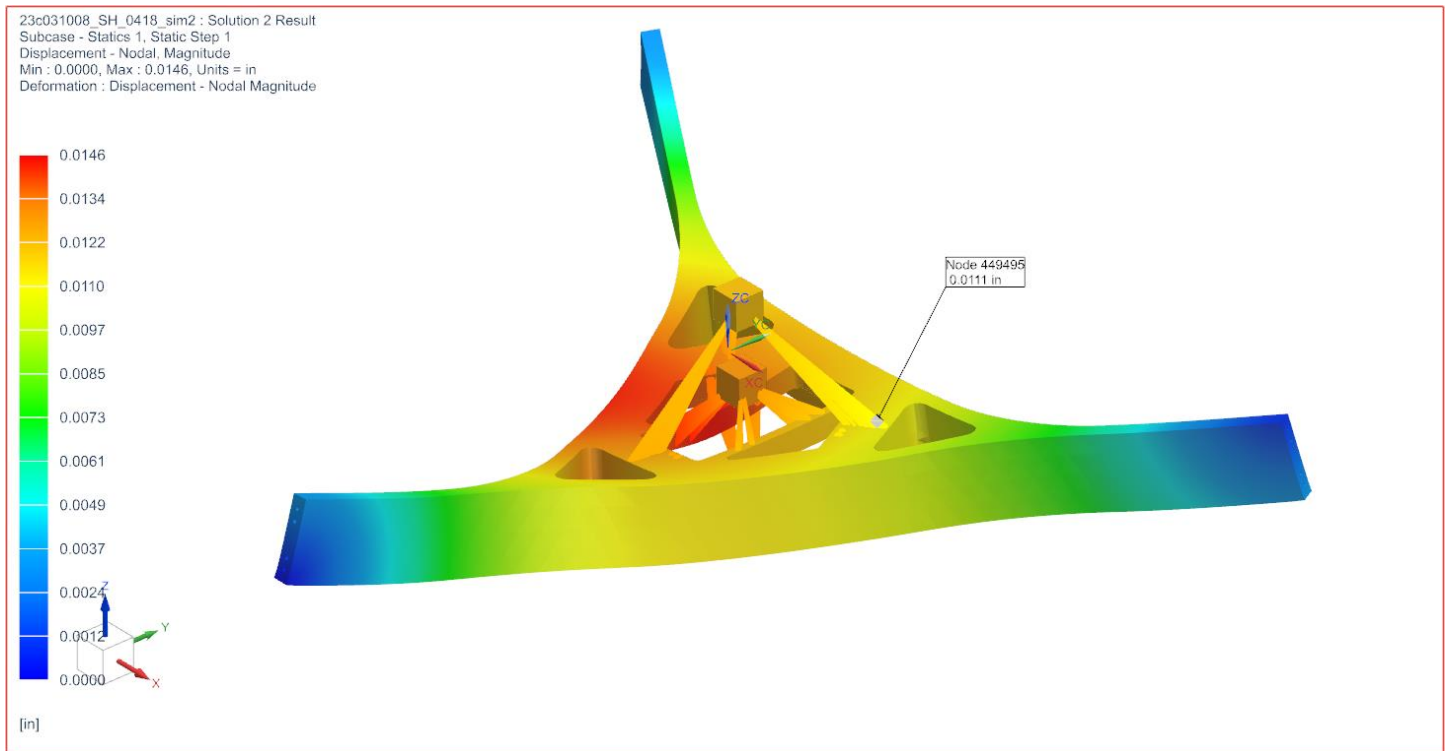


Figure 66: Displacement analysis of 60% scaled solid model with 8.9 lbf load.



Figure 67: Hammer test set up.

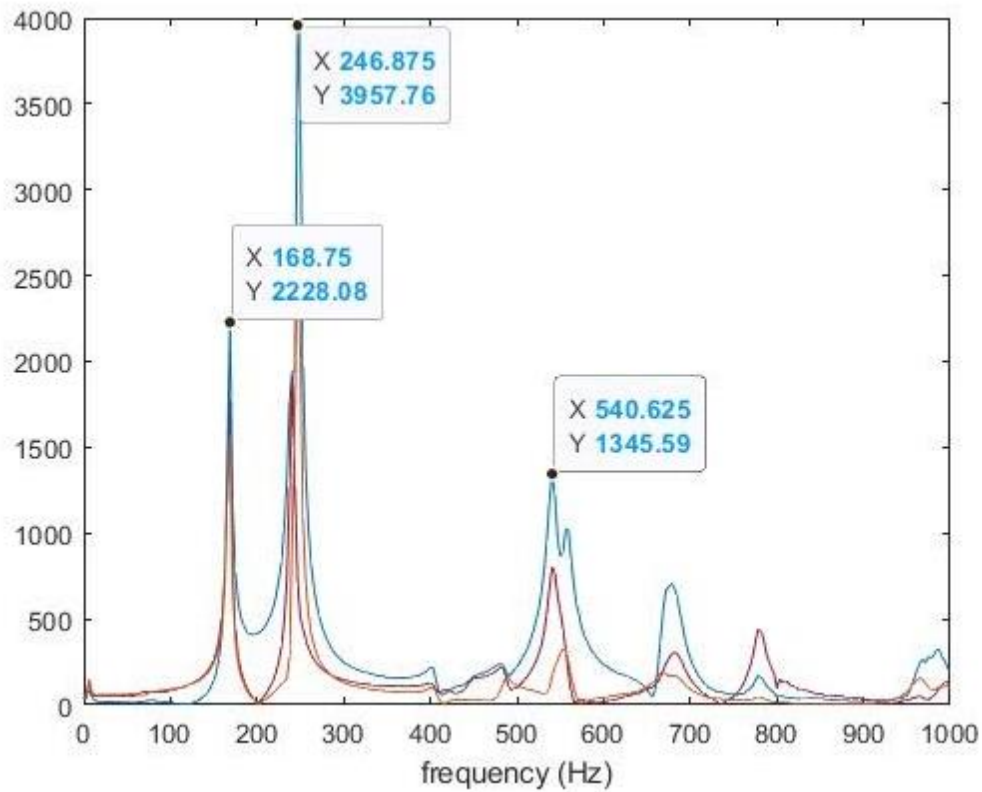
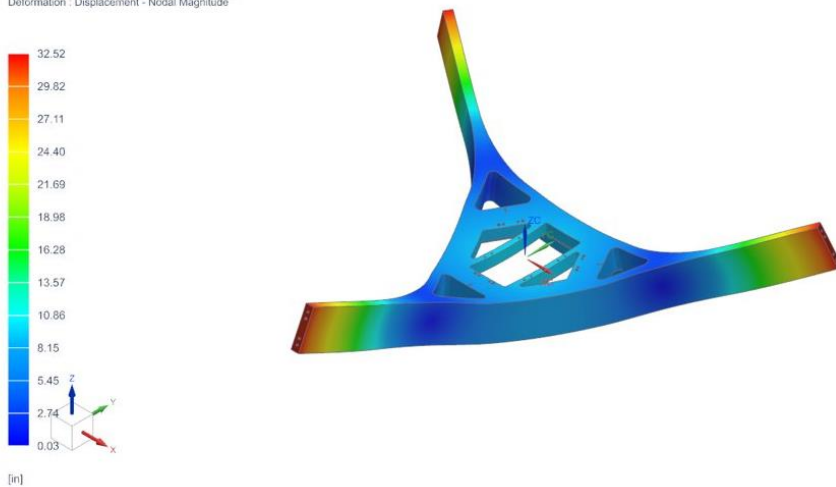


Figure 68: Mode frequencies of 3D printed solid model.

4-18-23

60% scaled solid structure modal analysis sim for real life hammer test

23c031006_SH_0418_sim2 - Solution 1 Result
 Subcase - Normal Modes 1, Mode 10, 176.29Hz
 Displacement - Nodal Magnitude
 Min : 0.03, Max : 32.52, Units = in
 Deformation : Displacement - Nodal Magnitude



Mechanical Engineering
 University of Rochester

Figure 69: Modal analysis simulation results on 60% scaled solid model for hammer test verification.

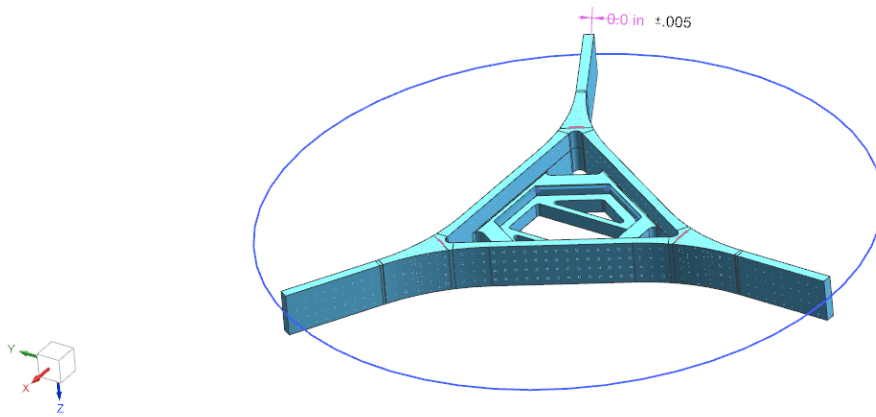


Figure 70: Tolerance verification for SMSS diameter.

4-20-23

Faro Arm measuring angle between legs

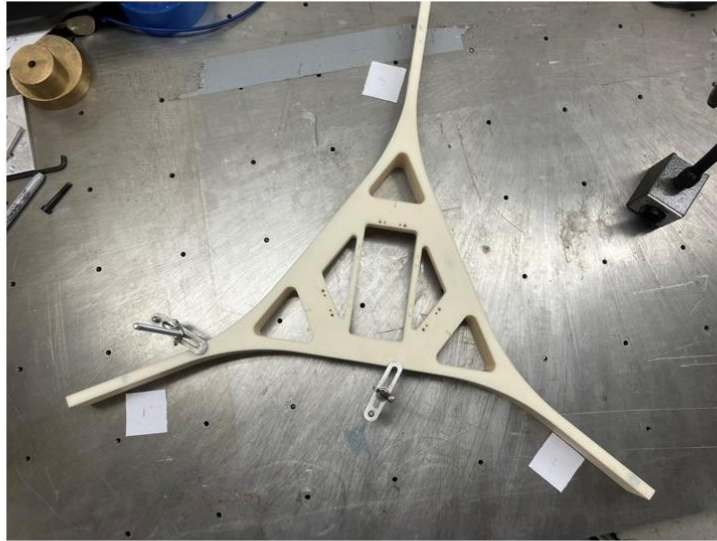


Mechanical Engineering
University of Rochester

Figure 71: Angle verification test using Faro arm.

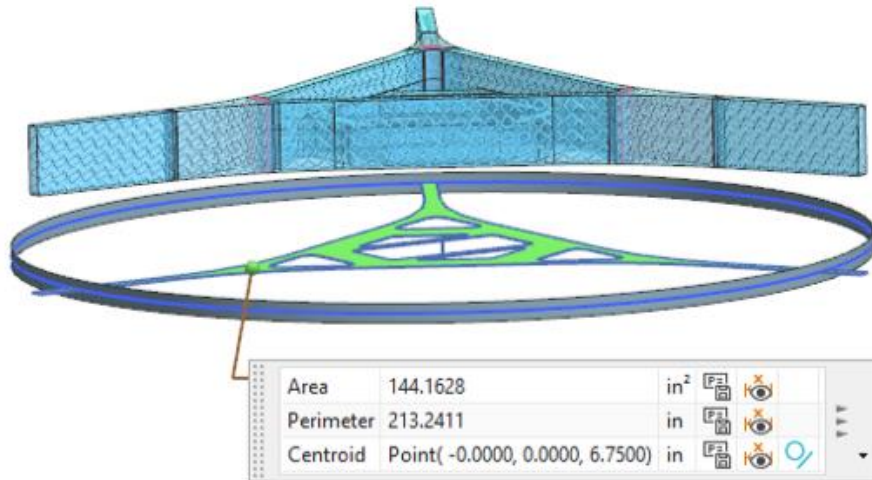
4-20-23

Set up for angle verification



 Mechanical Engineering
University of Rochester

Figure 72: Angle verification test set up. The model is fixed to prevent vertical movement.



Projected Area Percentage = Area of SMSS/ Area of Primary Mirror

'22 SMSS Area % = 144.1628 in² / 1319.073 in²

'22 SMSS Area % = 10.93%

Figure 73: Projected area verification calculation for specification #6.

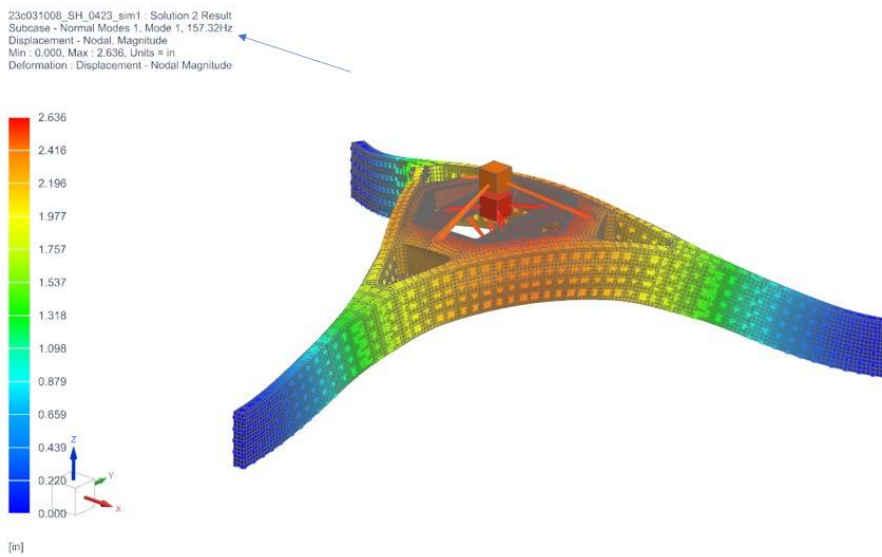


Figure 74: Hammer/Strike test analysis. Mode 1 frequency is 157.32 Hz.

Lattice Test Coupon

Solution 101
Material: ABS
MTS Test Result:
F = 100.119 N,
Extension = 0.07415 mm

NX Simulated Results:
F = 101.605 N,
Extension = 0.0694 mm

Percent Error = 6.8%

23/03/10/09_CP_04110_sim1 : Solution 1 Result
Subcase = 4562, Static Step 1
Displacement - Nodal Magnitude
Min: 0.0000, Max: 0.0694, Units = mm
Absolute Value
Deformation: Displacement - Nodal Magnitude

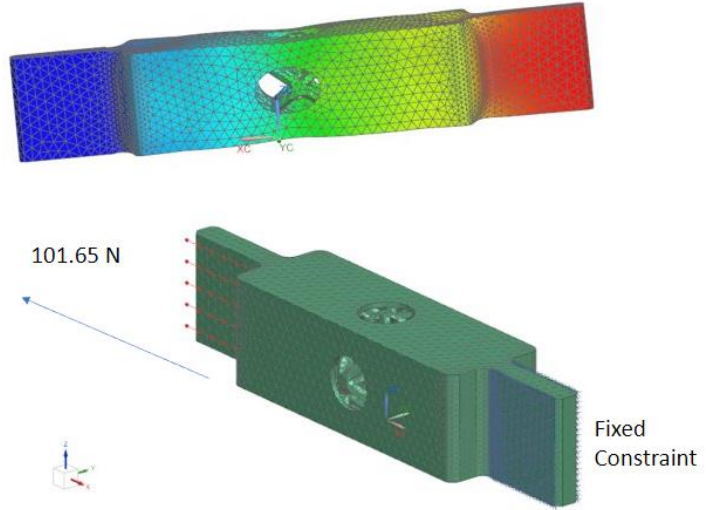


Figure 75: Lattice test coupon displacement analysis and comparison calculation to actual.

Hollow Test Coupon

Solution 101
Material: ABS
MTS Test Result:
F = 101.65 N, Extension = .1190 mm

NX Simulated Results:
F = 101.605 N, Extension = 0.0862 mm

Percent Error = 38%

23/03/10/09_sim2 : Solution 1 Result
Subcase = 4562, Static Step 1
Displacement - Nodal Magnitude
Min: 0.0000, Max: 0.0862, Units = mm
Absolute Value
Deformation: Displacement - Nodal Magnitude

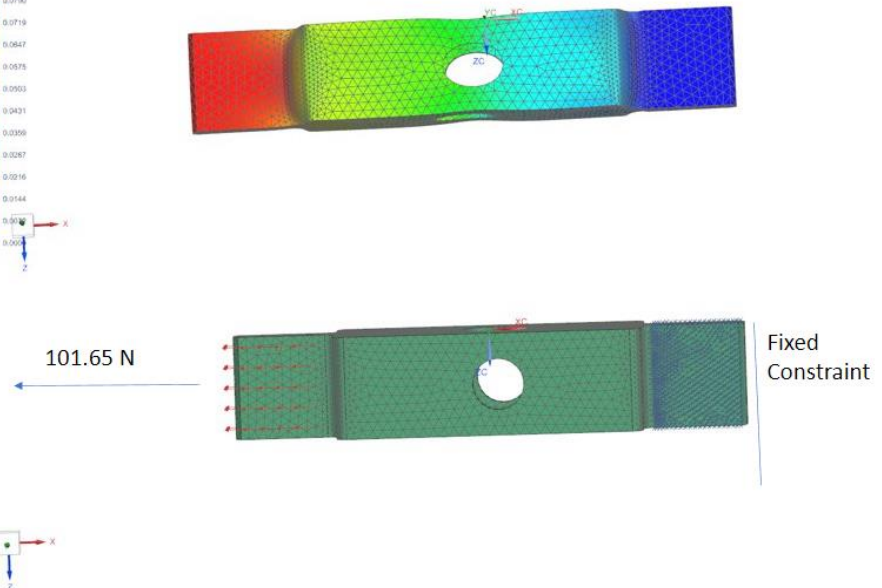


Figure 76: Hollow test coupon displacement analysis and comparison calculation to actual.

Subcase	Temperature (°C)	Axial Load Direction (° from X Axis)	Maximum Displacement (in)	Maximum Stress (psi)	Pass Reqs and Specs
1	35	0	7.264E-3	19910	Pass
2	35	45	4.968E-3	11010.58	Pass
3	35	90	5.332E-3	14860	Pass
4	5	0	7.178E-3	19790	Pass
5	5	45	4.901E-3	11047.41	Pass
6	5	90	5.554E-3	14550	Pass
7	20	0	7.22E-3	19850	Pass
8	20	45	4.933E-3	11028.56	Pass
9	20	90	5.443E-3	14650	Pass

Figure 77: Thermal load subcase results.

**3 Leg Lattice, and Base 1,2,3 Lattice, Split Lattice 1,2,3
2D Shell All Around, 2D Middle Shell**

File: 0423 FEM/SIM 7

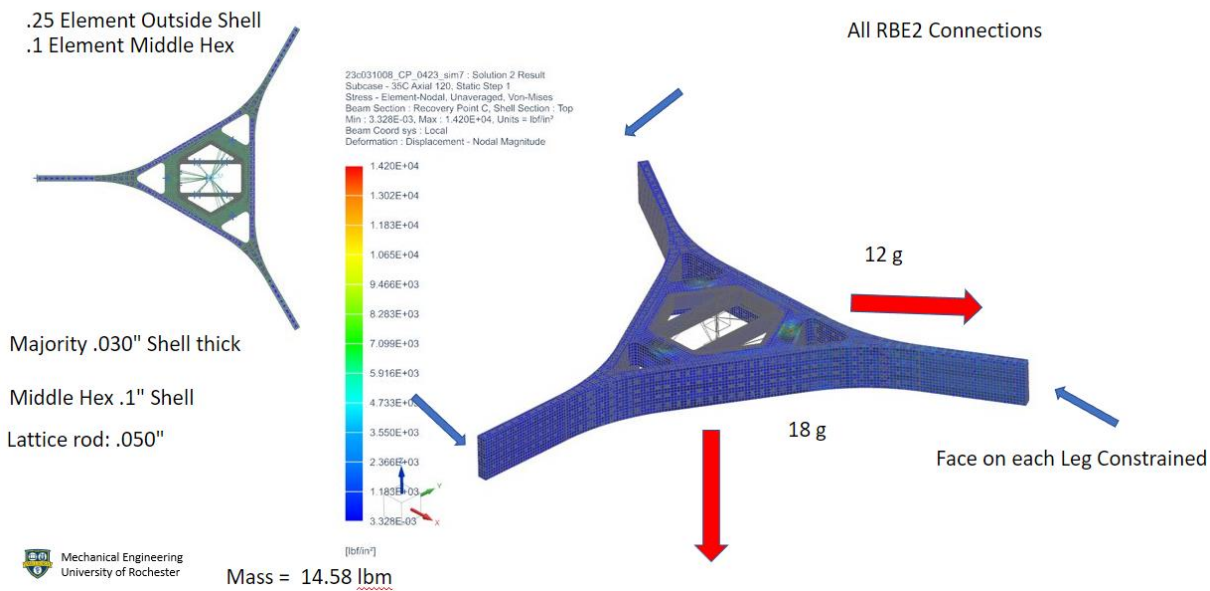


Figure 78: Von-mises stress analysis on shelled split lattice model.

**3 Leg Lattice, and Base 1,2,3 Lattice, Split Lattice 1,2,3
2D Shell All Around, 2D Middle Shell**

File: 0423 FEM/SIM 7

Lattice rod: .050"

All RBE2 Connections

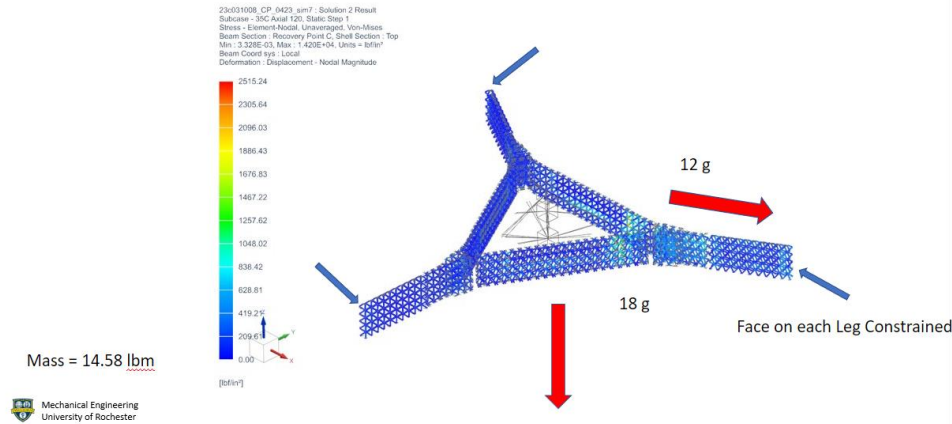


Figure 79: Von-mises stress analysis on lattice only in final model.

Testing --- Test Coupon

Hollow Test Coupon

MTS Test Result:

F = 51.78N, Extension = .0490 mm

NX Simulated Results:

F = 51.78N, Extension = 0.044 mm

Percent Error = 11%

Stiffness = 8.02 E+3 lbf/in

Lattice Test Coupon

MTS Test Result:

F = 100.119N, Extension = 0.0745 mm

NX Simulated Results:

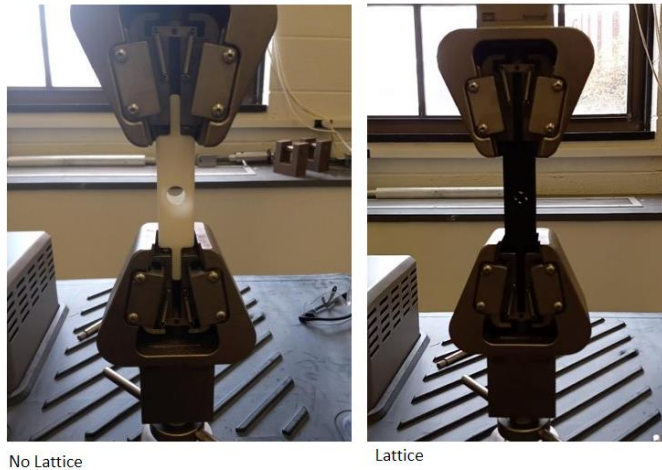
F = 101.605 N, Extension = 0.0694mm

Percent Error = 6.8%

Stiffness = 1.05E+04 lbf/in

**26.67% more stiffness in
Lattice Test Coupon**

**Difference of
Mass/Stiffness = 1.87%**



Mechanical Engineering
University of Rochester

Figure 80: Results of test coupon MTS physical test and following NX Simulation.

APPENDIX G: PATENTS

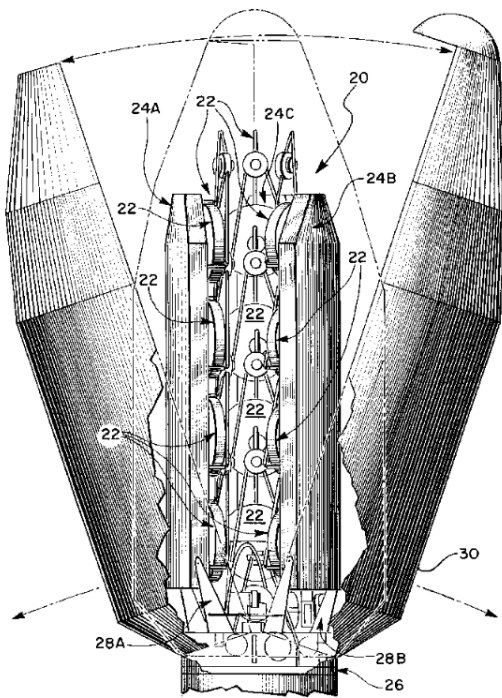


Figure 81: Patent example #1 of Lockheed Martin's secondary mirror support structure.

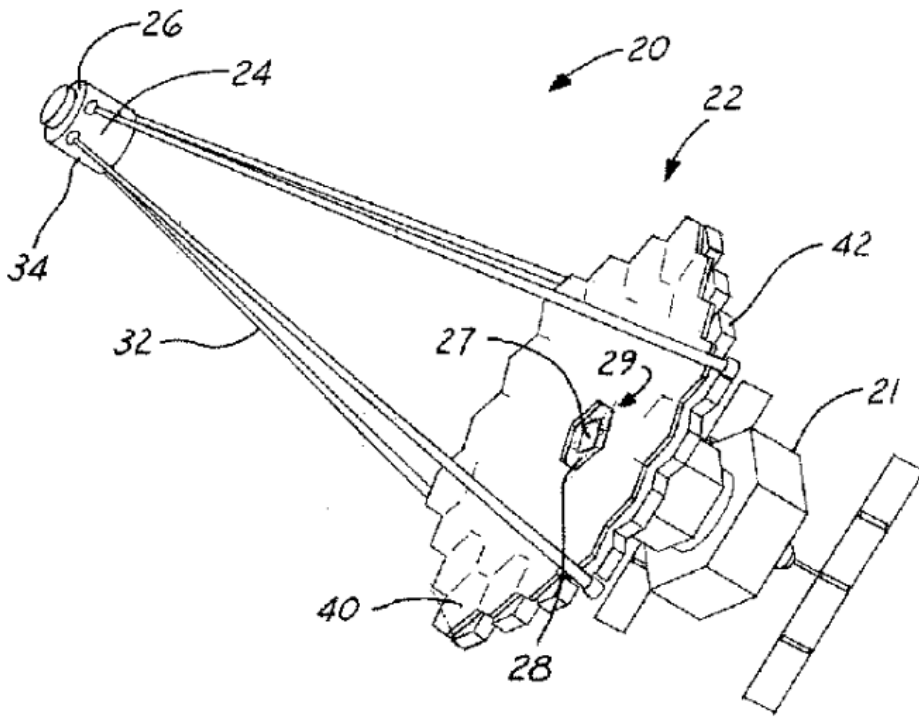


Figure 82: Patent example #2 of Lockheed Martin's secondary mirror support structure.